SISSA
Scuola
Internazionale
Superiore di
Studi Avanzati

Physics Area - PhD course in
Theoretical Particle Physics

Orientifolds in Dimer Models: General Aspects and Applications.

Candidate:
Shani Nadir Meynet

Advisor:
Matteo Bertolini

Academic Year 2020-21

Abstract

In this thesis we study orientifolds and D-branes at toric Calabi-Yau singularities using dimer model techniques. We present new general results concerning orientifold projections and we apply them, constructing the first example of fully stable dynamical supersymmetry breaking model.

The thesis is divided into three parts.

In the first part we present mostly background material. We start with a short review of the Gauge/Gravity duality and generalizations. In particular we consider D3-branes at the tip of singular toric Calabi-Yau threefolds, introducing the idea of quiver theory and its natural generalization, dimer models. We then present known results obtained using this tool to explore orientifold projections. Finally, we review two dynamical supersymmetry breaking models, that are the simplest ones that can be engineered on D3-branes in this framework and which will play a prominent role in the last part of the thesis.

The second part focuses on orientifolds. We present two new results: the first one links the geometry of the Calabi-Yau variety and the chiral anomaly of the orientifolded theory, in particular we will provide a criterium to determine whether an orientifold projection can be safely performed, i.e. without introducing uncancelled anomalies. The second concerns a new kind of orientifold projection related to glide involutions of the dimer model. This construction has the property to preserve superconformal invariance in the projected theory.

In the third and last part of this thesis, we investigate dynamical supersymmetry breaking vacua obtained by D-branes at Calabi-Yau singularities. We first review known models and we show that all those theories have instabilities along $\mathcal{N} = 2$ Coulomb branches. We then show that this instability can be overcome, with suitable generalizations of the models presented in the first part. Finally, using the results of the second part, we will show how to constrain the possible geometries able to host dynamical supersymmetry breaking models free of any instabilities. This will select a singular Calabi-Yau, that we dubbed the Octagon, which furnishes the first instance of a model able to host a fully stable dynamical supersymmetry breaking model within the Gauge/String correspondence.

Forward

This thesis is divided into three parts. In the first one I revise some background material about Gauge/Gravity duality and the tools we used in our research, namely dimer models and orientifolds. In the second part I present new results obtained studying orientifolded toric Calabi-Yau singularities. In the final part I use the tools developed in the second section to build stable dynamical supersymmetry breaking models in the framework on Gauge/Gravity duality.

The thesis is based on the following papers

1. R. Argurio, M. Bertolini, S. Meynet, and A. Pasternak, *On supersymmetry breaking vacua from D-branes at orientifold singularities*, *JHEP* **12** (2019) 145, [arXiv:1909.04682]

2. R. Argurio, M. Bertolini, S. Franco, E. García-Valdecasas, S. Meynet, A. Pasternak, and V. Tatitscheff, *Dimers, Orientifolds and Stability of Supersymmetry Breaking Vacua*, *JHEP* **01** (2021) 061, [arXiv:2007.13762]

3. R. Argurio, M. Bertolini, S. Franco, E. García-Valdecasas, S. Meynet, A. Pasternak, and V. Tatitscheff, *Dimers, Orientifolds and Anomalies*, *JHEP* **02** (2021) 153, [arXiv:2009.11291]

4. R. Argurio, M. Bertolini, S. Franco, E. García-Valdecasas, S. Meynet, A. Pasternak, and V. Tatitscheff, *The Octagon and the Non-Supersymmetric String Landscape*, *Phys. Lett. B* **815** (2021) 136153, [arXiv:2005.09671]

5. E. García-Valdecasas, S. Meynet, A. Pasternak, and V. Tatitscheff, *Dimers in a Bottle*, *JHEP* **04** (2021) 274, [arXiv:2101.02670]

Contents

Part I
Background

Introduction

The Quantum Theory of Fields (QFT), and in particular, the Standard Model, provides the most complete description of fundamental interactions. At the perturbative level, it is able to predict scattering amplitudes, decay rates and particle production with an impaired precision. In the last century, not only it was able to reproduce many observed phenomena, but also allowed the prediction of new particles, e.g. the Higgs Boson. Despite this huge success, there are still some open and fundamental questions we are not able to answer:

- First of all we lack an analytical formulation of strongly coupled systems. Yang-Mills' mass gap, chiral symmetry breaking, confinement are just a few examples of observed properties of matter which are not fully explained in the context of QFT.

- Second, the Standard Model provides a description of all observed fundamental forces but gravity, which, upon quantization, leads to non-renormalizable observables, making impossible to give any reliable prediction.

In order to address these problems, physicists tried to generalize the tools provided by QFT and the first instance of this work is Supersymmetry.

Supersymmetry is a special kind of symmetry which relates bosons and fermions. The presence of such symmetry strongly constrains the content and interactions of a theory, allowing reliable computations also at strong coupling. Using the power of holomorphicity and non-renormalization theorems, many results were achieved in the context of supersymmetric field theory, such as the computation of partition functions via localization and the proof of confinement for supersymmetric QCD. However, no sign of supersymmetry has been found yet. This opened a new direction of research, both formal and phenomenological, for mechanisms which could lead to supersymmetry breaking, if present in nature.

A second great revolution in the field of theoretical physics came with the advent of String Theory. Born as a model to describe the confinement of quarks, String Theory was soon recognized to be a candidate to describe all fundamental interactions, including gravity. It consists in a quantum field theory where the fundamental objects are not point like particles, but extended strings, propagating in space-time. In fact, it was later realized, [6], that String Theory not only describes one dimensional strings, but also extended objects, called D-branes. The study of

these objects allowed to engineer all kinds of field theory in various dimensions in a simple and clear language. Most important, D-branes were one of the crucial ingredient to understand one of the deepest property of String Theory: all various realizations of Supersymmetric String Theory are connected via a web of dualities, all describing some regimes of an underlying theory in which the fundamental objects are not only the strings, but also extended objects.

Finally, the discovery of D-branes paved also the path to what is probably the most striking development in theoretical physics in the last decades, namely the Gauge/Gravity or Gauge/String correspondence. In its original formulation, Gauge/Gravity duality relates a $d+1$-dimensional theory of gravity and a d-dimensional quantum field theory. One interesting aspect of this duality is that it is a strong/weak duality, relating the regime in which the gauge theory is at strong coupling to the regime in which the gravity dual is weakly coupled (and vice versa). The two theories have the same partition function and thus describe the same physics. In the late nineties, in his seminal work, [7], Maldacena explicitly constructed the first example of a theory admitting such a duality. This example was then further generalized and lead to the development of new tools to study not only the strong coupling regime of gauge theories, but also quantum corrections to gravitational systems.

The use of Gauge/Gravity duality to explore non-perturbative phenomena is well established in the context of supersymmetric field theories. Indeed, it is possible to study effects such as chiral symmetry breaking and confinement using the gravity dual. A natural question is weather it is possible to do the same also for non-supersymmetric theories. To this end we need to find models displaying dynamical supersymmetry breaking (DSB) in the framework of the Gauge/Gravity duality.

Finding DSB models with a gravity dual would be of great relevance both in the context of the Gauge/Gravity duality and, even more interestingly, in string compactifications. In this latter set-up they could be used for model building in GKP-like constructions [8]. Eventually, they might also have an impact on the swampland program [9, 10, 11] and recent related conjectures such as [12, 13, 14].

This thesis deals with the problem of constructing DSB models in the framework of Gauge/Gravity duality. Using known geometrical and physical results, we were able to obtain new and interesting ones in the context of model building, mostly thanks to the use of dimer models and orientifold projections. These results are then applied to solve the problem of constructing DSB models in the Gauge/Gravity framework.

1 Gauge/Gravity duality

One of the first examples of Gauge/Gravity duality was realized in [7] considering type IIB string theory with a stack of N coincident D3-branes placed in a 10 dimensional Minkowski space-time. This model admits two alternative descriptions.

From the branes point of view, if we limit ourselves to the study of the low energy theory, the only accessible modes are the massless ones. On the closed string side we have that the graviton decouples in the limit in which the string length goes to zero. On the other end, the open modes on the branes describe an $\mathcal{N} = 4$ super Yang-Mills (SYM) gauge theory.

The degrees of freedom are thus

$$\text{Free graviton in flat space} + \mathcal{N} = 4 \text{ SYM} \tag{1}$$

From the gravity point of view, we need to solve Einstein equation of motions in the presence of D3-branes which have both gravitational and electric charge, the second one under the Ramond-Ramond fields. Such a solution can be find in terms of a warped metric

$$\mathrm{d}s^2 = f(r)^{-1/2}(-\mathrm{d}t^2 + \mathrm{d}x^2 + \mathrm{d}y^2 + \mathrm{d}z^2) + f(r)^{1/2}(\mathrm{d}r^2 + r^2\mathrm{d}\Omega_5) \tag{2}$$

where

$$f(r) = 1 + \frac{R^4}{r^4}, \tag{3}$$

with R a constant that depends on the string coupling, string length and number of branes, while $\mathrm{d}\Omega_5$ is the infinitesimal five dimensional solid angle. We now consider two limits, $r \to \infty$ and $r \to 0$. In the first case the solution is asymptotically flat space. Near $r \to 0$, instead, we can perform the substitution $r \to \frac{R}{v}$, and the metric becomes

$$\mathrm{d}s^2 = \frac{1}{v^2}(-\mathrm{d}t^2 + \mathrm{d}x^2 + \mathrm{d}y^2 + \mathrm{d}z^2 + dv^2) + R^2\mathrm{d}\Omega_5, \tag{4}$$

describing an $AdS_5 \times S^5$ space, where now R corresponds to the common radius of AdS_5 and S^5.

In the low energy limit, gravitons with large enough energy do not feel the AdS geometry any more, effectively decoupling from the system. Excitations coming from $r \to 0$, instead, are redshifted at infinity such that the physics close enough the AdS throat does not affect the one at large distance. The system is now described by

$$\text{Free graviton in flat space} + \text{Type IIB on } AdS_5 \times S^5. \tag{5}$$

Looking at the right hand side of eq. (1) and eq. (5), Maldacena conjectured that the two should be one and the same. Identifying the corresponding partition functions, he was the first to establish the equivalence between $\mathcal{N} = 4$ SYM and type IIB string theory on $AdS_5 \times S^5$.

From this duality, one can construct a dictionary between operators in the gauge theory and fields in the theory of gravity. For example the graviton is dual to the energy momentum tensor and the gravitino to the supersymmetric current. Moreover, the global symmetries of the field theory are matched by the isometries of the gravity theory. Indeed the $SO(6)$ R-symmetry of $\mathcal{N} = 4$ SYM correspond to the isometries of S^5, while the conformal symmetry group $SO(2,4)$ of the gauge theory is the isometry group of the AdS_5 space.

In the next sections we will explore generalizations of this duality, introducing new geometries, with the property of reducing the number of supersymmetries of the theories living on branes, and new kind of branes, the so called fractional branes, which break the confromal invariance of the world volume theory. The discussion of orientifolds in this framework, a crucial ingredient for the construction of DSB models using D-branes, is postponed to section 2, where the language of dimers makes more easy their construction.

1.1 Quiver theories

Maldacena's duality can be generalized to systems with less supersymmetries. This is achieved considering D3-branes at the tip of a singular non compact Calabi-Yau (CY) threefold.

The metric on the CY can be written as

$$\mathrm{d}(CY_3)^2 = \mathrm{d}r^2 + r^2 \mathrm{d}SE_5, \tag{6}$$

where SE_5 is a five dimensional Sasaki-Einstein manifold.

Because of the CY geometry, the theory on the world volume of branes is, in general, an $\mathcal{N} = 1$ gauge theory. On the other side of the duality, we have that the gravitational dual is given by Type IIB on $AdS_5 \times SE_5$.

Because of the holographic dictionary, theories engineered using D3-branes at the singular locus of CY threefold can be expected to be conformal, because of the AdS_5 factor in the gravitational theory. However, the isometry group of SE_5 is not $SO(6)$ any more and supersymmetry is reduced to $\mathcal{N} = 2$ or $\mathcal{N} = 1$, depending on the geometry of the CY.

The first examples of this kind of construction where 4d $\mathcal{N} = 2$ theories, where the number of supersymmetries highly constrains not only the field contents of the theory on the branes, but also possible interactions.

A simple example is to consider the geometry $CY_3 = \mathbb{C} \times \mathbb{C}^2/\mathbb{Z}_2$. This singularity is obtained as an orbifold of flat space via the action

$$(z_1, z_2, z_3) \to (z_1, -z_2, -z_3), \tag{7}$$

where z_i are the complex coordinates of the Calabi-Yau manifold.

This induces an action on the Chan-Paton factors of the open string sector, which allows us to compute the massless spectrum of the theory,

$$\begin{pmatrix} A_1 & 0 \\ 0 & A_2 \end{pmatrix}, \begin{pmatrix} 0 & X_{12} \\ X_{21} & 0 \end{pmatrix}, \begin{pmatrix} 0 & Y_{12} \\ Y_{21} & 0 \end{pmatrix}, \begin{pmatrix} Z_1 & 0 \\ 0 & Z_2 \end{pmatrix}. \tag{8}$$

Here the A_i represent the gauge fields of the gauge group $SU(N) \times SU(N)$, X_{ij} and Y_{ij} are bifundamental fields and the Z_i are adjoint fields. The adjoint scalars and the vectors combine into an $\mathcal{N} = 2$ vector multiplet, while the bifundamentals combine into hyper multiplets. Given the matter content and the number of supersymmetries, the lagrangian for this theory is fully determined. We can summarize the matter content and gauge group of the theory, in a graphical way, fig. 1.

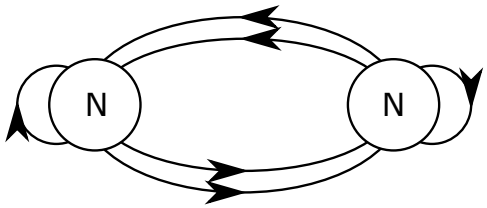

Figure 1: Quiver of $\mathbb{C}^2/\mathbb{Z}_2$.

This kind of oriented graph is called a quiver. To every node we associate a gauge group $SU(N)$, the number in the node gives the rank of the gauge group, and to every oriented arrow a bifundamental field, charged under the two gauge groups it is connecting. For general orbifold $\mathbb{C}^2/\Gamma$, where Γ is a discreet subgroup of $SU(2)$, the quivers are known to be related to the affine Dynkin diagram of the group Γ.

This result holds only for theories with $\mathcal{N} = 2$ supersymmetry. For a generic threefold, the theory on the branes' world volume is an $\mathcal{N} = 1$ gauge theory. For such theory, even if the quiver can be obtained by geometrical means, the superpotential cannot be uniquely determined.

Computing the full spectrum and interactions of 4d $\mathcal{N} = 1$ theories on D3-branes at Calabi-Yau singularities is a really hard problem that nowadays still doesn't have a complete answer. However, for a special class of geometries, known as toric, the corresponding field theory can be fully determined.

A toric threefold is a variety with an $U(1)^3$ isometry. The simplest examples of toric geometries are flat space orbifolds. Starting from this geometry, it is possible

to perform partial resolutions and obtain new varieties that will still be toric. We are interested in these geometries because we can easily compute the theory living on branes at the tip of an orbifold singularity. Once we obtain the field theory corresponding to flat space orbifold, partial resolutions are realized in field theory language via Higgsing specific fields. This provides a systematic way construct the field theory for any toric variety. This procedure allowed to construct an infinite number of 4d $\mathcal{N} = 1$ SCFT.

We do not give an example of how this procedure works, since we will provide much stronger tools to investigate the relation between geometry and field theory, namely dimer models, in section 2.

1.2 Fractional branes

Thanks to the rich geometrical struncture of Sasaki-Einstein manifolds, we can construct effective D3-branes by wrapping D5 and D7-branes on, respectively, 2 and 4 shrinking cycles of the toric Calabi-Yau. Shrinking cycles are cycles that, at the singularity of the Calabi-Yau, have zero volumes. Brane wrapped on them source an NS 2-form flux through the cycle, stabilizing it. The wrapped brane is now an effective D3-brane, with less degrees of freedom, since it is stuck at the tip of the singularity.

We focus on D5-branes wrapping 2-cycles whose dual 4-cycle is non compact. This allows to the flux sourced by the wrapped brane to escape at infinity, avoiding possible RR-tadpoles. These kind of branes have the remarkable property of breaking conformal invariance on the world volume theory. This is because, as we already mentioned, they are stuck at the singularity. This has the effect of setting to zero some modes on the branes, resulting on a reduced symmetry of the brane system. In order to understand this fact more clearly, let us look at the field theory description of these objects.

In the quiver framework, every node corresponds to an $SU(N)$ gauge group and every arrow to a bifundamental. Rank assignments that are free of chiral anomaly corresponds to fractional branes. If we consider again the theory obtained from the singularity $\mathbb{C}^2/\mathbb{Z}_2$, we see that there is such an assignment, fig. 2.

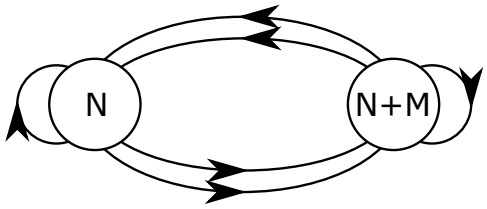

Figure 2: Quiver of $\mathbb{C}^2/\mathbb{Z}_2$ with a non anomalous rank assignment.

Upon computing the β-function of the model, we see that it is indeed non vanishing

$$\beta_{N+M} = 3(N+M) - \frac{1}{2}(4N + 2(N+M)) = 2M\,, \tag{9}$$

$$\beta_N = 3N - \frac{1}{2}(2N + 4(N+M)) = -2M\,. \tag{10}$$

As stated in [15], fractional branes can be classified according to the effects they have on the dynamics of the field theory. Their classification is as follows:

- $\mathcal{N} = 2$ branes

  Geometrically, they correspond to D5-branes wrapped on shrinking 2-cycles whose singular locus is a whole complex line inside the Calabi-Yau. An example is the $\mathbb{C}^2/\mathbb{Z}_2$ singularity previously discussed. In this case, the only shrinking cycle is free to move along the $\mathbb{C}$ line in the threefold at zero energy. This corresponds to give a VEV to the adjoint scalar in the vector multiplet. In this configuration, the theory on the world volume of the fractional brane is a 4d $\mathcal{N} = 2$ theory.

- Deformation branes

  In this case, the shrinking cycle has zero volume only at the tip of the Calabi-Yau. The presence of this kind of fractional branes triggers a cascade of Seiberg dualities in the field theory, as described in [16]. At the bottom of the cascade, these fractional branes causes some 3-cycles to develop a non vanishing volume, corresponding to a complex structure deformation in the geometry, thus the name "deformation branes". On the field theory side, at the bottom of the cascade the gauge groups confine, and the strong coupling scale is related to the volumes of the 3-cycles.

- DSB branes

  Any other kind of anomaly free rank assignment usually leads to a dynamically generated superpotential and hence breaks supersymmetry dynamically [17] (though into a runaway direction). These branes are called DSB fractional branes.

2 Dimer Models

Thanks to the development in the description of supersymmetric gauge theories from D-branes at CY singularities, a simple and powerful link was established between toric geometry and quiver gauge theories: Dimer Models.

This tool not only allowed faster and easier computations of field theory starting from toric diagrams, with respect to previous approaches, but also gave a new combinatiorial perspective to the theory, making more intuitive operations such has Higgsing, Seiberg duality as well as the addition of orientifolds.

In this section we delve into the origin and the formal aspects of dimer models, recalling know results and introducing new ones. All the tools we develop now will be used in the reminder of the thesis.

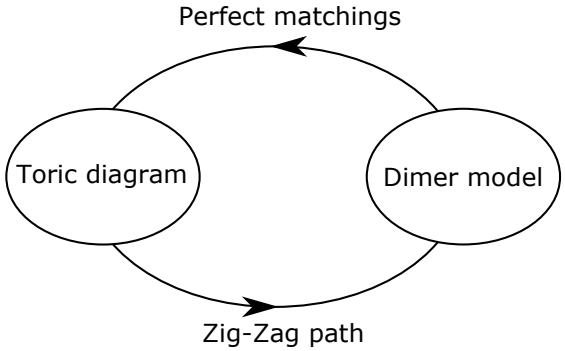

Figure 3: A picture representing the link between toric diagram, i.e. geometry, and dimer models, i.e. field theory. The link between the two is provided by ZZP and perfect matchings.

2.1 Brane tiling

In order to motivate the use of dimer models to study gauge theories on D3-branes at CY singularities, we start discussing systems of D5-branes and NS5-branes. In this context, the notion of bipartite graph, related to the concept of dimer model, arises naturally.

In the general setting, we have D5-branes in flat space which intersect NS5-branes along an holomorphic Riemann surface. Since it is hard to extract informations on the field theory living on the branes in this picture, we consider, instead, the strong coupling limit of this configuration, i.e. $g_s \to \infty$. In this limit, the D5-branes are parallel to the NS5-branes along 0123 directions, while along 45 we have that NS5-branes can either be parallel or perpendicular to the D5-branes, as depicted in table 1.

	0	1	2	3	4	5	6	7	8	9
N D5	×	×	×	×	×	×				
NS5	×	×	×	×	×		×			
NS5'	×	×	×	×		×		×		

Table 1: System of D5 branes and NS5. D5 and the NS5-branes are parallel along directions 0123. Along 4 we have D5 and NS5 parallel, NS5' are perpendicular, while along 5 the converse is true.

If we now take direction 4 and 5 to be compact, the bound states of D5-NS5-branes cut this torus into distinct regions. The regions are classified as follows: $(N, 0)$ are regions on which we have only N parallel D5-branes, $(N, \pm 1)$ are regions where both NS5 and D5 are parallel, respectively in the same or opposite orientation, see fig. 4 for an example.

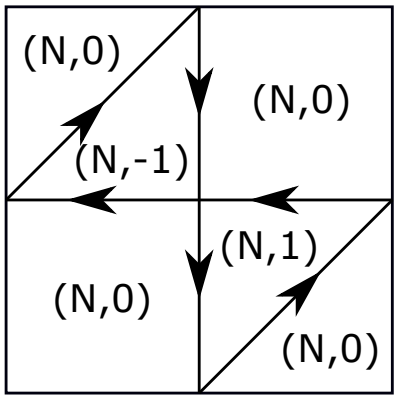

Figure 4: An example of tiling. The oriented lines represent the NS5 branes meeting the D5, the convention is that on the left of the arrow the NS5 is parallel to the D5, on the right antiparallel.

Since the bound state of branes is wrapping a torus, the net charge of the branes must be single valued, thus winding of both α and β cycles of the torus, taken with sign, must sum to zero. This imposes a topological constraint on the bound states. Given $a_\mu = (p_\mu, q_\mu)$, the vector whose components are winding numbers of branes on the torus, we have

$$\sum_\mu a_\mu = 0. \tag{11}$$

We now want to determine the gauge theory on the world volume of the D5-branes. It can be shown, [18], that the coupling of the gauge theory is proportional to the compactification radius, R, the string length, l_s, and the string coupling,

$$\lambda \propto \frac{R^4}{g_s l_s^2}. \tag{12}$$

We now consider the limit in which the radius of the torus and the string length vanish, $R, l_s \to 0$, keeping the gauge coupling fixed. In this limit, the theory can be read as follows: every $(N, 0)$ region gives a $SU(N)$ factor; points where two of such regions meet give rise to tensionless strings, producing bifundamental matter; every $(N, \pm 1)$ region gives a non-dynamical $SU(N)$ factor and can be interpreted as a tree-level disk amplitude corresponding to a superpotential term, whose sign depend on the charge of the D5-NS5 bound state, see for example fig. 5.

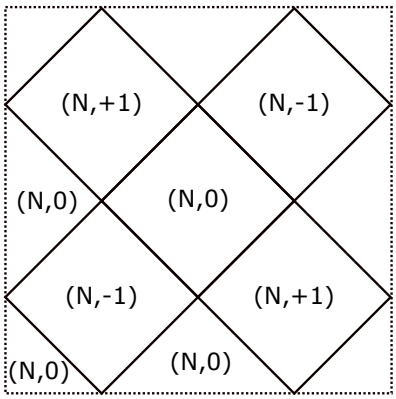

Figure 5: The solid lines are bound states of D5-NS5 and the dashed ones are the edges of the fundamental cell of the torus in directions 4-5.

Upon T-duality along the direction 4 and 5, the brane configuration becomes

	0	1	2	3	4	5	6	7	8	9
D3	×	×	×	×						
CY_3					-	-	-	-	-	-

Table 2: After T-duality, the system of D5-branes and NS5-branes becomes the desired configuration of D3-branes at the singularity of a CY threefold.

which is precisely the desired configuration of D3-branes probing the CY threefold. In particular, as we will see in the next section, the previous example is the complex cone over the zeroth Hirzebruch surface, F_0.

2.2 Bipartite graph

The previous picture gives us a hint on how to summarize the information of the brane tiling. We can associate to every $(N, \pm 1)$ region a vertex, colored with white for $+1$ and black for -1. Every $(N, 0)$ region is now a face, and the contacts points between different faces are edges. What we described just now is a bipartite graph.

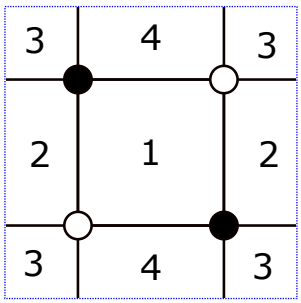

Figure 6: The bipartite graph corresponding to the tiling of fig. 5.

For a graph, being bipartite means that every edge starts on a vertex of one colour and end on one of the opposite colour. Since every edge is a bifundamental field and each vertex is a superpotential term, every field appears exactly twice in the superpotential with opposite sign

$$W = Y(X_1 \dots X_n) - Y(Z_1 \dots Z_m) + \dots \tag{13}$$

which ensures that the moduli space of the theory is toric. Indeed, a definition of toric variety is that the algebraic equations that define it are of the form "monomial=monomial". This is guaranteed by the structure of the superpotential.

Every vertex is at least three-valent. This is becasue a one-valent vertex has no sense, both from diagrammatical and the fivebrane point of view, and two-valent vertex corresponds to a mass term for some fields, which can be integratded out in the low energy limit.

Finally, the bipartite graph must be on a genus one surface in order for the theory to be conformal. Let us consider the β-function for every gauge factor

$$\beta_a = 2 + \sum_i (R_i - 1) = 0, \tag{14}$$

Brane Tiling	Quiver Gauge Theory
Face	$U(N_i)$ gauge factor
Edge between faces i and j	Chiral superfield in the bifundamental representation of groups i and j (adjoint representation if $i = j$). The chirality, i.e. orientation, of the bifundamental is such that it goes clockwise around black nodes and counter-clockwise around white nodes.
k-valent node	Superpotential term made of k chiral superfields. Its sign is $+/-$ for a white/black node, respectively.

Table 3: Dictionary relating brane tilings to quiver gauge theories.

where R_i is the R-charge of the fields, a runs over the number of gauge groups and i over the number of fields. Since every edge, i.e. a field, belongs to two faces, i.e. a gauge group, we have, summing all the β functions,

$$2F + 2\sum_i R_i - 2E, \tag{15}$$

and imposing that the R-charge of every superpotential term is exactly 2, we have

$$2F + 2V - 2E = 0. \tag{16}$$

This is nothing but the Euler identity, $F - E + V = 2g - 2$, telling us that the surface under consideration has genus one. There is only one orientable surface of genus one, which is, in fact, the torus[1].

For a complete proof of the correspondence between tilings and bipartite graphs, and in particular dimer models, see [19].

2.3 Dimer models

Despite being able to create a dictionary between bipartite graphs and field theory, table 3, we still need a way to connect the probed geometry with the graph. To solve these questions we introduce *dimer models*.

Given a bipartite graph we can define a perfect matching. This is a collection of edges such that no two edges share a vertex and every vertex is touched by one of these selected edges.

The collection of all perfect matchings of a graph is called Dimer Model.

[1]The non orientable one, the Klein Bottle, will be explored in section 5.

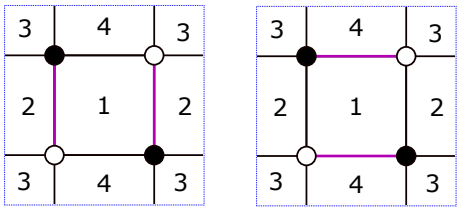

Figure 7: In purple, two possible choice of perfect matchings.

This object has been extensively studied in statistical physics and we can borrow some of these results, see [20] for an introduction, to help us in understanding how dimer models are related to the probed geometry.

It is possible to define the partition function of the dimer model. This is obtained summing over all perfect matchings, weighted by the number of times, with orientation, that perfect matchings intersects the fundamental cell. This is just the determinant of the Kasteleyn matrix of the dimer model, for detail see [21].

The partition function can be cast in the following form

$$P(x,y) = \sum_{i,j} c_i j x^i y^j, \tag{17}$$

where x, y are the weight of the perfect matchings in the dimer and the coefficients $c_{i,j}$ count the number of perfect matchings of weight (i,j). The Newton Polygon associated to the polynomial $P(x,y)$ is nothing but the toric diagram of the CY singularity producing the dimer model.

In fig. 7 there is example of two perfect matchings of height zero. It is easy to compute all the others and their weights. This leads to the polynomial

$$P(x,y) = x^{-1} + y^{-1} + x + y + 4, \tag{18}$$

and the associated Newton Polygon gives the toric diagram of the cone over F_0, the toric CY corresponding to the dimer model, see fig. 8.

This analysis allows us to go from the bipartite graphs to the geometry. To complete the picture given in fig. 3, we need a way to construct a dimer model starting from a toric diagram. To this end we introduce a new tool: the Zig-Zag path.

Given two external consecutive points on the perimeter of the toric diagram, we can compute the formal difference between the corresponding perfect matchings.

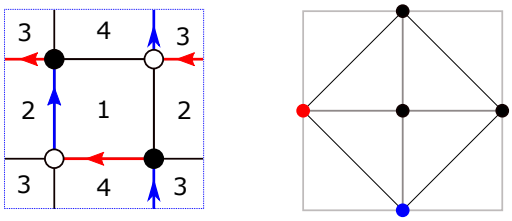

Figure 8: On the left the dimer model with coloured perfect matching corresponding to the colored vertices on the toric diagram, on the right

This gives a loop in the graph with winding number given precisely by $(b_2 - b_1, a_1 - a_2)$, where a_i, b_i are the coordinates of the two vertices of the toric diagram. This loop is called a Zig-Zag path (ZZP). These objects allow to construct the dimer model given a toric diagram.

To do so, we need to associate to every external edge in the toric diagram the corresponding ZZP. Then we must follow Thurston's triple crossings procedure, described in [22], in order to get a consistent graph. Eventually, we end up with a graph that is said to be non minimal, meaning that there are some two-valent nodes. Upon integrating out the massive fields, we end up with the desired dimer model.

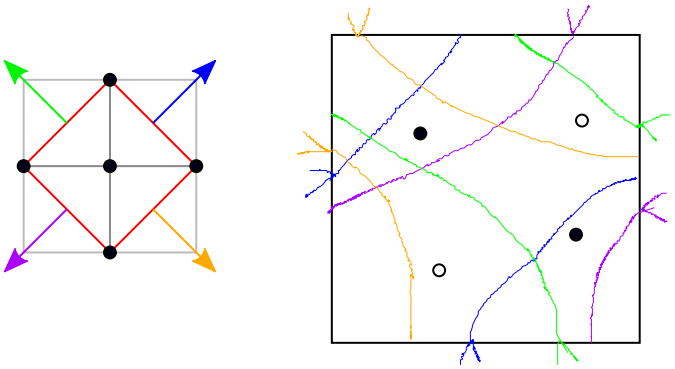

Figure 9: On the left the ZZP associated to the edges of the toric diagram. On the right we draw the ZZP on the fundamental cell, this reproduces the brane tiling, as the ZZP reproduce the NS5 branes intersection pattern.

This procedure, described for the first time in [23], allows to construct dimer models from a toric diagram, but the result it is not unique. Indeed, the dimer produced by this algorithm is unique up to Seiberg duality.

2.4 Branes constructions with dimers

In this section we show how to use the tool we introduced previously, i.e. dimer models, to study field theories engineered within toric geometries. Our focus will be mostly on fractional branes and orientifolds.

2.4.1 Fractional branes

As we already mentioned, there exist three classes of fractional branes, which differ by the IR dynamics they trigger: confinement, effective $\mathcal{N} = 2$ SYM or supersymmetry breaking. The existence of fractional branes, and their nature, can be argued directly from the dimer, as summarized below.

- Deformation branes:

  These branes correspond to isolated faces in the dimer touching each other at nodes (so, only gauge groups and no bifundamental fields are involved) or to isolated clusters of faces surrounding a given node. The gauge theory is then either a set of decoupled SYM theories, or SYM theories coupled via a superpotential term, respectively. In both cases, the low energy effective theory leads to confinement and the geometry undergoes a complex structure deformation.

  Two examples of deformation branes are reported in figure 10.

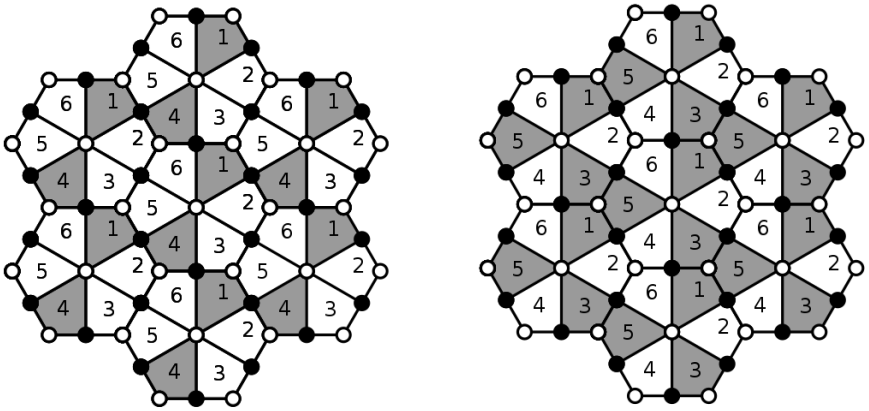

Figure 10: The dimer of the $dP3$ singularity, which admits both classes of deformation branes. Left figure: deformation fractional branes corresponding to isolated nodes. Right figure: deformation fractional branes corresponding to loops in the quiver.

- $\mathcal{N} = 2$ branes

  These other fractional branes correspond to paths along faces keeping, in our conventions, white nodes on the left and going across the unit cell without making any closed loop. This implies that the gauge invariant operator constructed along the closed path does not appear in the superpotential. The VEV of such operator is unconstrained and parametrizes a one-dimensional moduli space, along which the dynamics has $\mathcal{N} = 2$ supersymmetry.

  A simple such example is shown in figure 11.

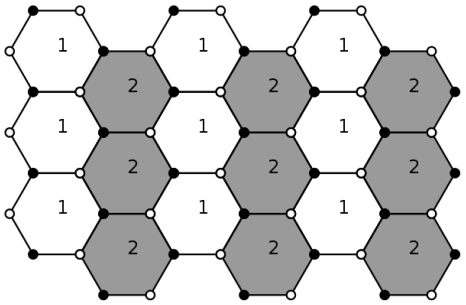

Figure 11: The dimer of the $\mathbb{C}^2/\mathbb{Z}_2 \times \mathbb{C}$ singularity with its $\mathcal{N} = 2$ fractional branes.

- DSB branes

  Any other kind of anomaly free rank assignment leads to DSB fractional branes. In thi case there is no general pattern to recognize them in the dimer.

Dimer techniques allow the easy construction of these fractional branes. To this end we now review a method for finding anomaly-free rank assignments on the dimers based on ZZPs [24].

We can regard every ZZP as defining an "anomaly-free wall" on the dimer. This is because, due to its definition, every time a ZZP overlaps with a face in the dimer, it does so over exactly a pair of consecutive edges.[2] These two consecutive edges correspond to an incoming and an outgoing arrow in the quiver for the gauge group associated to the face under consideration.[3] This implies that if we add some constant to the ranks of all the faces on one side of the ZZP, the anomaly cancellation condition (ACC) of the gauge group associated to the faces on the other side of the ZZP does not change, as illustrated in Figure 12.

[2]By overlapping with a face, we mean sharing an edge with it, not just touching it at a node.

[3]More generally, a ZZP might overlap with a given face more than once. Every overlap involves a pair of consecutive edges, so the previous discussion still applies.

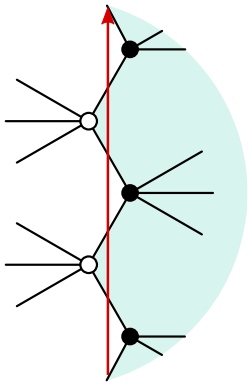

Figure 12: A ZZP as an anomaly wall. If all the ranks on the faces on the right of the ZZP are increased by a constant, the ACC is not modified. This is because all contributions from the edges along the ZZP are equal and with opposite sign.

With this insight, one recovers the algorithm to construct anomaly-free rank assignments for dimer models outlined in [24]:

1. The set of ZZPs is given by $\{(p_\Gamma, q_\Gamma)|\Gamma = 1, \ldots, n\}$, where p_Γ and q_Γ are the winding numbers of the ZZP Γ, with respect to a fixed unit cell. To every (p_Γ, q_Γ) assign an integer coefficient v_Γ.

2. Choose one face and assign rank zero to it.

3. In going from face a to an adjacent face b, the rank of the latter will be

$$N_b = N_a + v_\Gamma - v_\Delta \,, \tag{19}$$

   where v_Γ is the coefficient of the ZZP moving to the left with respect to the path from a to b, and v_Δ is the one in the opposite direction. This operation is well defined since we are working on an oriented surface, which implies that we can consistently speak of "right" and "left" of a ZPP.

4. Finally, one must impose two constraints which ensure that the rank assignment is single valued. Consider, for instance, moving along a loop along one of the two cycles of the fundamental cell. When returning to the initial face, the rank should be unchanged. This is granted by imposing

$$\Lambda = \sum_\Gamma v_\Gamma p_\Gamma = 0, \quad M = \sum_\Gamma v_\Gamma q_\Gamma = 0 \,. \tag{20}$$

   We will refer to these two conditions as the Λ and M *topological constraints*.

Every choice of values for the v_Γ's consistent with the topological constraints eq. (20) gives rise to an anomaly-free rank assignment. Moreover, notice that, by construction, every rank assignment is invariant under a global shift $v_\Gamma \to v_\Gamma + k$. One may use this freedom to fix one of the v_Γ's (equivalently, one of the ZZPs is not independent). There are thus two constraints and one redundancy to be fixed, giving a total of

$$\#\text{ZZPs} - 3 = \#\text{Fractional Branes} \,. \tag{21}$$

This kind of analysis will prove to be useful in the reminder of the thesis, where we will apply it to the case of orientifolded singularities.

2.4.2 Orientifold in dimer

We now discuss orienfitolding in the framework of D3-branes at CY singularities and, in particular, how this operation is realized in the framework of dimer models.

This operation, from the brane picrture, is defined by modding out the spectrum of the theory by $\Omega\mathcal{R}(-1)^{F_L}$, where Ω is the world sheet parity, $\mathcal{R}$ is a geometric $\mathbb{Z}_2$ isometry of the CY_3 and F_L the left-moving fermion number in spacetime. Extended objects are located at the fixed point of the R action and are called O-planes or orientifolds. They are non-dynamical objects which, however, have tension and an RR charge as D-branes do. The $\mathbb{Z}_2$ symmetry acts holomorphically on the internal coordinates. This translates to an action on the Kähler form J and the holomorphic 3-form Ω_3, that defines the CY, as follows

$$J \to J \quad \text{and} \quad \Omega_3 \to -\Omega_3 \,, \tag{22}$$

where the $-$ sign is necessary in order for the O-plane to preserve some common supercharges with the D3-branes. The resulting gauge theory is obtained by looking at the projected open string spectrum. The orientifold projection on Chan-Paton factors is essentially free. If we denote by λ the Chan-Paton matrix, the orientifold acts with a unitary matrix γ_Ω:

$$\Omega : \lambda \to \gamma_\Omega \lambda^T \gamma_\Omega^{-1} \,. \tag{23}$$

Orientifold projections on D-branes at singularities and their description on dimers were studied in [25]. In this framework, the orientifold projection corresponds to a $\mathbb{Z}_2$ involution acting on the torus that identifies faces, edges and vertices in an appropriate way. The authors studied involutions with fixed loci (see Figure 13 for examples) resulting in a set of rules needed to construct the projected theory that we now summarize.

Figure 13: (a) Orientifold of $\mathbb{C}^2/\mathbb{Z}_2$ with fixed points. (b) Orientifold of $\mathbb{C}^2/\mathbb{Z}_2$ with fixed lines.

1. Self-identified faces project to SO/USp groups, depending on the O-plane charge, $+$ or $-$ respectively. All other faces are identified with their image, merging to one SU group.

2. Every edge on top of a fixed locus becomes a symmetric or antisymmetric tensor (or their conjugate), depending on the O-plane charge, $+$ or $-$ respectively. The remaining edges are identified with their images, merging to bifundamental fields. More concretely, bifundamentals are identified as $(\,\overline{\square}_{\,i},\ \square_{\,j}) \sim (\,\overline{\square}_{\,j'},\ \square_{\,i'}) \to (\,\overline{\square}_{\,i},\ \square_{\,j})$, where i', j' are the images of gauge groups i, j.

3. The superpotential is found upon projection of the fields.

The introduction of orientifold planes is crucial for model building purposes, and in particular for DSB models.

Not only orientifold, as fractional branes, break, in general, conformal invariance, but also the projected theory admits different gauge groups from the unitary one, namely symmetric and symplectic, and field in different representations, such has symmetric and antisymmeric.

Orientifold projections will be heavily studied and generalized in the second part of this thesis, while on the third one they will be used to build DSB model in the context of Gauge/Gravity duality.

Before dealing with new results, and in order to get familiar with orientifolds in dimer models, we present in detail two examples of orientifold projections.

Fixed Points. In an orientifold of this type, there are four fixed points in a unit cell. In order to preserve supersymmetry, their signs must satisfy the so-called *sign*

rule: their product must be $(-1)^{n_W/2}$ where n_W is the number of superpotential terms.

In the example of Figure 13a, we chose the signs $(-+-+)$, starting with the fixed point at the origin of the unit cell and going clockwise. Face 1 is identified with face 2, meaning that the resulting theory will have only one gauge group $SU(N)$. The bifundamental fields are identified as follows

$$\begin{gathered} Y_{12} \sim Y_{12} \to \overline{\square}\,\square \;,\; X_{21} \sim X_{21} \to \square\square \\ Y_{21} \sim Y_{21} \to \square\,\overline{\square} \;,\; X_{12} \sim X_{12} \to \overline{\square\square} \\ Z_{11} \sim Z_{22} \to \text{Adj}\,. \end{gathered}$$

and the superpotential is given by

$$W = X_{12}Y_{21}Z_{11} - X_{21}Y_{12}Z_{11}\,, \tag{24}$$

where we implicitly take a trace over gauge indices.

To be sure that this projection preserves some supersymmetry, we need to check the action of the involution on Ω_3. To do so, we compute the mesonic moduli space of the theory, which correspond to the singularity D3-branes are probing. Mesonic operators are given by

$$\begin{array}{rclcrcl} x & = & X_{12}X_{21}\,, & y & = & Y_{12}Y_{21}\,, \\ w_1 & = & Y_{12}X_{21}\,, & w_2 & = & Y_{21}X_{12}\,, \\ z_1 & = & Z_{11}\,, & z_2 & = & Z_{22}\,. \end{array} \tag{25}$$

F-term equations impose $w_1 = w_2 = w$ and $z_1 = z_2 = z$, and the classical relation between the fields gives $xy = w_1w_2 = w^2$. Thus, the mesonic moduli space is the symmetric product of N copies of the A_1 singularity, $xy = w^2$, where N is the number of probe D3-branes. The three form, Ω_3, can be easily computed using the Poincaré residue formula:

$$\Omega_3 = \text{Res}\frac{\mathrm{d}x \wedge \mathrm{d}y \wedge \mathrm{d}w \wedge \mathrm{d}z}{w^2 - xy} = \frac{\mathrm{d}x \wedge \mathrm{d}y \wedge \mathrm{d}z}{2w}\,. \tag{26}$$

Under the involution, the fields are mapped in the following way

$$\begin{gathered} x \to x\,, \quad y \to y\,, \\ w \to -w\,, \quad z \to z\,, \end{gathered}$$

where the sign taken by a meson is given by the product of the fixed point charges it crosses. The orientifold action on the holomorphic 3-form is thus odd, $\Omega_3 \to -\Omega_3$, meaning that the O-plane in compatible with the supersymmetry charges preserved by the D3-branes. It is easy to see that sign configurations not respecting the sign rule are not supersymmetric.

Fixed Lines. In the example of Figure 13b, we have two fixed lines, each one coming with a sign, + or −, which is now unconstrained. We chose to assign − to the bottom line and + to the other. The faces are self-identified, leading to a gauge group $USp(N_1) \times SO(N_2)$. The identification of fields gives

$$\begin{aligned} Y_{12} \sim X_{21} \to Q^1_{12} \ , \quad & X_{12} \sim Y_{21} \to Q^2_{12} \\ Z_{11} \sim Z_{11} \to \ \square\!\!\square \ , \quad & Z_{22} \sim Z_{22} \to \ \square\square \ . \end{aligned} \tag{27}$$

and the superpotential is given by

$$W = (Q^2_{12} Q^{2T}_{12} - Q^1_{12} Q^{1T}_{12}) Z_{11} + (Q^{2T}_{12} Q^2_{12} - Q^{1T}_{12} Q^1_{12}) Z_{22} \, . \tag{28}$$

The mesons are the same as in the previous example, since the geometry is the same, but the action of the orientifold is different and given by

$$\begin{gathered} x \leftrightarrow y \, , \\ w \to -w \, , \quad z \to -z \, , \end{gathered}$$

where the fixed line exchanges two mesons and introduces a sign to the self-mapped mesons given by the product of the signs of the two fixed lines crossed. We can again see that the SUSY condition is respected

$$\Omega_3 = \frac{\mathrm{d}x \wedge \mathrm{d}y \wedge \mathrm{d}z}{2w} \to \frac{\mathrm{d}y \wedge \mathrm{d}x \wedge \mathrm{d}z}{2w} = -\Omega_3 \, . \tag{29}$$

In particular, we see that the signs of the fixed lines play no role in the last relation.

3 Dynamical Supersymmetry Breaking

We now briefly revise some models displaying DSB vacua that will play a central role in the last part of the thesis.

As all symmetries, supersymmetry can be broken by various means. The most interesting one is when supersymmetry is broken spontaneously by the strong coupling dynamics of the theory.

It is a well known fact, [26], that the tree level superpotential of supersymmetric gauge theories in 4d is quantum exact at the perturbative level, meaning that it does not get renotmalized by contribution coming from perturbative dynamics.

If we do not what to break supersymmetry explicitly, namely via the tree level superpotential, we need to consider non-perturbative contributions.

In [17], thanks to supersymmetry, such contributions to the superpotential were computed exactly. In particular, one of the effects of the condensation of gauge groups is to produce a non-perturbative superpotential term, called the Affleck-Dine-Seiberg (ADS) superpotential.

This superpotential usually leads to a runaway vacuum, meaning that the minimum of the potential is reached at infinity in the moduli space of the theory. However, the combination of tree level terms and the ADS one can lead to a stable, non zero, minimum of the potential, meaning that the theory sits in a non zero energy vacuum, effectively breaking supersymmetry.

In order to better understand this effect, let us go through two examples, the so called 3-2 models and $SU(5)$.

- **3-2**

  This is an $SU(3) \times SU(2)$ $\mathcal{N} = 1$ gauge theory with matter content given by

  $$Q = (\square_3, \overline{\square}_2) \ , \ \overline{U} = \overline{\square}_3 \ , \ \overline{D} = \overline{\square}_3 \ , \ L = \square_2 \, , \tag{30}$$

  where $\square_i$ is the fundamental representation under gauge group i, and $\overline{\square}_i$ is the antifundamental.

  The theory also has a tree level superpotential

  $$W = \lambda \overline{D} Q L \ , \tag{31}$$

  where λ is a coupling constant.

  The minimum of the theory can be ground by imposing D and F-term equations. The space of D-flat directions is parametrized by

  $$X_1 = Q\overline{D}L \, , \, X_2 = Q\overline{U}L \, , \, Y = \det(Q\overline{U}Q\overline{D}) \, . \tag{32}$$

This space is modified by the F-term equations. For L, the F-term equation is

$$\frac{\partial W}{\partial L} = \lambda \overline{D} Q = 0 \ , \tag{33}$$

contracting with L and $Q\overline{U}$, the previous equation implies that $X_2 = Y = 0$, as VEVs in the moduli space. Imposing the F-term equation for $\overline{D}$ and contracting with $\overline{U}$ sets $X_1 = 0$ as well. This classical anlysis shows that the theory admits a supersymmetric vacuum at the origin of the moduli space.

We now have to consider the low energy regime, where the $SU(3)$ or the $SU(2)$ factors could condense, given the number of flavours and colours.

Let us consider the regime in which $SU(3)$ condenses. In this case a non-perturbative ADS superpotential is generated

$$W_{non-pert} = \frac{\Lambda_3^7}{Y} \, . \tag{34}$$

This extra term allows the system to break supersymmetry dynamically.

In fact, it is easy to see that, in term of low energy degrees of freedom, there is no solution to the F-term equations, once the non-perturbative contribution is taken into account

$$W_{eff} = \lambda X_2 + \frac{\Lambda_3^7}{Y} \, . \tag{35}$$

Hence supersymmetry is broken.

The analysis can be repeated for a regime in which is the $SU(2)$ factor who condenses first, as well as when both reach strong coupling at comparable energies, leading to one and the same result, namely supersymmetry is broken.

- **SU(5)**

  This is an $SU(5)$ $\mathcal{N} = 1$ gauge theory with matter content given by

  $$A = \begin{array}{|c|}\hline \ \ \\ \hline \ \ \\ \hline \end{array} \ , \ \ \overline{Q} = \begin{array}{|c|}\hline \ \ \\ \hline \end{array} \, , \tag{36}$$

  without superpotential.

  No gauge invariant operator can be constructed and no D-flat direction hence is present. At the origin of the moduli space, where the gauge group is unbroken, there is a supersymmetric vacuum and the theory most likely confines.

Even if it is really hard to perform any reliable computation, we can infer that supersymmetry is broken at low energies.

A sufficient condition for supersymmetry breaking is that a theory, with no classical flat directions, has a broken global symmetry. The UV theory has two global non-anomalous $U(1)$ symmetries, under which the fields have charge $A = (-1, 1)$ and $\overline{Q} = (3, -9)$, imposed by the cancellation of chiral anomalies. Once the theory undergoes confinement, the low energy degrees of freedom should reproduce the 't Hooft anomalies of the UV theory. To achieve this the number of fields is at least five, with rather bizarre charges, if we ask for charges smaller then ≈ 50. This rather peculiar charge assignment can be interpreted as the actual impossibility of matching the anomalies of the IR and UV theory, leading to the conclusion that the global symmetry should be broken.

If the global $U(1)$ symmetry is broken, we have a theory without classical flat directions and with a broken global symmetry, which, as said, is a sufficient condition for supersymmetry breaking.

We will show, in the following of this thesis, that these two models are the simplest that can be engineered in the context of branes at orientifolded Calabi-Yau singularities. Moreover, some of their variants will play a crucial role in the quest of constructing stable DSB models using D-branes.

Part II
Orientifolds in Dimer Models: general aspects

4 Anomaly Cancellation Conditions in Orientifolds

In this section we investigate the relation between geometry and anomalies. In particular we study the ACC of orientifolded theories in the absence of flavour branes, providing and algorithmical approach that allows to link them with the ZZP of the dimer model of the theory at hand.

Our result permits to discriminate whether an orientifold projection will be anomalous, or not, looking directly at the geometry of the singularity under consideration, without going through the, sometimes, painful task of finding the corresponding dimer model.

As we will see in next sections, this result will prove to be useful in model building scenarios, giving severe constraints on which singularities can be consistently orientifolded without the need of flavour branes.

4.1 Systematic approach to anomalies

Determining whether an orientifolded theory admits anomaly-free solutions and, if so, finding them is a relatively straightforward task in a case by case basis. Indeed, writing down the set of anomaly equations for every gauge group and looking for solutions is not more complicated than for non-orientifolded models. In this section we systematize this calculation, introducing an algorithm for finding anomaly-free solutions in the presence of orientifolds. This, in turn, will allow us to relate the calculation to the one in the unorientifolded theory and, at a later stage, to extend the geometric determination of solutions in terms of zig-zag paths to orientifolds.

In what follows, we will refer to the original, unorientifolded theory as the *mother theory*. Similarly, we will dub the orientifolded theory the *daughter theory*. We also define the matrix $\tilde{A}_{IJ}$, whose entry are the number of bifundamental, i.e. edges, which are antifundamental with respect to I and fundamental with respect to J. It's antisymmetric part, which we dub as the *adjacency matrix*, corresponds to the ACC of the gauge groups. Finding anomaly-free rank assignment amounts to find the kernel of the adjacency matrix. When considering the daughter theory, tensor matter modifies the ACC, dovetailing the contribution of the O-planes to the RR-charges that must cancel in compact homology. In general, the anomaly/tadpole problem of orientifolded theories corresponds to a

non-homogeneous linear system of the form:

$$\bar{A} \cdot N = f \,, \tag{37}$$

where $\bar{A}$ is the adjacency matrix of the daughter theory, and f stands for the additional contribution of tensor matter. The difference between two solutions of the system eq. (37) is a solution of the corresponding homogeneous one, i.e. it is in the kernel of $\bar{A}$. If one knows a particular solution N_{part} of eq. (37), every solution N can be expressed as:

$$N = N_{\text{hom}} + N_{\text{part}} \,, \tag{38}$$

where N_{hom} is a solution of the homogeneous system $\bar{A} \cdot N_{\,\text{hom}} = 0$.

Remarkably, we will show that whether eq. (37) has solutions or not can be directly determined from the toric diagram of the singularity under consideration. In other words, we will establish a geometric criterion for the satisfiability of the ACC in orientifolded theories.

4.1.1 The Adjacency Matrix of Orientifolded Theories

Consider a toric singularity and a corresponding dimer admitting a $\mathbb{Z}_2$ involution. We can divide the n_g gauge groups of the mother theory into two sets: pairs of faces identified under the involution, and self-identified ones. Therefore, the adjacency matrix of the mother theory, A_{IJ} with $I, J = 1, \ldots, n_g$, can be suitably rearranged as follows:

$$A = \left(\begin{array}{c|c|c} B_{11} & B_{12} & B_{13} \\ \hline B_{21} & B_{22} & B_{23} \\ \hline B_{31} & B_{32} & B_{33} \end{array}\right) \begin{array}{l} \Big\} i \\ \Big\} i+k \\ \Big\} a \end{array} \quad . \tag{39}$$

$$\underbrace{\phantom{B_{11}}}_{j} \quad \underbrace{\phantom{B_{12}}}_{j+k} \quad \underbrace{\phantom{B_{13}}}_{b}$$

Here faces $i, j = 1, \ldots, k$ are the surviving ones out of those in the pairs of faces that are mapped into each other (for every pair, we are free to keep any of the two faces). Faces $i + k, j + k$, with $i, j = 1, \ldots, k$, are their images. Finally, the remaining faces $a, b = 1, \ldots, n_g - 2k$ are those that are self-identified. The B matrices are the adjacency matrices between these different subsets. For example,

B_{13} is the adjacency matrix between surviving faces and self-identified faces, while B_{23} is the adjacency matrix between the image faces and the self-identified ones. The matrix A is by definition antisymmetric, which in terms of the submatrices B implies that

$$\begin{aligned} B_{11} &= -B_{11}^T\,, \quad B_{22} = -B_{22}^T\,, \quad B_{33} = -B_{33}^T\,, \\ B_{12} &= -B_{21}^T\,, \quad B_{13} = -B_{31}^T\,, \quad B_{23} = -B_{32}^T\,. \end{aligned} \tag{40}$$

The $\mathbb{Z}_2$ symmetry of the phase under consideration endows it with further symmetry properties. The $\mathbb{Z}_2$ projection acts on the bifundamental fields as follows:

$$\begin{array}{ccc} \text{Mother theory} & & \text{Daughter theory} \\ (\overline{\square}_i, \square_j),\, (\overline{\square}_{j+k}, \square_{i+k}) & \to & (\overline{\square}_i, \square_j) \\ (\overline{\square}_i, \square_{j+k}),\, (\overline{\square}_j, \square_{i+k}) & \to & (\overline{\square}_i, \overline{\square}_j) \\ (\overline{\square}_{i+k}, \square_j),\, (\overline{\square}_{j+k}, \square_i) & \to & (\square_i, \square_j) \\ (\overline{\square}_a, \square_i),\, (\overline{\square}_{i+k}, \square_a) & \to & (\square_a, \square_i) \\ (\overline{\square}_i, \square_a),\, (\overline{\square}_a, \square_{i+k}) & \to & (\square_a, \overline{\square}_i) \\ (\overline{\square}_a, \square_b),\, (\overline{\square}_b, \square_a) & \to & (\square_a, \square_b) \end{array} \quad . \tag{41}$$

These projections imply that:

$$\begin{aligned} B_{11} &= B_{22}^T\,, \quad B_{12} = B_{12}^T\,, \quad B_{21} = B_{21}^T\,, \\ B_{31} &= B_{23}^T\,, \quad B_{13} = B_{32}^T, \quad B_{33} = B_{33}^T\,. \end{aligned} \tag{42}$$

We can apply eqs. (40) and (42) together to find further relations between the B's,

$$\begin{aligned} B_{11} &= -B_{22}\,, \quad B_{12} = -B_{21}\,, \\ B_{13} &= -B_{23}\,, \quad B_{31} = -B_{32}\,, \quad B_{33} = 0\,, \end{aligned} \tag{43}$$

so that eventually the adjacency matrix is entirely determined by B_{11}, B_{12} and B_{13}:

$$A = \begin{pmatrix} B_{11} & B_{12} & B_{13} \\ -B_{12} & -B_{11} & -B_{13} \\ -B_{13}^T & B_{13}^T & 0 \end{pmatrix}\,. \tag{44}$$

In order to illustrate these relations, let us consider the complex cone over PdP_{3b}, as studied in [1]. The dimer, which is shown in fig. 14, admits a $\mathbb{Z}_2$ symmetry with two fixed lines. The numbering of the faces has already been chosen such that the adjacency matrix reads

$$A = \left(\begin{array}{cc|cc|cc} 0 & 1 & -1 & 0 & 1 & -1 \\ -1 & 0 & 0 & 1 & 1 & -1 \\ \hline 1 & 0 & 0 & -1 & -1 & 1 \\ 0 & -1 & 1 & 0 & -1 & 1 \\ \hline -1 & -1 & 1 & 1 & 0 & 0 \\ 1 & 1 & -1 & -1 & 0 & 0 \end{array}\right)\,, \tag{45}$$

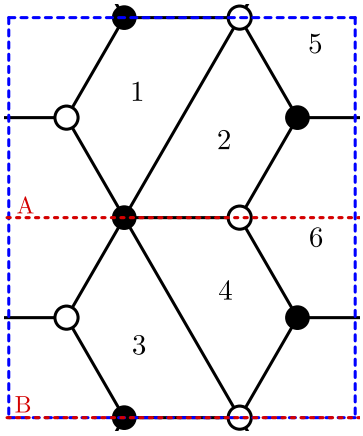

Figure 14: Dimer diagram for $PdP3_b$ with two horizontal fixed lines (dotted red).

which showcases the general structure in eqs. (40), (42) and (43).

Let us now turn our attention to the daughter theory. To compute the ACC for the orientifolded theory we first note that SO/USp groups are automatically anomaly-free and play no role. Further, for the ACC of the non-self-identified faces we have to take into account both the contributions from fields such as $(\overline{\square}_i, \square_j)$, that are counted by B_{11}, and fields such as $(\square_i, \square_j)$ and $(\overline{\square}_i, \overline{\square}_j)$ that are counted by B_{12}, see eq. (41). This leads to the homogeneous ACC for the projected theory given by

$$\overline{A} = \left(\begin{array}{c|c} B_{11} + B_{12} & B_{13} \end{array} \right) . \tag{46}$$

Applying this to the PdP_{3b} example we get

$$\overline{A} = \left(\begin{array}{cc|cc} -1 & 1 & 1 & -1 \\ -1 & 1 & 1 & -1 \end{array} \right) . \tag{47}$$

4.1.2 The Homogeneous Problem

In the previous section, we have constructed the homogeneous part of the ACC for an orientifolded theory. We now show how solutions to the homogeneous problem, namely elements of $\ker(\overline{A})$, are obtained from symmetric rank assignments of the mother theory, which form a subspace of $\ker(A)$. This will allow us to extend the method explained in section 2.4.1 to the homogeneous problem of orientifolded theories.

We say that a rank assignment of the mother theory N_I^S is symmetric with

respect to the $\mathbb{Z}_2$ involution if it satisfies

$$N_i^S = N_{i+k}^S\,, \quad N_a^S \ \text{free}\,. \tag{48}$$

If this rank assignment is anomaly-free in the mother theory (i.e. if it is in the kernel of A), we have

$$A_{IJ}N_J^S = 0\,, \tag{49}$$

where here and henceforth, summation over repeated indices is understood.

Expanding this equation in terms of the B matrices and exploiting the symmetry properties given in eq. (48), it becomes

$$\begin{aligned}(B_{11}+B_{12})_{ij}N_j^S + (B_{13})_{ia}N_a^S &= 0\,,\\ (B_{21}+B_{22})_{ij}N_j^S + (B_{23})_{ia}N_a^S &= 0\,,\\ (B_{31}+B_{32})_{aj}N_j^S + (B_{33})_{ab}N_b^S &= 0\,.\end{aligned} \tag{50}$$

From eq. (43), we conclude that the first two equations are actually one and the same, while the third equation is trivially satisfied for any symmetric rank assignment. From the first two equations we learn that any symmetric rank assignment N_I^S in the mother theory which satisfies the ACC, defines a solution of the homogenous ACC system of the daughter theory given in eq. (37):

$$N_{\text{hom}} = (N_i^S|N_a^S)\,. \tag{51}$$

Equation (50) indeed implies that such a vector satisfies:

$$\overline{A}\cdot N_{\text{hom}} = 0\,. \tag{52}$$

Conversely, if one starts with a vector $(N_i^S|N_a^S)$ satisfying eq. (52), the vector $(N_i^S|N_{i+k}^S|N_a^S)$ is a symmetric rank assignment of the mother theory. The definition of $\overline{A}$ in eq. (46) implies that the equations in eq. (50) hold for $(N_i^S|N_{i+k}^S|N_a^S)$, i.e. that the latter satisfies the ACC of the mother theory. Hence, we have proved the following:

> Rank assignments in the daughter theory which satisfy the homogeneous ACC are in one-to-one correspondence with symmetric rank assignments in the mother theory which satisfy the ACC.

In the special case where tensors are absent from the daughter theory, the ACC are actually a homogeneous problem and the symmetric rank assignments in the mother theory provide directly the orientifold solutions. The regular brane is such a solution that always exists, and thus guarantees that an orientifold without tensors always admits a non-anomalous solution.

4.1.3 The Non-Homogeneous Problem

Finding solutions to the ACC in orientifolded theories with tensors is not trivial because their very existence is not guaranteed, since the full system of ACC given in eq. (37) has a non-homogeneous part coming from the tensor matter. The Rouché-Capelli theorem gives us a criterion for its solvability: a non-homogeneous system,

$$\bar{A} \cdot N = f \,, \tag{53}$$

admits a solution if and only if

$$\text{rank}(\bar{A}) = \text{rank}(\bar{A}|f) \,, \tag{54}$$

where $(\bar{A}|f)$ is the matrix obtained appending the column f to the matrix $\bar{A}$. For us f encodes the contribution to the ACC of the tensor matter, i.e. of the self-identified chiral fields.

In other words, every set of numbers r_i such that

$$r_i \bar{A}_{i\bar{J}} = 0 \tag{55}$$

holds for all $\bar{J} = j, a$, must satisfy

$$r_i f_i = 0 \tag{56}$$

for the system to be solvable. In this section we show that the coefficients r_i which satisfy eq. (55) correspond precisely to the antisymmetric rank assignments of the mother theory.

Suppose that some coefficients r_i satisfying eq. (55) exist. Using eq. (43) for $\bar{J} = j$, one can show that it implies

$$r_i (B_{11})_{ij} - r_i (B_{21})_{ij} = 0 \,. \tag{57}$$

Using eq. (43), this is equivalent to

$$r_i (B_{12})_{ij} - r_i (B_{22})_{ij} = 0 \,. \tag{58}$$

For $\bar{J} = a$, using eq. (43), we find that

$$r_i (B_{13})_{ia} - r_i (B_{23})_{ia} = 0 \,. \tag{59}$$

We write

$$N_I^A = (r_i| \, - r_i|0) \,, \tag{60}$$

and equations eq. (57) to eq. (59) can be expressed as

$$N_I^A A_{IJ} = 0 = A_{JI} N_I^A \,, \tag{61}$$

where the second equality merely uses the antisymmetry property of A. Hence, we have proved that any set of r_i satisfying eq. (55) defines an antisymmetric rank assignment N_I^A of the mother theory, which satisfies the mother ACC.

Conversely, starting with an antisymmetric rank assignment N_I^A in the mother theory

$$N_i^A = -N_{i+k}^A, \quad N_a^A = 0 \,, \tag{62}$$

which satisfies the ACC, one can use equations eq. (57) to eq. (59) backwards, and thus obtain a set of r_i such that eq. (55) holds for all $\bar{J} = j, a$.

Let us emphasize that while symmetric rank assignments in the mother theory are in one-to-one correspondence with solutions of the homogeneous system of ACC in the daughter theory (which by definition form the kernel of $\overline{A}$), the antisymmetric rank assignments in the mother theory correspond rather to the elements of the cokernel of $\overline{A}$, that we will see merely as technical tools. They are useful for determining whether a given daughter theory admits an anomaly-free rank assignment, since the elements in the cokernel of $\overline{A}$ encode the relations between the lines of $\overline{A}$, from which one can row-reduce $\overline{A}$.

Coefficients of trivial linear combination of lines of $\overline{A}$ are in one-to-one correspondence with the anomaly-free antisymmetric rank assignments in the mother theory.

To rephrase what we wrote at the beginning of the section, there are anomaly-free rank assignments in the daughter theory if and only if

$$N_i^A f_i = 0 \tag{63}$$

for every antisymmetric solution N_I^A of the mother theory, where f is easily computed from the dimer and its orientifold. We call this the "Rouché-Capelli condition."

In general, note that any rank assignment N_I can be split into a symmetric and an antisymmetric component,

$$(N_i|N_{i+k}|N_a) = \frac{1}{2}(N_i + N_{i+k}|N_{i+k} + N_i|2N_a) + \frac{1}{2}(N_i - N_{i+k}|N_{i+k} - N_i|0) \,. \tag{64}$$

Both parts are then half-integer valued. Multiplying such a possibly unphysical (in the case it is half integer-valued) rank vector by an even number yields a physical rank vector with the required (anti)symmetry. All of the reasoning of the last two subsections is pure linear algebra, and does not know about the need of integrality for rank assignments, which entirely comes from physics.

4.2 A Zig-Zag Algorithm for Orientifolds

We will now generalize the procedure discussed in section 2.4.1 to find (anti)symmetric rank assignments in orientifolded theories. The precise details of the algorithm depend on whether the $\mathbb{Z}_2$ involution leaves fixed lines or points. This difference comes from the fact that involutions with fixed lines map nodes to nodes of the same color, while involutions with fixed points map nodes to nodes with opposite color.

We illustrate this difference in Figure 15. There we can see that ZZPs around a node make a clockwise or counterclockwise loop. If a node is mapped to a node of the same color it means that the orientation of the loop is preserved, while, in the opposite case, it is reversed.[4] This observation will become crucial when we define (anti)symmetric rank assignment in both the case of fixed lines and points.

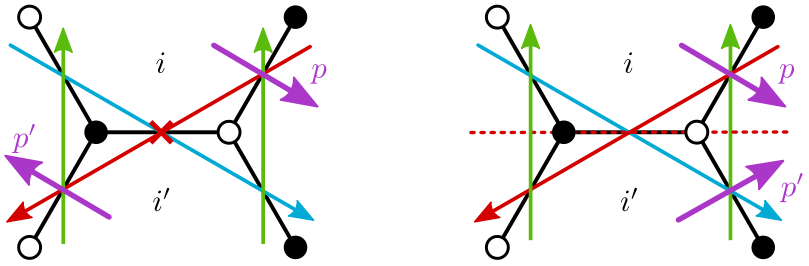

Figure 15: The orientifold actions with fixed points (a) and fixed lines (b). p is a path from one face to an adjacent one, and p' its image. In (a) the red and blue ZZPs are self-identified, while the green ones are mapped into each other. In (b), the red and blue ZZPs are mapped into each other, and the green ones are self-identified.

For the forthcoming analysis, we find it useful to introduce the notation $\{\Gamma\} = \{\alpha, \overline{\alpha}, \gamma\}$ to describe the set of ZZPs: every pair (α, $\overline{\alpha}$) corresponds to ZZPs mapped into each other under the orientifold projection, while γ labels self-identified ZZPs.

[4]We recall that under both involutions, a dimer is sent to a dimer with all ZZPs going in the opposite direction. The map between ZZPs is understood after additionally reversing the direction of every ZZP, as in [27].

4.2.1 Fixed Line Orientifolds

Due to how they act on ZZPs, orientifolds with fixed lines in the dimer correspond to toric diagrams with axes of $\mathbb{Z}_2$ reflection symmetry.[5] fig. 16 illustrates the general structure of such axes and the map between a ZZP and its image in the cases of orientifolds with diagonal and horizontal O-lines (which is analogous to the case with vertical O-lines). Let us elaborate on this kind of figure. Naively, the orientation of the reflection axis in these toric diagrams can be modified by an $SL(2,\mathbb{Z})$ transformation, potentially eliminating the distinction between the diagonal and vertical/horizontal O-line cases. However, the toric diagram after such $SL(2,\mathbb{Z})$ transformation would no longer be symmetric with respect to the axis. Alternatively, we can think about the toric diagrams with reflection axes as coming from specific dimers with fixed lines. In this context, an $SL(2,\mathbb{Z})$ transformation translates into a change of the unit cell of the dimer. But the unit cell is fixed by the specific orientifold under consideration: not any $SL(2,\mathbb{Z})$ transformation is permitted once we have chosen an orientifold identification. In other words, the orientifold obstructs $SL(2,\mathbb{Z})$ transformations.

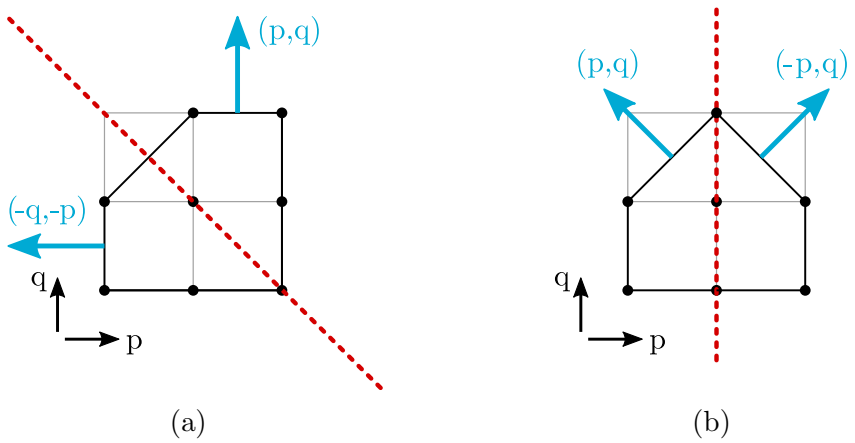

Figure 16: The toric diagrams for fixed line orientifolds have an axis of reflection symmetry. The corresponding axes for: (a) diagonal and (b) horizontal O-lines. In both cases we show in blue a generic ZZP and its image.

Symmetric rank assignments. For $\mathbb{Z}_2$ involutions with fixed lines, symmetric rank assignments correspond to symmetric ZZP value assignments:

$$v_\alpha = v_{\overline{\alpha}}, \quad v_\gamma \text{ free} \tag{65}$$

[5]We will refer to such lines of reflection symmetry in the toric diagram as *axes* in order to avoid confusion with the fixed lines in the dimer (which we also call O-lines).

First, recall from section 2.4.1 that the difference between the ranks of any two faces in the dimer is equal to a sum (with signs) of the values of the ZZPs one crosses as one goes between the two faces. ACC at each face of the dimer ensure that the value of this sum is invariant under smooth (homological) deformations of the path one follows. Furthermore, the topological constraints guarantee that the value of the sum is independent of the homology class of the path on the torus.

Consider two faces i and j and a path p connecting them, and i', j' and p' their respective images under the $\mathbb{Z}_2$ symmetry. Every time p crosses a ZZP α, its image p' crosses α', and these two crossings have the same sign, since the orientation is preserved. From this, it is clear that, if the ZZP value assignment is symmetric, the rank assignment generated by the method in section 2.4.1 is also symmetric.

In the case of dimer models with involutions fixing lines, symmetric rank assignments correspond bijectively to symmetric ZZP value assignments (up to the global shift in the values, and such that the topological constraints are satisfied).

For symmetric value assignments, the topological constraints read:

- Diagonal line ($p_{\bar{\alpha}} = -q_\alpha, q_{\bar{\alpha}} = -p_\alpha$):

$$0 = \Lambda = \sum_\alpha v_\alpha (p_\alpha - q_\alpha) + \frac{1}{2} \sum_\gamma v_\gamma (p_\gamma - q_\gamma) = -M = 0 \,. \tag{66}$$

- Vertical lines ($p_{\bar{\alpha}} = -p_\alpha, q_{\bar{\alpha}} = q_\alpha$):

$$\begin{aligned} M &= 2 \sum_\alpha v_\alpha q_\alpha + \sum_\gamma v_\gamma q_\gamma = 0 \,, \\ \Lambda &= 0 \,, \end{aligned} \tag{67}$$

The case of horizontal lines follows exchanging p_Γ with q_Γ and Λ with M.

We can now compute the total number of symmetric rank assignments. If the dimer under consideration has n ZZPs, symmetric rank assignments correspond to a choice of v_Γ, such that $v_\alpha = v_{\overline{\alpha}}$, and such that topological constraints hold. We also have the freedom to shift the rank of all gauge groups, since regular branes respect the required symmetry. Putting all this together, the number of independent symmetric rank assignments modulo some (possibly half-integer) number of regular branes is

$$\dim(\ker(\overline{A})) - 1 = \frac{1}{2}(n + n_s) - 2 \,, \tag{68}$$

where n_s is the number of self-identified ZZPs.

Antisymmetric rank assignments. Antisymmetric rank assignments are found in a similar fashion, by imposing the antisymmetry explicitly on the ZZP values, i.e. $v_\Gamma = -v_\Gamma$, or equivalently

$$v_\alpha = -v_{\overline{\alpha}}, \quad v_\gamma = 0\,. \tag{69}$$

This follows from the same reasoning as in the symmetric case: due to the geometric action of the symmetry, it is clear that antisymmetric ZZP value assignments lead to antisymmetric rank assignments in the dimer. Furthermore, if the ZZP value assignment is not antisymmetric *up to a shift*, it is straightforward to see that the rank assignment cannot be antisymmetric either.

In this case there is a subtlety that was not present in the symmetric case. First, the ZZP value method only knows about differences of ranks in the dimer. Equivalently, it only describes anomaly-free rank assignments up to some (half-integer) number of regular branes. The relevant point here is that regular branes are not antisymmetric. Hence, starting from an antisymmetric value assignment, it can well be that the rank assignment one constructs is not antisymmetric per se, but merely antisymmetric after having added some number of regular branes (we will see examples of this later). Then, in the method of section 2.4.1, a global shift of the ZZP values does not change the resulting rank assignment. The global shift does not preserve antisymmetry, so among the family of value assignments corresponding to a given rank assignment (modulo regular branes), there is a special representative which is an antisymmetric value assignment. Thus instead of focusing on the bijection between the set of antisymmetric rank assignments up to a (half-integer) number of regular branes, and the set of ZZP value assignments which satisfies the topological constraints, and which can be transformed into antisymmetric value assignments thanks to the global shift, one can consider the only representative of such a class of ZZP value assignments, which is antisymmetric. We have proven the following:

> In the case of dimer models with involutions fixing lines, antisymmetric rank assignments correspond bijectively to antisymmetric ZZP value assignments which satisfy the topological constraints.

When combined with eq. (69), the topological constraints $\Lambda = M = 0$ again merge into a single constraint, regardless of the type of fixed line orientifold. The surviving combination however depends on the nature of the fixed lines:

- Diagonal line:

$$\Lambda = \sum_\alpha v_\alpha (p_\alpha + q_\alpha) = -M = 0\,. \tag{70}$$

- Vertical lines:

$$\Lambda = 2\sum_{\alpha} v_\alpha p_\alpha = 0\,,$$
$$M = 0\,. \tag{71}$$

For horizontal lines we merely need to exchange p_α with q_α, and Λ with M.

The number of antisymmetric rank assignments is easily computed to be

$$\dim(\mathrm{coker}(\overline{A})) = \frac{1}{2}(n - n_s) - 1 \tag{72}$$

Adding eq. (68) and eq. (72), we find that the total number of independent either symmetric or antisymmetric anomaly-free rank assignments is $n-3$, as should be the case since it is the number of anomaly-free rank assignments in the mother theory, up to (half) regular branes.

Below we illustrate these ideas with a few explicit examples, containing both diagonal and vertical/horizontal fixed lines.

No Anomaly-Free Solution: PdP_4 with Diagonal Fixed Line

Consider PdP_4. Figure 17 shows the dimer and toric diagram for the orientifold under consideration. The anomaly-free rank assignments of the mother theory are given by:

$$\mathbf{N} = (-v_7, v_2, v_6 - v_1, -v_1, v_6, v_2 - v_7, 0)\,. \tag{73}$$

The topological constraints are:

$$\Lambda : v_4 + v_3 = v_6 + v_7\ , \tag{74}$$
$$M : v_4 + v_5 = v_1 + v_2\,. \tag{75}$$

Adjacency matrices. The adjacency matrices of the mother and daughter theories are:

$$A = \left(\begin{array}{ccc|ccc|c} 0 & 0 & 1 & -1 & -1 & 0 & 1 \\ 0 & 0 & 1 & -1 & -1 & 0 & 1 \\ -1 & -1 & 0 & 0 & 0 & 1 & 1 \\ \hline 1 & 1 & 0 & 0 & 0 & -1 & -1 \\ 1 & 1 & 0 & 0 & 0 & -1 & -1 \\ 0 & 0 & -1 & 1 & 1 & 0 & -1 \\ \hline -1 & -1 & -1 & 1 & 1 & 1 & 0 \end{array}\right), \qquad (\bar{A}|f) = \left(\begin{array}{ccc|c|c} -1 & -1 & 1 & 1 & -4 \\ -1 & -1 & 1 & 1 & -4 \\ -1 & -1 & 1 & 1 & +4 \end{array}\right)\ , \tag{76}$$

where, for concreteness, we have assumed that the sign of the orientifold line is negative.

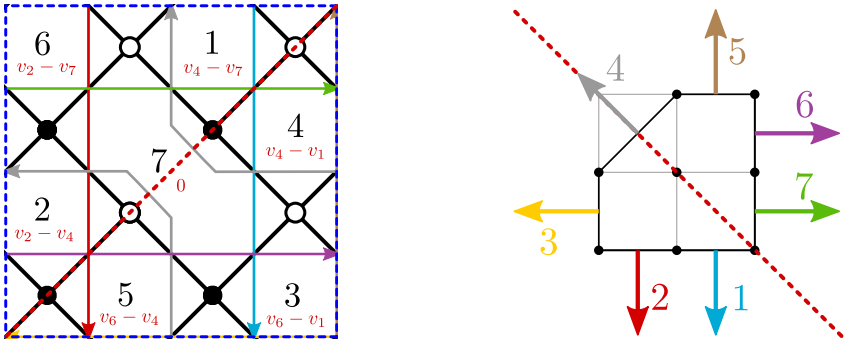

(a) (b)

Figure 17: (a) Dimer diagram for PdP_4 with a diagonal fixed line (dotted red). We show the ZZPs and the rank assignments coming from them. (b) The toric/web diagram with the corresponding symmetry axis.

Symmetric rank assignments. Impose $v_3 = v_5$, $v_2 = v_6$, $v_1 = v_7$. The constraints $M = 0$, $\Lambda = 0$ combine into $v_4 = v_1 + v_2 - v_3$. We can use the global shift freedom to set $v_4 = 0$, which leads to $\mathbf{v^S} = (v_1, v_2, v_1 + v_2, 0, v_1 + v_2, v_2, v_1)$. The resulting symmetric rank assignments in the mother and daughter theories are

$$\begin{aligned} \mathbf{N^S} &= (-v_1, v_2, v_2 - v_1, -v_1, v_2, v_2 - v_1, 0) \\ \overline{\mathbf{N}}^{\mathbf{S}} &= (-v_1, v_2, v_2 - v_1, 0) \ . \end{aligned} \tag{77}$$

Note that $\overline{\mathbf{N}}^{\mathbf{S}}$ should be understood as the column vector whose first three elements refer to the faces 1–3 that have an image, while the last refers to the self-identified face 7. When considered as a row vector, one should drop the last element.

Antisymmetric rank assignments. Impose $v_1 = -v_7$, $v_2 = -v_6$, $v_3 = -v_5 = 0$, $v_4 = 0$. We also need to impose the constraint $v_1 + v_2 = -v_3$ with no global shift freedom. We then find a two-parameter family of antisymmetric assignments for the v_Γ, $\mathbf{v^A} = (v_1, v_2, -v_1 - v_2, 0, v_1 + v_2, -v_2, -v_1)$. The corresponding antisymmetric rank assignment is

$$\mathbf{N^A} = (v_1, v_2, -v_1 - v_2, -v_1, -v_2, v_1 + v_2, 0) \ . \tag{78}$$

In the daughter theory, this rank assignment gives rise to the two row vectors

$$\overline{\mathbf{N}}^{\mathbf{A}}_{\mathbf{1}} = (1, 0, -1)v_1, \quad \overline{\mathbf{N}}^{\mathbf{A}}_{\mathbf{2}} = (0, 1, -1)v_2 \tag{79}$$

Let us denote by $\mathbf{f} = (-4, -4, 4)^T$ the inhomogeneous part of $(\overline{A}|f)$. We find $\overline{\mathbf{N}}^{\mathbf{A}}_{\mathbf{1}} \cdot \mathbf{f} = -8$ and $\overline{\mathbf{N}}^{\mathbf{A}}_{\mathbf{2}} \cdot \mathbf{f} = -8$. We conclude that anomalies cannot be cancelled in this theory.

An Anomaly-Free Example: PdP_{3b} with Two Fixed Lines

Figure 18 shows the dimer and toric diagram for an orientifold of PdP_{3b} with two fixed lines. This theory was studied in [1], where it was shown that the daughter theory admits an anomaly-free rank assignment if the two O-lines have opposite signs. Note that the horizontal fixed lines in the dimer correspond to a vertical axis of symmetry in the toric diagram.

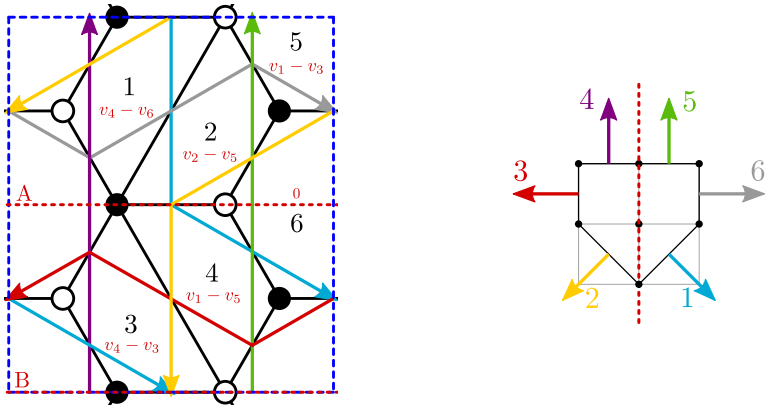

(a) (b)

Figure 18: (a) Dimer diagram for PdP_{3b} with two horizontal fixed lines (dotted red). We show the ZZPs and the rank assignments coming from them. (b) The toric/web diagram with the corresponding symmetry axis.

Adjacency matrices. The adjacency matrices of the mother and daughter theories are:

$$A = \left(\begin{array}{cc|cc|cc} 0 & -1 & 1 & 0 & -1 & 1 \\ 1 & 0 & 0 & -1 & -1 & 1 \\ \hline -1 & 0 & 0 & 1 & 1 & -1 \\ 0 & 1 & -1 & 0 & 1 & -1 \\ \hline 1 & 1 & -1 & -1 & 0 & 0 \\ -1 & -1 & 1 & 1 & 0 & 0 \end{array}\right), \qquad (\bar{A}|f) = \left(\begin{array}{cc|cc|c} 1 & -1 & -1 & 1 & -4\cdot\mathrm{sign}(B) \\ 1 & -1 & -1 & 1 & +4\cdot\mathrm{sign}(A) \end{array}\right), \tag{80}$$

where $\mathrm{sign}(A)$, $\mathrm{sign}(B)$ are the signs of the two O-lines. Let us now turn to the study of symmetric and antisymmetric rank assignments.

Symmetric rank assignments. Let us impose $v_2 = v_1$, $v_6 = v_3$. The constraint $\Lambda = 0$ is trivially satisfied, while $M = 0$ becomes (keeping v_1 and v_3):

$$2v_1 - v_4 = v_5\,. \tag{81}$$

Setting $v_4 = 0$, we get

$$\mathbf{v^S} = (v_1, v_1, v_3, 0, 2v_1, v_3)\,, \tag{82}$$

giving in turn

$$\mathbf{N^S} = (-v_3, -v_1, -v_3, -v_1, v_1 - v_3, 0)\,. \tag{83}$$

Projecting down this vector, we obtain the solutions to the homogeneous problem in the daughter theory.

Antisymmetric rank assignments. We now impose $v_2 = -v_1$, $v_3 = -v_6$, $v_4 = v_5 = 0$. As expected, M is trivially satisfied and one just needs to impose $\Lambda = 0$, which reads $v_3 = v_1$. Remember that the global shift has already been fixed. We then find a one-dimensional family of antisymmetric assignments for the v_Γ:

$$\mathbf{v^A} = (v_1, -v_1, v_1, 0, 0, -v_1)\,. \tag{84}$$

The corresponding antisymmetric rank assignment is $\mathbf{N^A} = (v_1, -v_1, -v_1, v_1, 0, 0)$. In the daughter theory this rank assignment gives $\overline{\mathbf{N}}^{\mathbf{A}} = (1, -1)v_1$. One may now use it to row reduce $\overline{A}$. Denote by $\mathbf{f} = (-4 \cdot \mathrm{sign}(B), +4 \cdot \mathrm{sign}(A))^T$ the inhomogeneous part of $(\overline{A}|f)$. We find $\overline{\mathbf{N}}^{\mathbf{A}} \cdot \mathbf{f} = -4 \cdot \mathrm{sign}(B) - 4 \cdot \mathrm{sign}(A)$. If $\overline{\mathbf{N}}^{\mathbf{A}} \cdot \mathbf{f} \neq 0$, the theory is anomalous, so we need $\mathrm{sign}(A) = -\mathrm{sign}(B)$, as anticipated.

Anomaly-free rank assignments. As explained in the introduction of the current section, since we have a parametrization of the symmetric rank assignments, we merely need a single solution of the tadpole-cancellation system to write all of them.

Looking at the adjacency matrix of the daughter theory in eq. (80) with $\mathrm{sign}(A) = +$ and $\mathrm{sign}(B) = -$, a straightforward solution to the rank assignment is $N_1 = 4$ and $N_2 = N_5 = N_6 = 0$ (in the daughter theory we keep faces $1, 2, 5$ and 6). This gives the following three-parameter family of solutions to the ACC, where we have added $N + v_1 + v_3$ regular branes:

$$\begin{cases} N_1 &= N + v_1 + 4 \\ N_2 &= N + v_3 \\ N_5 &= N + 2v_1 \\ N_6 &= N + v_1 + v_3\ . \end{cases} \tag{85}$$

These examples consist of an orientifold with a diagonal fixed line and an orizontal one. The first case turned out to lead to a theory in which anomalies cannot be cancelled, while the second one admitted a solution to the ACC. This is not by chance, in section 4.4.1 we will provide a general criterion for orientifold with fixed lines.

4.3 Fixed Point Orientifolds

In orientifolds with fixed points, every ZZP is mapped to a ZZP with the same winding numbers [27]. The image of a ZZP can therefore be either itself or another ZZP, if more than one ZZP with the same winding numbers exist.

Contrarily to the cases with fixed lines, in fixed point orientifolds nodes in the dimer are mapped to nodes of the opposite color. In analogy with the case of line orientifolds, let us consider a path p going from a face i to a face j, and its image p' going from the image of i to the image of j. If p crosses a ZZP α, then p' crosses its image α', but since the color of the nodes is inverted in the image, the signs of the crossings are opposite. This implies that a symmetric, respectively antisymmetric, rank assignment is associated to an antisymmetric, respectively symmetric, value assignment for the ZZP. We therefore have:

> In dimer models with fixed point involutions, symmetric rank assignments up to (half)-regular branes correspond bijectively to antisymmetric ZZP value assignments which satisfy the topological constraints. Similarly, antisymmetric rank assignments correspond bijectively to symmetric ZZP value assignments which satisfy the topological constraints and up to a global shift.

We have seen that in the cases of fixed point orientifolds, symmetric rank assignments correspond to ZZP value assignments such that:

$$v_\alpha = -v_{\overline{\alpha}}, \quad v_\gamma = 0\,. \tag{86}$$

One can easily verify that the topological constraints are always satisfied by this choice of v_Γ, hence the number of symmetric rank assignment is:

$$\dim(\ker(\overline{A})) = \frac{1}{2}(n - n_s)\,. \tag{87}$$

Antisymmetric rank assignments, conversely, correspond to:

$$v_\alpha = v_{\overline{\alpha}}, \quad v_\gamma = \text{free}\,. \tag{88}$$

In this case both topological constraints Λ and M are not trivial:

$$\begin{cases} \Lambda = \sum_\alpha p_\alpha v_\alpha + \sum_{\overline{\alpha}} p_{\overline{\alpha}} v_{\overline{\alpha}} + \sum_\gamma p_\gamma v_\gamma = 2\sum_\alpha p_\alpha v_\alpha + \sum_\gamma p_\gamma v_\gamma = 0 \\ M = \sum_\alpha q_\alpha v_\alpha + \sum_{\overline{\alpha}} q_{\overline{\alpha}} v_{\overline{\alpha}} + \sum_\gamma q_\gamma v_\gamma = 2\sum_\alpha q_\alpha v_\alpha + \sum_\gamma q_\gamma v_\gamma = 0 \end{cases} \tag{89}$$

This leads to:

$$\dim(\text{coker}(\overline{A})) = \frac{1}{2}(n + n_s) - 3\,. \tag{90}$$

Upon summing the contributions of symmetric and antisymmetric rank assignments, we retrieve the total number of fractional branes, $n - 3$, modulo regular branes.

4.3.1 An Example: PdP_{3b}

We now consider PdP_{3b} as an example for our algorithm in the case of fixed points.

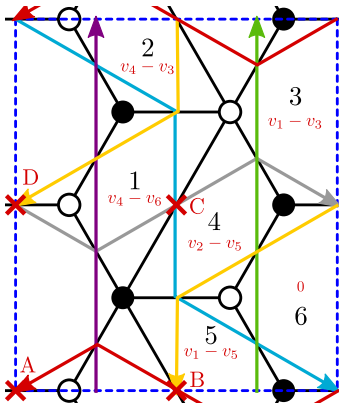

Figure 19: Dimer diagram for PdP_{3b} with fixed points. We show the ZZPs and the rank assignments coming from them.

Adjacency matrices. The adjacency matrices of the mother and daughter theories are:

$$A = \left(\begin{array}{ccc|ccc} 0 & 1 & -1 & -1 & 0 & 1 \\ -1 & 0 & 1 & 0 & 1 & -1 \\ 1 & -1 & 0 & 1 & -1 & 0 \\ \hline 1 & 0 & -1 & 0 & -1 & 1 \\ 0 & -1 & 1 & 1 & 0 & -1 \\ -1 & 1 & 0 & -1 & 1 & 0 \end{array}\right), \quad (\bar{A}|f) = \left(\begin{array}{ccc|c} -1 & 1 & 0 & +4\cdot\mathrm{sign}(C) \\ -1 & 1 & 0 & -4\cdot\mathrm{sign}(B) \\ 2 & -2 & 0 & -4\cdot\mathrm{sign}(A)+4\cdot\mathrm{sign}(D) \end{array}\right), \tag{91}$$

where $\mathrm{sign}(A)$ to $\mathrm{sign}(D)$ are the signs of the O-points. Note that the ZZPs 4 and 5 are interchanged by the projection, while all other ZZPs are mapped to themselves. Let us now turn to the study of antisymmetric and symmetric rank assignments.

Symmetric rank assignments. This time we start with antisymmetric ZZP assignments, since for point orientifolds they provide symmetric rank assignments. Let us impose $v_4 = -v_5$, $v_1 = v_2 = v_3 = v_6 = 0$. As already said, the topological constraints are both trivially satisfied. Note that there is no global shift to fix. We obtain a one-parameter family of v_Γ assignments:

$$(0, 0, 0, 1, -1, 0)v_4\,. \tag{92}$$

The corresponding rank assignment is:

$$\mathbf{N^S} = (1,1,0,1,1,0)v_4\,, \tag{93}$$

which is symmetric, as expected. Projecting down this vector, one obtains the solutions to the homogeneous problem in the daughter theory.

Antisymmetric rank assignments. We now turn to symmetric ZZP assignments, responsible for the antisymmetric rank assignments. We only need to impose $v_4 = v_5$. We further fix the global shift by choosing $v_4 = 0$. The topological constraints become:

$$\begin{aligned} Ł : v_3 &= v_1 - v_2 + v_6\ , \\ M : v_2 &= -v_1\ . \end{aligned} \tag{94}$$

We find a two-dimensional family of symmetric assignments for the v_Γ:

$$(1,-1,2,0,0,0)v_1 + (0,0,1,0,0,1)v_6\,. \tag{95}$$

The corresponding antisymmetric rank assignments are:

$$\mathbf{N}^A = (0,-2,-1,-1,1,0)v_1 + (-1,-1,-1,0,0,0)v_6\ . \tag{96}$$

Which, up to half regular branes is equal to:

$$\mathbf{N}^A = (1,-3,-1,-1,3,1)\frac{v_1}{2} + (-1,-1,-1,1,1,1)\frac{v_6}{2}\,, \tag{97}$$

which is antisymmetric, as expected. Let us split it into two vectors and project them down to the daughter theory to obtain,

$$\overline{\mathbf{N}}_1^A = (1,-3,-1)\frac{v_1}{2}, \quad \overline{\mathbf{N}}_2^A = (-1,-1,-1)\frac{v_6}{2}\ . \tag{98}$$

Again, let us use these rank assignments to row reduce $\overline{A}$ by denoting $\mathbf{f} = (+4\cdot \text{sign}(C), -4\cdot\text{sign}(B), -4\cdot\text{sign}(A) + 4\cdot\text{sign}(D))^T$. One finds that, for the theory to admit non-anomalous solutions, one must satisfy,

$$\begin{aligned} \overline{\mathbf{N}}_1^A\cdot\mathbf{f} =& \frac{v_1}{2}\left(\text{sign}(C) + 3\text{sign}(B) + \text{sign}(A) - \text{sign}(D)\right) = 0\ , \\ \overline{\mathbf{N}}_2^A\cdot\mathbf{f} =& \frac{v_6}{2}\left(-\text{sign}(C) + \text{sign}(B) + \text{sign}(A) - \text{sign}(D)\right) = 0\ . \end{aligned} \tag{99}$$

Anomaly-free rank assignments. The solution to eq. (99) depends on the sign choices for the four fixed points. Consider for example

$$\text{sign}(A) = \text{sign}(C) = +, \quad \text{sign}(B) = \text{sign}(D) = - \,, \tag{100}$$

which is consistent with the sign rule for fixed point orientifolds. In this case, we go back to eq. (91) to find a two-parameter family of solutions:

$$\begin{cases} N_1 &= N + v_4 \\ N_2 &= N + v_4 + 4 \\ N_3 &= N \ . \end{cases} \tag{101}$$

4.4 General Criteria for Anomaly-Free Orientifolds

In this section we present a general study of the solutions to the non-homogeneous system of ACC of the daughter theory. Remarkably, we can exploit the algorithm of the previous section to determine the existence of such solutions directly from toric data, regardless of the particular phase of the theory. This gives a purely geometric criterion determining whether an orientifolded theory may admit a toric phase with non-anomalous rank assignments.

4.4.1 Diagonal Line Orientifolds

Let us consider orientifolds with a diagonal fixed line. Without loss of generality, we assume that the fixed line has winding numbers $(1, 1)$ in the fundamental cell of the dimer. The mapping of ZZPs in this kind of orientifolds has been studied in [27] and we presented a preliminary discussion in section 4.2.1. The diagonal fixed line in the dimer translates into a reflection symmetry axis in the toric diagram with slope -1, as we already illustrated in fig. 16a. This $90°$ rotation of the symmetry axis of the toric diagram with respect to the fixed line in the dimer was explained in [28].

Reflection with respect to the axis of the toric diagram maps a ZZP with winding (p, q), to a ZZP with winding $(-q, -p)$. fig. 20 shows an example of a generic toric diagram with a diagonal line orientifold.

- Let l be the number of pairs $\{v_\alpha, v_{\overline{\alpha}}\}$,with $\alpha = 1, .., l$, of ZZPs mapped one to another, which are not parallel to the symmetry axis of the toric diagram.

- Let $l_\parallel$ be the number of self-identified ZZPs $\{v_\gamma\}$ for $\gamma = 1, ..., l_\parallel$, which are parallel to the symmetry axis of the toric diagram.

From the previous section, we know how to produce the coefficients of the trivial linear combinations of rows. They are the ranks of the projected SU groups that

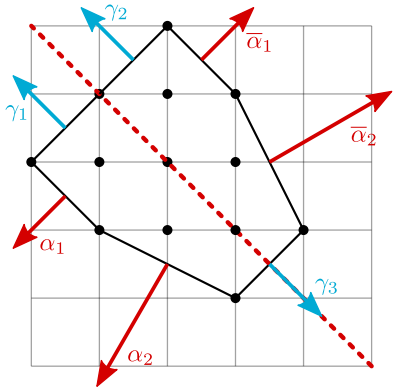

Figure 20: A generic toric diagram with a diagonal axis symmetry.

result from imposing the following conditions on the v_Γ:

$$\begin{aligned} v_\alpha &= -v_{\overline{\alpha}}\,, \\ v_\gamma &= 0 \end{aligned} \tag{102}$$

for all α and γ's. The topological constraints Λ and M are given by:

$$\Lambda = \sum_{\alpha,\overline{\alpha}} (v_\alpha p_\alpha + v_{\overline{\alpha}} p_{\overline{\alpha}}) = \sum_\alpha v_\alpha (p_\alpha + q_\alpha) = -M \tag{103}$$

where we used $p_{\overline{\alpha}} = -q_\alpha$.

We now recall the Rouché-Capelli theorem: A non-homogeneous linear system has solution *iff* the rank of the associated homogeneous matrix is equal to the rank of the matrix associated to the full system. A trivial linear combination of rows of the homogenous matrix is still trivial when considering the matrix associated to the full system. This can be stated as:

$$\sum_i N_i f_i = 0 \tag{104}$$

where f_i is the non-homogeneous contribution to the ACC matrix of the orientifolded theory, coming from the tensor matter.

We now need to derive an expression for N_i in terms of the v_Γ. The Rouché-Capelli theorem tells us that the ACC system admits a solution *iff* eq. (104) holds for every value of v_Γ consistent with the topological constraints.

Faces with at Most One Tensor

Let us first focus on the simpler case where every gauge group has at most one tensor field. This result will be easily extended later to cases with more tensors.

Consider a face of the mother theory with an edge on top of a fixed line. The rank assignment providing the coefficients for row reduction is given by the condition $N_i = -N_{i+k}$, $v_\alpha = -v_{\overline{\alpha}}$, and the difference between the ranks of two adjacent faces is given by $N_i - N_{i+k} = v_\alpha - v_{\overline{\alpha}}$. Combining these two results, we obtain

$$2N_i = N_i - N_{i+k} \;=\; v_\alpha - v_{\overline{\alpha}} = 2v_\alpha \,. \tag{105}$$

Let us now determine the f_i from the toric data. The method we are going to discuss below can be regarded as a generalization to orientifolds of the algorithm for finding the (minimal) matter content of a quiver in terms of basic knowledge of the (p, q) winding numbers of its ZZPs (equivalently of the external legs of the (p, q) web dual to the toric diagram). The intersection number between a given ZZP and the fixed line is

$$\det \begin{pmatrix} p & 1 \\ q & 1 \end{pmatrix} = p - q \,. \tag{106}$$

At every such crossing this ZZP, if not self-identified, will intersect its image on the line. The edge on which they cross will produce a tensor or conjugate tensor field, depending on the orientation of the crossing. This is depicted in fig. 21.

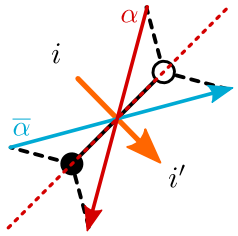

Figure 21: Crossing between a ZZP (and its image) over an edge on top of a diagonal fixed line. We show the corresponding bifundamental field in the mother theory.

From the discussion above, it is clear that the non-vanishing components of f_i are exactly those corresponding to the faces with a tensor, for which we have just determined the rank in terms of the ZZP values. Taking into account that the same ZZP can be related to $p_\alpha - q_\alpha$ tensors, this allows us to write eq. (104) as

$$\sum_i N_i f_i = (\pm 4) \sum_\alpha v_\alpha (p_\alpha - q_\alpha) = 0 \,, \tag{107}$$

where we have factorized the choice of sign for the diagonal O-line.

It is worth noting that the intersection with sign is a topological quantity that counts the minimal number of intersections of the ZZP with the fixed line in the dimer. This is, in fact, a homological invariant. In principle, more intersections

are allowed, but they will come in pairs, one with positive and one with negative intersection, as shown in fig. 22. When computing the total contribution they cancel, leaving us with eq. (107), which does not depend on the particular phase we are considering.

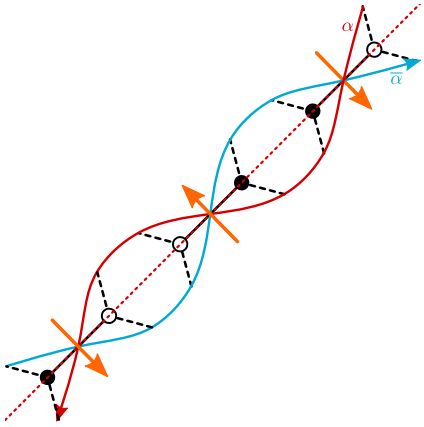

Figure 22: When ZPPs are deformed, additional intersections are added in pairs. We show the corresponding bifundamental fields in the mother theory.

We use the topological constraint eq. (103) to express the value assigned to v_1, as

$$v_1 = -\frac{1}{p_1 + q_1} \sum_{\alpha \neq 1} v_\alpha (p_\alpha + q_\alpha) \,. \tag{108}$$

Plugging this expression into eq. (107) and rearranging the terms, we reach the following equality:

$$\sum_{\alpha \neq 1} v_\alpha \left(p_\alpha q_1 - p_1 q_\alpha \right) = 0 \,. \tag{109}$$

Then, the Rouché-Capelli theorem can be satisfied for generic v_α *iff*

$$p_\alpha q_1 - p_1 q_\alpha \equiv \det \begin{pmatrix} p_\alpha & p_1 \\ q_\alpha & q_1 \end{pmatrix} = 0 \,, \tag{110}$$

which implies that $p_\alpha = p_1, q_\alpha = q_1$ for every α. We dub the corresponding class of toric diagrams the *trapezoids*. An example of such a trapezoid is shown in fig. 23. Among trapezoids, we of course include also *triangles*.

Note also that there is a subset of trapezoids for which eq. (107) is trivially satisfied. They have $p_\alpha = q_\alpha$ for every α so we refer to them as the *rectangles*, and describe orbifolds of F_0. See fig. 24 as an example. We remark that rectangles are the toric diagrams that give rise to line orientifolds without tensors in the spectrum. Thus, we recover the result that the latter always admit a non-anomalous solution.

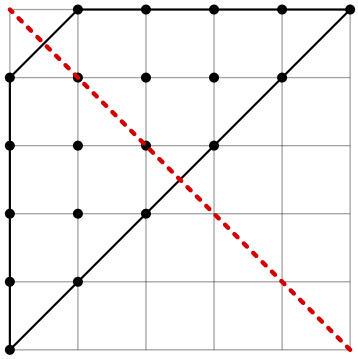

Figure 23: An example of a trapezoid for which you can find a non-anomalous diagonal line orientifold.

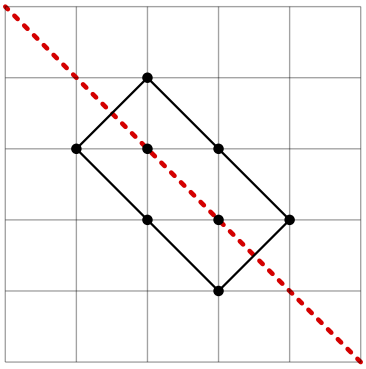

Figure 24: An example of a rectangle toric diagram with its diagonal axis of symmetry.

Preliminary result for diagonal line orientifolds: Unless the toric diagram of the singularity under consideration is a trapezoid, any orientifold theory obtained from a dimer symmetric with respect to its diagonal, *and in which every face has at most one edge along this diagonal*, does not admit anomaly-free solutions.

Faces with Multiple Tensors

Faces with multiple tensors arise in examples as simple as the conifold or $\mathbb{C}^2/\mathbb{Z}_{2n+1}$ orbifolds, upon orientifolding with respect to a diagonal line. We now discuss how the previous discussion is extended to these cases. We start by considering how multi-tensor faces may be embedded in the dimer. We will see that there are restrictions on the number of tensors a face can have. Moreover, their existence is non-trivial and imposes constraints on the toric diagrams. The analysis of this

case is slightly different from the one in the previous section but will lead to the same result.

Interestingly, it is possible to find an upper bound on the number of tensors a face in the dimer can have. Figure 25 shows a face with two self-identified edges on the same side of the O-line. If they were adjacent, they would be connected at a 2-valent node, which corresponds to a mass term and then they could be integrated out. Naively, we might imagine that this can be avoided by introducing additional structure between the two edges, which is represented as a blob in fig. 25. But the ZZPs generating the edges on the line are the only ones that participate in the blob. In other words, the orange and purple ZZPs in fig. 25 must be identified with the blue and green ZZPs, with the precise identification depending on the number of intermediate edges. Therefore, the blob can only correspond to a sequence of edges connected by mass terms. After integrating them out, we are left with either zero or one tensor for an even or odd number of edges, respectively. This implies that a given face can only support more than one tensor in two cases: if they belong to different O-lines or if they belong to the same O-line but are coming from different copies of the unit cell as illustrated in fig. 26. In both cases, the previous analysis applies to each instance that the face touches a fixed line, so we conclude that the maximum possible number of tensors at a given face is two. The total number of tensors in the full theory is, however, unrestricted.

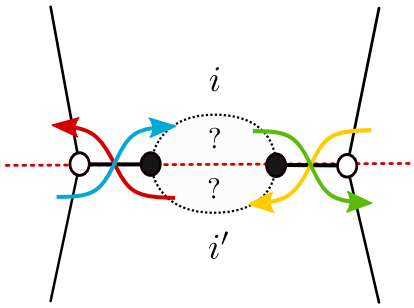

Figure 25: Two edges of a given face on a fixed line, separated by a general structure.

From fig. 26, we see that there can be three types of ZZPs: ZZPs parallel to the fixed line, which are forbidden since they would have to go through the face with two tensors, spoiling it; ZZPs orthogonal to the fixed line, i.e. self-identified ZZPs, which do not give rise to tensors; finally, ZZPs which intersect in pairs on self-identified edges giving rise to tensors. Thus, the singularity can only have self-identified ZZPs, those of the γ kind, and at most two couples of ZZPs of the α kind. Moreover, the (p, q) numbers of the latter are also subject to constraints. They cannot cross faces i and i' otherwise than passing by the O-lines, so they can intersect the grey dotted axis in fig. 26 at most twice if only one couple of ZZPs α

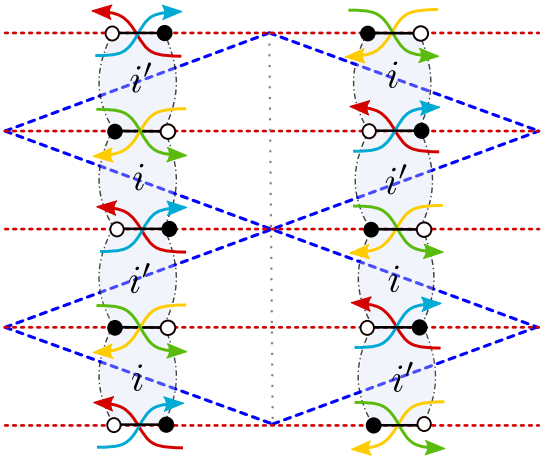

Figure 26: Faces with edges on top of the fixed line at different copies of the unit cell.

is involved:

$$|p_\alpha + q_\alpha| \leq 2 \quad \text{for } \alpha = 1\,, \tag{111}$$

and once in the case of two couples:

$$|p_\alpha + q_\alpha| = 1 \quad \text{for } \alpha = 1, 2\,. \tag{112}$$

Those relations apply both for ZZPs α and $\bar{\alpha}$, for which the sums are respectively negative and positive.

If there is only one couple, the singularity corresponds to a trapezoid as the ones discussed in the previous section. Indeed, we have only one couple of ZZPs of the α kind and the topological constraint imposes $v_1 = 0$ for them, turning the RC condition into a trivial equation.

For two couples, the topological constraints and eq. (112) impose

$$v_1 = -v_2\,. \tag{113}$$

This is the counterpart of the fact that faces i and i' in fig. 26 have to be of opposite ranks, following section 4.4.1. Now, we can write the RC condition allowing faces to support one or two tensors in terms of v_1 only:

$$\sum_i N_i f_i = (\pm 4)(v_1(p_1 - q_1) - v_1(p_2 - q_2)) = 0\,. \tag{114}$$

Knowing eq. (112), the only solution is $(p_1, q_1) = (p_2, q_2)$ so that we recover trapezoids. Let us note that the last equation considered with eq. (113) can be brought to the form of eq. (109) for two couples of ZZPs α, hence it is not surprising that

a subset of trapezoids appears again as solutions in this context. For instance, the conifold does not provide a non-anomalous diagonal line orientifold while $\mathbb{C}^2/\mathbb{Z}_{2n+1}$ orbifolds do.

We conclude with a general result for diagonal line orientifolds:

Diagonal line orientifolds: Unless the toric diagram of the singularity is a *trapezoid*, any orientifold theory obtained from a dimer with a diagonal O-line is anomalous.

See fig. 27 for more examples.

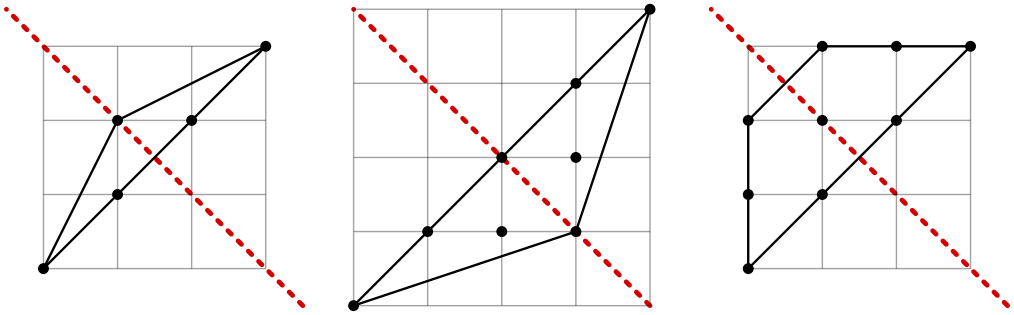

Figure 27: Examples of trapezoids, which admit anomaly-free fixed line orientifolds.

4.4.2 Horizontal/Vertical Line Orientifolds

In this section we consider horizontal fixed lines. The case of vertical lines is trivially related by rotation. The reasoning is essentially the same as the one described previously for the case of diagonal lines. This allows us to go fast to the main result for this class of orientifolds. In particular, we will not comment here about rectangles and faces with many tensors since the previous results are easily generalized.

Horizontal symmetry lines in the dimer correspond to a vertical symmetry in the toric diagram. The $\mathbb{Z}_2$ action maps a ZZP with winding (p, q) to a ZZP with winding $(-p, q)$. Again, we distinguish two different types of ZZPs:

- Pairs of ZZPs $\{v_\alpha, v_{\overline{\alpha}}\}$ for $\alpha = 1, ..., l$, where v_α and $v_{\overline{\alpha}}$ are exchanged under the symmetry, thus not parallel to the axis of symmetry.
- Self-identified ZZPs $\{v_\gamma\}$ for $\gamma = 1, ..., l_\parallel$, with winding numbers $(0, 1)$ or $(0, -1)$.

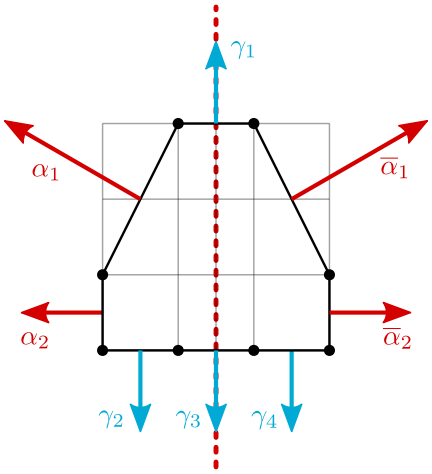

Figure 28: A generic singularity with a vertical axis symmetry.

A general illustration of this is depicted in fig. 28.

In order to find the antisymmetric solutions to the ACC, we need to look at the antisymmetric value assignments of the ZZPs and impose the topological constraint

$$Ł = 2\sum_{\alpha} v_\alpha p_\alpha = 0 \ . \tag{115}$$

Let us now consider the Rouché-Capelli condition. A ZZP of type α with winding numbers (p, q) crosses both fixed lines $-q$ times, counted with sign. The Rouché-Capelli condition can be expressed as

$$\sum_i N_i f_i = -\sum_\alpha v_\alpha q_\alpha (4 \text{ sign}(A) + 4 \text{ sign}(B)) = 0 \,, \tag{116}$$

where sign(A) and sign(B) indicate the signs of the two fixed lines. Unlike the case of diagonal lines, the Rouché-Capelli condition in eq. (116) becomes trivial as soon as sign(A) and sign(B) are different. In that case, the orientifold theory is always anomaly-free.

If the two fixed lines have the same sign, eq. (115) allows us to express v_1 in terms of the remaining v_α, as in the case of diagonal lines. Plugging this expression into Equation (116) leads to

$$\sum_{\alpha \neq 1} v_\alpha \left(p_\alpha q_1 - p_1 q_\alpha\right) = 0 \,. \tag{117}$$

With the same analysis of the previous section, we find that singularities with two horizontal lines of the same sign admit a solution to the ACC only if they are trapezoids, just as in the case of diagonal lines. See Figure 29 for examples.

Horizontal/vertical line orientifold: Toric diagrams symmetric with respect to a horizontal/vertical axis always lead to anomaly-free orientifold theories when the two O-lines have *opposite signs*. When the signs are the same, instead, in order to yield a non-anomalous orientifold theory the toric diagram of the singularity must be a *trapezoid*.

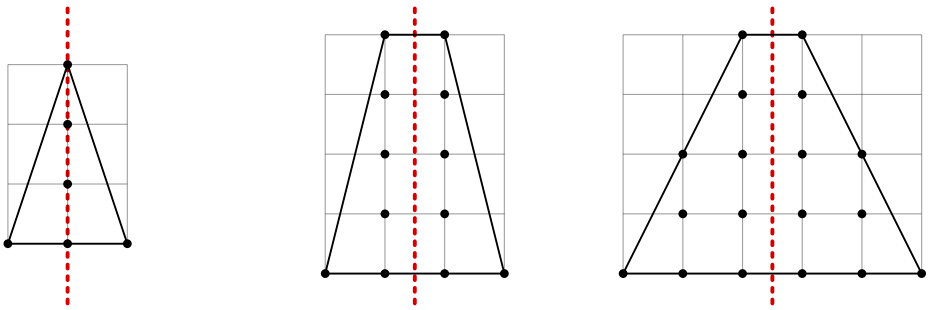

Figure 29: Examples of trapezoids, which admit anomaly-free horizontal fixed line orientifolds.

4.4.3 Fixed Point Orientifolds

Finally, we address the case of fixed point orientifolds. We should state right away that the results in this case are less conclusive than for fixed lines. Indeed, one can easily anticipate that having a larger number of signs to fix (at the four fixed points), it will be straightforward to satisfy the ACC just by a wise choice, similarly to the case with horizontal/vertical line. On the other hand, if one sticks with a 'wrong' choice, the restriction on the allowed geometries is not as nicely characterizable as in the previous case.

As already explained in section 4.2, the action of the orientifold on every ZZP is to map it either to itself or to another ZZP with the same winding numbers. We thus divide the ZZPs into two sets:

- Pairs of distinct ZZPs $\{v_\alpha, v_{\overline{\alpha}}\}$ for $\alpha = 1, \cdots, k$ that are exchanged.
- Self-identified ZZPs $\{v_\gamma\}$, for $\gamma = 1, \cdots, l$.

The total number of ZZPs is $n = 2k + l$.

In this kind of orientifolds, tensors arise whenever a pair of self-identified ZZPs intersect over a fixed point. Moreover, a ZZP going through a fixed point necessarily goes through a second fixed point [27]. As a result, it is easy to convince oneself that the number of tensors, if present at all, must be between 2 and 4, and it coincides with the total number of self-identified ZZPs that cross a fixed point.

In order to find the antisymmetric solutions to the ACC, we need to consider symmetric value assignments for the ZZPs, as explained in section 4.2, subject to the topological constraints

$$\begin{aligned} \Lambda &= 2\sum_\alpha v_\alpha p_\alpha + \sum_\gamma v_\gamma p_\gamma = 0\,, \\ M &= 2\sum_\alpha v_\alpha q_\alpha + \sum_\gamma v_\gamma q_\gamma = 0\,. \end{aligned} \tag{118}$$

The RC equation becomes

$$\sum_i N_i f_i = \sum_{\gamma\neq\gamma'} (v_\gamma - v_{\gamma'})(\pm 4) = 0\,. \tag{119}$$

where the sum in the middle runs over the tensors. The signs depend on the sign of the fixed points and on the orientations of the self-identified edges. Depending on which of the two faces adjacent to the edge we preserve in the projection, we get tensors or their conjugates, contributing with opposite signs to the ACC.

We recall that the signs of the fixed points, in contrast with fixed lines, are constrained by the *sign rule* [25]. The rule prescribes that the product of the four signs is $(-1)^{n_W/2}$, with n_W the number of superpotential terms.[6]

We now consider the different possibilities, i.e. $l = 2$, 3 and 4 tensors. Our analysis is general and does not distinguish between faces with single or multiple tensors.

- $l = 2$: In this case we have two tensors, meaning that two ZZPs cross each other on two fixed points. Equation (119) reads

  $$(v_1 - v_2)(\pm_1 4) \pm (v_1 - v_2)(\pm_2 4) = 0\,, \tag{120}$$

  where the $\pm_i$ indicate the signs of the fixed points, while the additional $\pm$ signs depends on whether the tensors are conjugated or not.

  Since only two fixed points are involved in this case, their signs can always be chosen such that this equation is trivially satisfied, while satisfying the sign rule. However, it is interesting to consider whether there are other ways to satisfy this constraint. We can impose $v_1 = v_2$ using the two equations of the topological constraint. Expressing v_1 and v_2 as function of the other v_α's we get

  $$\begin{aligned} v_1 &= \frac{2}{p_1 q_2 - p_2 q_1}(p_2 \sum_\alpha v_\alpha q_\alpha - q_2 \sum_\alpha v_\alpha p_\alpha)\,, \\ v_2 &= \frac{2}{p_1 q_2 - p_2 q_1}(q_1 \sum_\alpha v_\alpha p_\alpha - p_1 \sum_\alpha v_\alpha q_\alpha)\,, \end{aligned} \tag{121}$$

[6] Generically, it is not known whether the parity of $n_W/2$ can be deduced from the toric diagram.

where we have assumed $p_1 q_2 - p_2 q_1 \neq 0$. Equating v_1 and v_2, we obtain

$$\sum_\alpha v_\alpha (p_\alpha (q_1 + q_2) - q_\alpha (p_1 + p_2)) = 0\,. \tag{122}$$

Since this equation must hold for all v_α, the only possibility is that all terms in the summation vanish, thus $p_\alpha(q_1 + q_2) = q_\alpha(p_1 + p_2)$ for all α. Solutions are of the form $p_1 = -p_2$ and $p_\alpha = 0$, up to $SL(2,\mathbb{Z})$ transformations. Those correspond to trapezoids (not necessarily symmetric with respect to any axis) with an even number of ZZPs on each base and only one ZZP on each side.

If $p_1 q_2 - p_2 q_1 = 0$, it means that $(p_1, q_1) = -(p_2, q_2)$, since the two ZZPs are parallel and, in order to intersect in a consistent way, they must have opposite winding numbers. In this case, the topological constraint imposes $v_1 = v_2$ if $p_\alpha q_{\alpha'} - q_\alpha p_{\alpha'} = 0$ where $\alpha \neq \alpha'$. It means that all non self-identified ZZPs have to be either parallel or anti-parallel to each other. This condition is satisfied by all toric diagrams with the shape of a rectangle or a parallelogram where there is an even number of non self-identified ZZPs. Together with the solutions of the previous paragraph, they constitute a class of trapezoids for which any sign assignment for the fixed points leads to an anomaly free theory when two tensors are involved.

As an illustration, consider fixed point orientifolds of $\mathbb{C}^3/\mathbb{Z}_6$ with actions (1,1,4) and (1,2,3), whose toric diagrams are shown in fig. 30. Both of them admit an orientifold with two tensors. Our analysis implies that only the first one admits tensors with any sign, as it can easily be checked by explicitly solving the ACC.

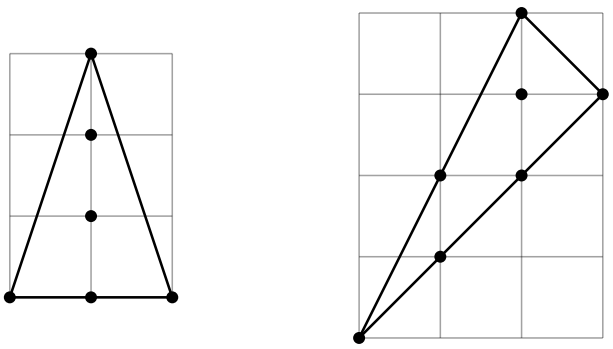

(a) (b)

Figure 30: The toric diagrams for the $\mathbb{C}^3/\mathbb{Z}_6$ orbifolds with actions: (a) (1,1,4) and (b) (1,2,3).

An interesting scenario is when tensors arise from the orientifold projection of adjoints in the mother theory, namely from edges separating self-identified

faces. In this case, the ACC of the self-identified gauge group is trivially zero, since it is either SO or USp. In this situation, the two self-identified ZZPs intersect all other ZZPs only once. This can be understood as follows. Let us consider a line passing through the fixed points under consideration. All the non self-identified ZZPs must be parallel to this line, since otherwise their intersections with the line would imply that they go through the self-identified face, which in turn would spoil the fact that it is self-identified. The $\mathbb{C}^2/\mathbb{Z}_{2m}$ orbifolds are examples in this class, see fig. 31.

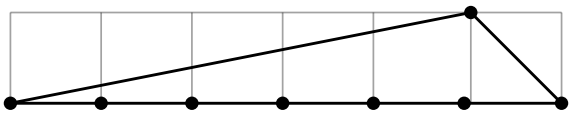

Figure 31: The toric diagram of $\mathbb{C}^2/\mathbb{Z}_6$, as an example of the $\mathbb{C}^2/\mathbb{Z}_{2m}$ family.

- $l = 3$: In this case we have three tensors, i.e. three ZZPs intersecting on three fixed points. Equation (119) reads

$$(v_1 - v_2)(\pm_1 4) \pm (v_2 - v_3)(\pm_2 4) \pm (v_3 - v_1)(\pm_3 4) = 0 \ . \tag{123}$$

  Since only three of the fixed points are involved, it is possible to pick their signs such that this equation is trivially satisfied. These choices in turn determine the sign of the fourth fixed point due to the sign rule.

  If instead we have a different combination of signs, we end up with an equation of the form

$$v_\gamma - v_{\gamma'} = 0 \, , \tag{124}$$

  with γ and γ' two of the three ZZPs above. The missing $v_{\gamma''}$ in the previous equation depends on the choice of fixed point signs in eq. (125). Therefore, in order to have a solution for all possible fixed point sign assignments we need to impose $v_1 = v_2 = v_3$ with the topological constraint. This means that the ZZPs have winding numbers of the form $(p_1, 0)$, $(-p_1, q_2)$ and $(0, -q_2)$, up to $SL(2, \mathbb{Z})$ transformations. The only solution is $p_1 = q_2 = 1$, corresponding to $\mathbb{C}^3$, i.e. flat space.

  A face with multiple tensors imposes constraint(s) of the form $v_1 - v_2 = \pm(v_2 - v_3)$, leading to an RC constraint of the form

$$(v_1 - v_2)(\pm_1 4) \pm (v_1 - v_2)(\pm_2 4) \pm (v_3 - v_1)(\pm_3 4) = 0 \ . \tag{125}$$

  Again, the existence of solutions depends on the signs of the fixed points. Solutions for generic signs can be obtained only when $v_1 = v_2 = v_3$, i.e. for flat space.

- $l = 4$:

  This case, in contrast with the previous ones, does not always admit a solution to the ACC. The reason for this is that the four fixed points are used, their signs are constrained by the sign rule and we no longer have the freedom of unused fixed points.

  The RC equation can take two different forms, depending on the ZZP intersections:

$$\begin{aligned}(v_1 - v_2)(\pm_1 4) \pm (v_2 - v_3)(\pm_2 4) \pm (v_3 - v_4)(\pm_3 4) \pm (v_4 - v_1)(\pm_4 4) = 0 \ , \\ (v_1 - v_2)(\pm_1 4) \pm (v_1 - v_2)(\pm_2 4) \pm (v_3 - v_4)(\pm_3 4) \pm (v_3 - v_4)(\pm_4 4) = 0 \ .\end{aligned} \tag{126}$$

  Since the signs of the fixed points are constrained, it is not always possible to trivially solve the RC equation.

  Moreover, it is also impossible to find general non-trivial solutions by using the topological constraint to force some of the v_i to be equal. For the first equation, we need all the v_i to be equal. To do so, we need at least three equations, but the topological constraint provides only two. In the second case, we can impose $v_1 = v_2$ and $v_3 = v_4$ with the following ZZPs: $(1, 0)$, $(-1, 0)$, $(0, 1)$ and $(0, -1)$, which define the conifold singularity. Unfortunately, the conifold gives rise to an RC of the first kind, not of the second one.

To conclude, this partial analysis retained only one toric diagram that can accommodate any signs for its fixed points: flat space. We eventually found some particular trapezoids for which we can freely chose the signs of the tensors when only two are present, but those singularities also allow *in principle* for fixed point orientifolds with four tensors, where our analysis showed its limits. Thus, we cannot say in general that they provide every kind of anomaly-free orientifolds. As an illustrative example, one can check that the orientifold of fig. 30a with four tensors does not allow for every combination of signs satisfying the sign rule, although it does with only two tensors.

It would be interesting to investigate further whether it is possible to determine the solvability of the ACC from the toric diagram. We leave this question for future work. In the meantime, orientifolds with four self-identified ZZPs need to be studied in a case by case basis.

4.5 Conclusions

In this section we studied anomalies in gauge theories living on D-branes probing orientifolds of toric singularities, focusing on pure D3-brane theories, namely without the addition of extra flavors.

We introduced a new, geometric algorithm for finding anomaly-free solutions based on zig-zag paths. The main virtue of this procedure is not so much its practicality over the direct solution of the ACC in explicit examples, but the fact that it allows us to make general statements regarding anomalies directly from geometry. Indeed, we managed to derive stringent no-go theorems that establish the conditions for anomaly-free solutions in these orientifolds. Such results are extremely useful, since until now the cancellation of anomalies in this class of theories was analyzed on a case-by-case basis.

We can summarize our findings as follows, from the most stringent case to the less conclusive one:

- For orientifolds with a fixed diagonal line, for which one has to choose only one sign, we find that only singularities whose toric diagram is a trapezoid with respect to the diagonal axis of symmetry allow for a non-anomalous D-brane gauge theory.

- For orientifolds with fixed horizontal lines, we have two signs to choose. All singularities lead to anomaly-free theories if the two signs are chosen to be opposite to each other. If the singularity has a toric diagram which is a trapezoid with respect to the vertical axis of symmetry, then the theory is non-anomalous also for equal signs.

- For orientifolds with fixed points, there are four signs to choose, up to a constraint on their product. Moreover, the relation between the fixed points in the dimer and the toric diagram of the singularity is less direct. Because of these two facts, it is more difficult to summarize the few instances where a restriction is indeed obtained on the singularities that lead to non-anomalous theories. The particular cases have been detailed in section 4.4.3.

As an illustration of the power of the ideas introduced in this section, in section 7 we will use them to guide the search of models of D-branes at singularities that display dynamical supersymmetry breaking.

5 New orientifold projections: the Klein bottle

In this section we construct a new orientifold projection in dimer models corresponding to a glide involution of the fundamental cell. This projection has the remarkable property that the orientifolded theory is superconformal, despite the presence of O-planes.

The result of this chapter completes the dictionary between orientifold projections and smooth toric involutions.

5.1 Torus involutions

There are five inequivalent non-trivial smooth involutions [29], i.e. involutive diffeomorphisms, on a torus[7]. Three of them have a fixed locus and the two others do not. To list all of them we consider a square torus, with complex structure[8] $\tau = i$. We take z as the complex coordinate on the torus, the periodicity condition is $z \sim z + m + ni$, with $m, n \in \mathbb{Z}$. The involutions are given by:

1. Two fixed lines: $z \to \bar{z}$. The fixed loci are two parallel lines located at $\mathrm{Im}(z) = 0, 1/2$ along the real axis. Under this involution the torus is projected to an annulus.

2. Single fixed line: $z \to i\bar{z}$. The fixed line is $\mathrm{Re}(z) = \mathrm{Im}(z)$, corresponding to a diagonal line of the unit cell. The resulting surface is a Moebius strip.

3. Fixed points: $z \to -z$. In this case we have four fixed points, $z = 0, 1/2, i/2$ and $(1+i)/2$. The resulting topology is that of a sphere.

4. Glide reflection: $z \to \bar{z}+1/2$. There are no fixed loci. The resulting topology is that of a Klein bottle.

5. Shift: $z \to z + 1/2$. Again, the involution has no fixed loci. The torus is projected to another torus.

As already mentioned, 1, 2 and 3 are involutions with fixed loci correspond to orientifold operations already studied in the literature. In this section, we will focus on 4, the glide reflection, studying the consistency of such projection and its properties. Regarding involution 5, we will show that the shift is not compatible with the required properties to preserve supersymmetry.

[7] They are classified by the topology of their orbit set which is always one of the parabolic 2-orbifolds listed in [30].

[8] We are interested only in smooth involutions, the complex structure doesn't play any role in the analysis, thus we fixed it to a handy value. The use of complex coordinates will be useful for later observations.

Let us ad some comments on the properties involutions should respect. First, involutions with fixed loci teach us that if the involution is holomorphic, $z \to f(z)$, nodes in the dimer are mapped to nodes of opposite color, while if it is antiholomorphic, $z \to f(\bar{z})$, nodes are mapped to nodes of the same color. This is a requirement from the orientifold mapping of chiral superfields. It gives us a hint for the unexplored involutions. Indeed, we expect 5 to be consistent with an orientifold identification only if nodes are mapped to nodes of the opposite color, while 4 would be consistent only if the mapping is between vertices of the same color. Second, we stress that the involution should be not only a symmetry for the torus, but also for the embedded dimer model. In particular, a generic fundamental cell for a dimer model has the shape of a parallelogram. The symmetry may be present in the abstract graph, but in order to be shown explicitly, consider the case of say 2, one has to deform the embedding in such a way that the resulting fundamental cell is now a rhombus, displaying a symmetry with respect to one of the diagonals. From this observation we conclude that in order to display a glide symmetry, the fundamental cell must be a rectangle. Third, a $\mathbb{Z}_2$ glide reflection with diagonal axis is described by the map $z \to i\bar{z} + (1+i)/2$ which has $\Re(z) = \Im(z) + 1/2$ as fixed line, hence they are nothing else than reflections about a diagonal axis. In particular, they do not correspond to a class of smooth involutions not listed above.

5.2 Glide Orientifolds

In this section we investigate glide reflection orientifolds. We start with orbifold examples, motivating our results in the dimer from the open string projection on the Chan-Paton indices. We also explicitly check that it preserves supersymmetry, in particular, it acts on the CY 3-form as $\Omega_3 \to -\Omega_3$. We extend our results to orbifolds of the conifold, considering the cascade in the presence of deformation fractional branes. Finally, we discuss anomalies, or rather their absence, and conformality in the presence of these orientifolds.

5.2.1 Orbifold $\mathbb{C}^2/\mathbb{Z}_2$

We consider the recipe directly applied in the dimer and then check that it is indeed predicted by open-string computation.

Projection on the dimer model. We present in fig. 32 the dimer for the orbifold $\mathbb{C}^2/\mathbb{Z}_2$ where the glide reflection is a combined operation of a horizontal shift by one half of the length of the unit cell followed by a reflection with respect to the dashed red horizontal axis. Nodes are mapped to nodes of the same color, as we want from the analysis in section 5.1. Note that this operation leaves no

(a) (b)

Figure 32: (a) Dimer diagram for the orbifold $\mathbb{C}^2/\mathbb{Z}_2 \times \mathbb{C}$. The unit cell and the reflection axis are depicted in blue and red respectively. (b) The Klein bottle we obtain with the orientifold projection.

fixed loci in the unit cell. The projected theory is embedded in a Klein Bottle drawn on one half of the original unit cell, as illustrated in fig. 32b.

The edge X_{12} is identified with Y_{12}, X_{21} with Y_{21} and Z_{11} with Z_{22}. Following the rules summarized in section 2.4.2, the resulting theory has gauge group $SU(N)_1$ with matter content given by two tensors[9] and one adjoint field. Note that the tensor fields are not in an irreducible representation, so we split them in their symmetric and antisymmetric parts;

$$\begin{aligned} \mathcal{X}_{S,A} &= \overline{\square\square}_{\,1},\ \overline{\begin{smallmatrix}\square\\\square\end{smallmatrix}}_{\,1}\,, \\ \mathcal{Y}_{S,A} &= \square\square_{\,1},\ \begin{smallmatrix}\square\\\square\end{smallmatrix}_{\,1}\,, \\ \mathcal{Z} &= \mathrm{Adj}_1\,. \end{aligned} \tag{127}$$

The superpotential is obtained by explicitly projecting the original one and keeping half of the terms,

$$W = \mathcal{X}\mathcal{Y}\mathcal{Z}^T - \mathcal{Y}\mathcal{X}\mathcal{Z} = \mathcal{X}_A\mathcal{Y}_S\mathcal{Z} - \mathcal{X}_S\mathcal{Y}_A\mathcal{Z}\,. \tag{128}$$

In a SUSY-preserving orientifold in type IIB, the holomorphic 3-form must map to minus itself. This is easy to check by noting that the orientifold action on the mesons is

$$x \leftrightarrow y \qquad w \to w \qquad z \to z\,. \tag{129}$$

The action on the 3-form is then

$$\Omega_3 = \frac{\mathrm{d}x \wedge \mathrm{d}y \wedge \mathrm{d}z}{2w} \to \frac{\mathrm{d}y \wedge \mathrm{d}x \wedge \mathrm{d}z}{2w} = -\Omega_3\,. \tag{130}$$

[9]The two tensors are of the form ($\overline{\square}_{\,1}$, $\overline{\square}_{\,1}$) and ($\square_{\,1}$, $\square_{\,1}$).

It is also clear from the matter content and the first equality of eq. (128) that the gauge theory preserves $\mathcal{N}=2$ supersymmetry[10].

It is worth noting that the theory, unlike many examples of projections with fixed loci, is free from any local gauge anomaly, regardless of the gauge group rank. Although this example is rather trivial, we will see that this feature is general and related to tensor fields being absent or coming in pairs, symmetric and antisymmetric, cancelling each other's contribution to the anomaly cancellation conditions (ACC). We also note that the projected theory is actually conformal. Indeed, the β-function of the gauge group can be shown to be zero. The fact that these orientifolds naturally lead to SCFT's will be discussed in section 5.4.

Open string projection. We now consider the orientifold projection on the Chan-Paton indices of the open string spectrum. For D-branes localized on the $\mathbb{C}^2/\mathbb{Z}_2\times\mathbb{C}$ singularity the open string spectrum is obtained by promoting the flat space one to $2N\times 2N$ matrices with a restricted set of non-zero entries:

$$A_\mu=\begin{pmatrix} A_{1\mu} & 0\\ 0 & A_{2\mu}\end{pmatrix},\quad \Phi_1=\begin{pmatrix} 0 & X_{12}\\ X_{21} & 0\end{pmatrix},\quad \Phi_2=\begin{pmatrix} 0 & Y_{12}\\ Y_{21} & 0\end{pmatrix},\quad \Phi_3=\begin{pmatrix} Z_{11} & 0\\ 0 & Z_{22}\end{pmatrix}, \tag{131}$$

where the gauge group is $SU(N)_1\times SU(N)_2$ and matther fields transform in the following representations,

$$X_{ij},Y_{ij}=(\ \square_{\,i},\ \overline{\square}_{\,j}),\quad Z_{ii}=\mathrm{Adj}_i\,. \tag{132}$$

Decomposing the $\mathbb{C}^3$ fields the orbifold superpotential becomes,

$$\begin{aligned} W &= [\Phi_1,\Phi_2]\,\Phi_3\\ &= X_{12}Y_{21}Z_{11}-Y_{21}X_{12}Z_{22}+X_{21}Y_{12}Z_{22}-Y_{12}X_{21}Z_{11}\,, \end{aligned} \tag{133}$$

where an overall trace over gauge indices is understood.

A general orientifold projection on the $\mathbb{C}^3$ fields acts as,

$$A_\mu = -\gamma_\Omega A_\mu^T\gamma_\Omega^{-1}\,, \tag{134}$$

$$\Phi_i = R_{ij}\gamma_\Omega\Phi_j^T\gamma_\Omega^{-1}\,, \tag{135}$$

where γ_Ω is a $2N\times 2N$ matrix acting on gauge group (Chan-Paton) indices and R_{ij} acts on space indices i,j running from 1 to 3. Different choices for these matrices

[10]The attentive reader might have noticed that this orientifolded theory is identical to the one obtained with fixed points in section 2.4.2, although the involution acts differently on the coordinates. This is however an artifact of the orbifold $\mathbb{C}^2/\mathbb{Z}_2$ since glide reflections will not provide tensors in general.

lead to different orientifold projections. In order to reproduce the glide reflection orientifold, we specifically choose

$$\gamma_\Omega = \begin{pmatrix} 0 & \mathbb{1}_N \\ \mathbb{1}_N & 0 \end{pmatrix}, \quad \text{and} \quad R = \begin{pmatrix} 0 & 1 & 0 \\ 1 & 0 & 0 \\ 0 & 0 & 1 \end{pmatrix}, \tag{136}$$

so that Φ_1 and Φ_2 coordinates are exchanged by the orientifold. Section 5.2.1 translates into

$$A_{1\mu} = -A_{2\mu}^T, \tag{137}$$

which tells us that the two gauge groups are now identified as one $SU(N)_1$ in the orientifolded theory. Section 5.2.1 maps the superfields in the following way:

$$\begin{array}{rcrcl} X_{12} & = & Y_{12}^T & \equiv & \mathcal{X}_{A,S}\,, \\ Y_{21} & = & X_{21}^T & \equiv & \mathcal{Y}_{A,S}\,, \\ Z_{11} & = & Z_{22}^T & \equiv & \mathcal{Z}\,. \end{array} \tag{138}$$

We recognise the same field content of the theory obtained with the dimer technique. It is easy then to show that we recover the superpotential advertised in eq. (128) (up to an irrelevant numerical factor). We thus conclude that the glide reflection on the dimer reproduces the orientifold projection we just computed in string theory.

In the following, we discuss the dimer construction in more involved examples. It is clear that not all dimer models have the required symmetry, and in section 5.6 we provide a necessary condition for a given toric CY_3 to admit a glide reflection directly from its toric diagram.

5.2.2 More orbifold examples

The previous example has so much symmetry that it could be misleading. Let us start our journey to less symmetric theories by considering $\mathbb{C}^2/\mathbb{Z}_4$, whose dimer model and relevant involution we present in fig. 33. From the four initial gauge groups, only two of them are kept after the projection, $SU(N_1)_1 \times SU(N_2)_2$. The surviving fields are

$$\begin{array}{lll} \mathcal{X}_{12} = (\,\overline{\square}_1,\,\square_2\,), & \mathcal{X}_{21} = (\,\overline{\square}_2,\,\overline{\square}_1\,), & \mathcal{Y}_{21} = (\,\overline{\square}_2,\,\square_1\,), \\ \mathcal{Y}_{12} = (\,\square_1,\,\square_2\,), & \mathcal{Z}_{11} = \mathrm{Adj}_1\,, & \mathcal{Z}_{22} = \mathrm{Adj}_2\,. \end{array} \tag{139}$$

and the resulting superpotential is found to be

$$W = \mathcal{X}_{12}\mathcal{Y}_{21}\mathcal{Z}_{11} - \mathcal{Y}_{21}\mathcal{X}_{12}\mathcal{Z}_{22} + \mathcal{X}_{21}\mathcal{Y}_{12}\mathcal{Z}_{22} - \mathcal{Y}_{12}\mathcal{X}_{21}\mathcal{Z}_{11}^T\,. \tag{140}$$

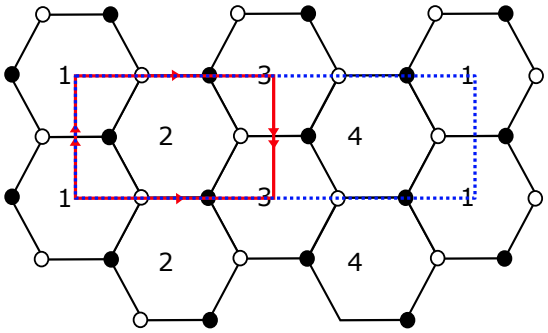

Figure 33: Dimer diagram for the orbifold $\mathbb{C}^2/\mathbb{Z}_4$. The unit cell is depicted in blue and we show in red the Klein bottle obtained from the orientifold projection.

The open string projection computation for this example can be found in appendix D. Note that despite its similarities with the orbifold $\mathbb{C}^2/\mathbb{Z}_2$ (without orientifold), this model has a different matter content, which cannot be obtained from dimer models.

The mapping of the mesons is the same as for $\mathbb{C}^2/\mathbb{Z}_2$ so that the holomorphic 3-form transforms as follows:

$$\Omega_3 = \frac{\mathrm{d}x \wedge \mathrm{d}y \wedge \mathrm{d}z}{4w^3} \to \frac{\mathrm{d}y \wedge \mathrm{d}x \wedge \mathrm{d}z}{4w^3} = -\Omega_3\,, \tag{141}$$

and hence suggests that our projection is indeed supersymmetric and the resulting gauge theory preserves $\mathcal{N} = 2$ supersymmetry. Note that the usual orientifold techniques in the dimer, fixed points and line(s), are not able to reproduce it.

Our observations make it clear that any orbifold $\mathbb{C}^2/\mathbb{Z}_{2n} \times \mathbb{C}$ will admit a glide reflection, for any integer n. More general orbifolds, such as $\mathbb{C}^3/\mathbb{Z}_n$ or $\mathbb{C}^3/\mathbb{Z}_p \times \mathbb{Z}_q$, can also enjoy the glide reflections, see an example in Figure 36a. In section 5.6 we will discuss the general geometric condition a singularity should meet in order to admit such orientifold.

$\mathcal{N} = 2$ fractional branes. Let us briefly comment on the fractional branes of the orientifolded theory [15]. The glide orientifold of $\mathbb{C}^2/\mathbb{Z}_4$ is free of local gauge anomalies for any rank N_1 and N_2. Hence, it has a fractional brane. We find that it is an $\mathcal{N} = 2$ fractional brane corresponding to a subset of the $\mathcal{N} = 2$ fractional branes of the parent theory. In section 5.6.2 we will discuss this fact in detail.

5.3 Conifold-like singularities

As we will explain in section 5.6, the conifold $\mathcal{C}$ itself does not admit a glide reflection, but conifold-like singularities like its orbifold $\mathcal{C}/\mathbb{Z}_2$ or the zeroth Hirzebruch surface F_0 do. We now study those examples in turn.

Non-chiral orbifold of the conifold $\mathcal{C}/\mathbb{Z}_2$. The dimer model and the glide orientifold of $\mathcal{C}/\mathbb{Z}_2$ are shown in fig. 34. The resulting gauge theory has gauge

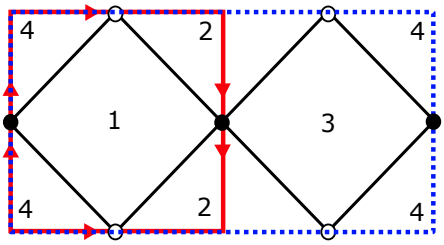

Figure 34: Dimer diagram for the orbifold of the conifold $\mathcal{C}/\mathbb{Z}_2$. The unit cell is depicted in blue and we show in red the Klein bottle obtained from the orientifold projection.

group $SU(N_1) \times SU(N_2)$ with matter content given by

$$\begin{array}{rclcrcl} A & = & (\,\overline{\square}_1,\,\overline{\square}_2\,), & & B & = & (\,\square_1,\,\square_2\,), \\ C & = & (\,\overline{\square}_1,\,\square_2\,), & & D & = & (\,\square_1,\,\overline{\square}_2\,), \end{array} \tag{142}$$

Note in passing that the ACC do not impose any constraint on the ranks, so that N_1 and N_2 may be chosen independently. The superpotential reads

$$W = ABCD - BAC^T D^T\,. \tag{143}$$

For details of computations using worldsheet techniques and a proof that the 3-form is odd under the orientifold action, see appendix E.1.

Zeroth Hirzebruch surface F_0. We show the dimer model and the glide orientifold of F_0 in fig. 35. After projection the gauge group becomes $SU(N_1)\times SU(N_2)$, while the matter content is given by

$$\begin{array}{rclcrcl} X & = & (\,\square_1,\,\overline{\square}_2\,), & & Y & = & (\,\square_1,\,\overline{\square}_2\,), \\ U_{S,A} & = & \overline{\square\square}_1,\,\overline{\square}_1\,, & & Z_{S,A} & = & \square\square_2,\,\square_2\,, \end{array} \tag{144}$$

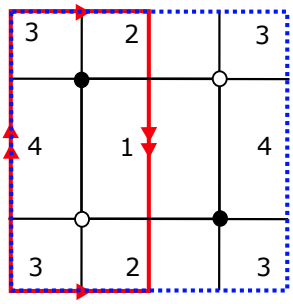

Figure 35: Dimer diagram for the Hirzebruch surface F_0. The unit cell is depicted in blue and we show in red the Klein bottle obtained from the orientifold projection.

In this case the ACC impose non-trivial constraints on the gauge group ranks, in particular they must be the same, $N_1 = N_2$. The superpotential reads

$$W = XU_S Y^T Z_A - X^T Z_S Y U_A \,. \tag{145}$$

The Chan-Paton computation and a proof that the 3-form is odd under the orientifold action are found in appendix E.2.

Deformation fractional branes. We have seen that the $\mathcal{C}/\mathbb{Z}_2$ glide reflection admits fractional brane since the ranks of the two gauge groups may be chosen freely. It is in fact a deformation brane [15, 24] of the parent theory that survives the orientifold projection, in the precise sense described in [3]. A natural question is whether such fractional branes may trigger a non-trivial RG-flow giving rise to a cascade of Seiberg dualities [31, 32]. We study this process in appendix E.3 and verify that the cascade steps are: $SU(N+M)_1 \times SU(N)_2 \to SU(N-M)_1 \times SU(N)_2$, with the same matter content and superpotential, as we flow towards the IR. For N being a multiple of M, the deep IR of this gauge theory is expected to reproduce the same features as for a deformed conifold. Notably, on the baryonic branch one finds the vacuum of SYM, displaying confinement and chiral symmetry breaking.

We will see later that it is a fact that the orbifolds of the conifold $\mathcal{C}/\mathbb{Z}_m \times \mathbb{Z}_n$ compatible with the glide projection preserve some of their deformation branes. The compatibility of fractional branes of the parent theory with the glide reflection is discussed in section 5.6.

5.4 General properties

As we have seen, and since the glide reflection leaves no fixed loci, we don't expect any self-identified face (i.e. SO or USp gauge group) to show up in the dimer

projection. This restricts the number of gauge groups of the parent theory to be even. A further consequence of not having fixed loci is that there are no self-identified bifundamentals, therefore, tensor matter, if present, always comes in antisymmetric-symmetric pairs, cancelling the contributions to the chiral anomaly. This is precisely what happens in the $\mathbb{C}^2/\mathbb{Z}_2$ orbifold, where two edges, charged under two identified groups, are identified, leading to a reducible two index tensor, which splits into the sum of a symmetric and an antisymmetric one. We now see how these facts translates in the absence of non-homogenous terms in the anomaly cancellation conditions, allowing always a solution to the latter, and how such projected theories are actually SCFTs.

Borrowing the notation of [3], we know that the ACC matrix of the projected theory is deduced from that of the parent theory. Denote the latter as,

$$A = \left(\begin{array}{c|c|c} B_{11} & B_{12} & B_{13} \\ \hline B_{21} & B_{22} & B_{23} \\ \hline B_{31} & B_{32} & B_{33} \end{array} \right) \begin{array}{l} \} i \\ \} i+k \\ \} a \end{array} \quad , \tag{146}$$
$$\underbrace{\phantom{B_{11}}}_{j} \quad \underbrace{\phantom{B_{12}}}_{j+k} \quad \underbrace{\phantom{B_{13}}}_{b}$$

where indices $i, j = 1, \ldots, k$ label the gauge groups surviving the orientifold projection and the corresponding entries represent the anomaly contribution of the field between faces i and j. Indices $i+k$ and $j+k$ represent gauge groups that are identified with i and j under the orientifold action, respectively. The a, b indices label the self identified gauge groups. Finally, the ACC system takes the form

$$A \cdot N = 0 \,, \tag{147}$$

where N is a vector whose entries, $N_{(j|j+k|a)}$ are the ranks of the corresponding gauge group.

From what we said earlier, we know that $B_{\star 3} = B_{3\star} = B_{33} = 0$, since there are no self-identified gauge groups. Furthermore, we have no net contributions from tensors to the ACC, meaning that there are no non-homogenous terms in the projected theory ACC. From [3], we know that the projected ACC can be written as

$$\overline{A} \cdot N = \left(\; B_{11} + B_{12} \; \right) \cdot N = 0 \,. \tag{148}$$

It is then easy to see that the all-equal-rank solution in the parent theory is still a solution. Indeed, a general solution for the orientifolded theory has a trivial part, corresponding to a stack of regular branes in the parent theory, and a non-trivial part, corresponding to "symmetric" fractional branes of the parent theory.

Fixed loci orientifolds have the remarkable property of producing, in general, non-conformal theories. However, this is not true for glide orientifolds. The theory they describe is an SCFT when the ranks of the gauge groups are all the same. This fact can be seen as follows, consider the β-function of the parent theory with N probes D-branes,

$$\beta_{SU(N)_i} = 3N - \sum_{i=1}^{n} \frac{N}{2}(1-\gamma_i) = 0\,, \tag{149}$$

where γ_i are the anomalous dimensions of the matter fields[11]. From this we can read the β-function of the projected theory whose general form is

$$\beta_{SU(N)_i} = 3N - \sum_{i=1}^{n} \frac{N+b_i}{2}(1-\gamma_i)\,, \tag{150}$$

where the coefficients b_i vanish for fundamental fields and are ± 2 for, respectively, symmetric or antisymmetric fields. If we assume that the anomalous dimensions of the fields are the same up to $1/N$ corrections and, since all tensors come in pairs of opposite parity, we see that the β-function of the gauge groups of the projected theory vanishes as long as all ranks are equal. This dovetails the fact that a Klein Bottle has zero Euler characteristic and, as explained in [19], such surfaces may embed a dimer model describing an SCFT[12]. Franco and Vegh pointed out that the Franklin graph would be a good candidate to be embedded in a Klein Bottle and host a SCFT not embedded in a torus. Indeed, it can be readily found via a glide reflection of $\mathbb{C}^3/\mathbb{Z}_{12}$, see fig. 36. This not only confirms their intuition, but it is, to the best or our knowledge, the first instance of such a construction within string theory.

5.5 Type IIA picture and the brane tiling

Fixed loci in the dimer have been related to actual orientifold planes in the physical realization of the dimer [21, 35]. In fact, one may consider the D3-branes probing a singularity with an orientifold and track the position of the orientifold in the

[11] We consider Adj fields as couple of anti-fundamentals fields charged under the same gauge group.

[12] Other kind of surfaces obtained from orientifolds with fixed loci were found to accommodate SCFTs in [33, 34].

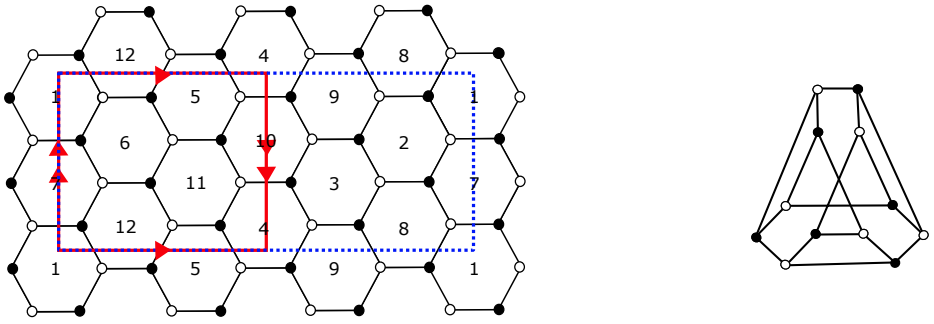

(a) (b)

Figure 36: (a) Dimer diagram for the orbifold $\mathbb{C}^3/\mathbb{Z}_{12}$ with action $(1, 5, 6)$. The unit cell and the Klein bottle are depicted in blue and red respectively. (b) The Franklin graph.

ambient space to the fixed loci in the dimer through T-dualities. An immediate puzzle arises in the case of glide orientifolds, since there are no fixed loci on the torus, i.e. in the brane tiling. In this section we look at $\mathbb{C}^2/\mathbb{Z}_2$ and argue that these orientifolds, which have 8-dimensional fixed loci in the D3 picture (they are O7-planes), don't have a fixed locus in the tiling in the precise sense of [36, 37]. In the latter reference, the shift action is deduced to be T-dual to a pair of opposite charge O-planes on a circle.

Let us again consider N D3-branes at the tip of a singular toric CY_3. As reviewed in the introduction, the dimer presented in fig. 32 is physically realized as a web of D5 and NS5-branes. It is obtained by T-duality along two of the three toric cycles of the toric variety. In particular along those corresponding to mesonic symmetries in the field theory, rather than R-symmetry. Focusing on the case at hand, $\mathbb{C}^2/\mathbb{Z}_2 \times \mathbb{C}$, one may take local coordinates such that x_7, x_9 correspond to the two toric cycles that are to be T-dualized. The D-brane configuration is then as in table 4 which, after two T-duality should become that of table 5. Note that we have avoided including an orientifold plane in the T-dual, as the dimer shift seems to suggest.

After T-duality one finds D5-branes wrapping the dual cycles with local coordinates x'_7, x'_9. These are in turn identified as the coordinates of the torus $\mathbb{T}^2$ where the 5-brane web lives.

To study the location of the O-plane in the singular geometry, let us introduce the coordinates z_1, z_2 and z_3 of flat space $\mathbb{C}^3$. We define the coordinates of the variety transverse to the D3-branes, $\mathbb{C}^2/\mathbb{Z}_2 \times \mathbb{C}$, by constructing invariants under

	0	1	2	3	4	5	6	7	8	9
$\mathbb{C}^2/\mathbb{Z}_2$					$\times$	$\times$	$\times$	$\times$		
D3	$\times$	$\times$	$\times$	$\times$						
O7	$\times$	$\times$	$\times$	$\times$	$\times$	$\times$			$\times$	$\times$

Table 4: D3-branes sitting at the tip of $\mathbb{C}^2/\mathbb{Z}_2$ in the presence of O7-planes.

	0	1	2	3	4	5	6	$7'$	8	$9'$
NS5	$\times$	$\times$	$\times$	$\times$			$-$	$-$	Σ	$-$ $-$
D5	$\times$	$\times$	$\times$	$\times$				$\times$		$\times$

Table 5: The brane tiling. Σ is the holomorphic curve in the $67'89'$-space wrapped by the NS5-brane.

the orbifold action:

$$x = z_1^2\,, \quad y = z_2^2, \quad w = z_1 z_2, \quad \text{and} \quad z = z_3\,, \tag{151}$$

with the following relation holding,

$$xy = w^2\,. \tag{152}$$

As explained in section 5.2.1, the orientifold action on the dimer implies that it acts on z_1, z_2, z_3 as $z_1 \leftrightarrow z_2$,. In terms of the orbifold invariant coordinates the orientifold action is then,

$$x \leftrightarrow y\,, \quad w \text{ and } z \text{ fixed.} \tag{153}$$

Thus, the orientifold plane extends on the surface defined by $x = y = t$, $t^2 = w^2$. From eq. (152) we read two toric $U(1)$ isometries of the orbifold:

$$\begin{array}{lllll} U(1)_\alpha : & x \to e^{i\alpha} x\,, & y \to e^{-i\alpha} y\,, & w \to w\,, \\ U(1)_\beta : & x \to e^{i\beta} x\,, & y \to e^{i\beta} y\,, & w \to e^{i\beta} w\,. \end{array} \tag{154}$$

We can think about these two isometries as generators of two 1-cycles, α, β. We can introduce local coordinates parametrizing these cycles, defined whenever they are non-singular,

$$\theta_\alpha \equiv \frac{1}{2}\left(\mathrm{Arg}(x) - \mathrm{Arg}(y)\right) \tag{155}$$

$$\theta_\beta \equiv \frac{1}{2}\left(\mathrm{Arg}(x) + \mathrm{Arg}(y)\right) \tag{156}$$

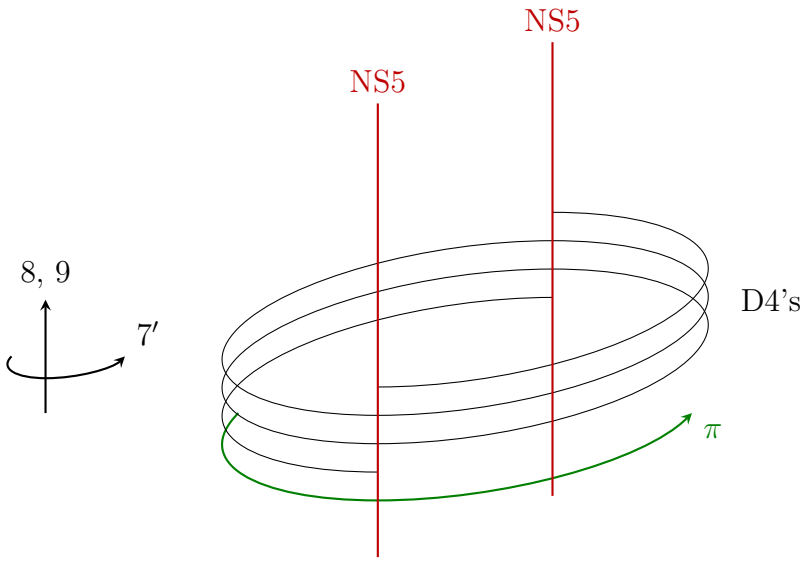

Figure 37: Type IIA picture with the orientifold mapping given by a π rotation along x_7' (in green).

We can now identify these two coordinates in terms of the coordinates in table 4: $(\theta_\alpha, \theta_\beta) \sim (x_7, x_5)$. The action of the orientifold on these two cycles, T-dual to the physical torus, are just $\theta_\alpha \to -\theta_\alpha$, $\theta_\beta \to \theta_\beta$. We thus learn that the orientifold plane spans x_5 and is located at $x_7 = 0, \pi$. In fact, there are two orientifold planes of opposite charge such that the total flux cancels with no further sources. One may also argue for the signs being opposite by noting the absence of net RR-charges coming from the O-planes in the dimer picture. This can be seen in the absence of SO/USp groups and the corresponding lack of non-homogeneous terms in the ACC, which can be thought of as Gauss law for compact cycles. Quite remarkably, the T-dual of such a cycle with opposite-charge O-planes, is known to be precisely an orientifold acting as a shift on the T-dual cycle. The absence of fixed loci for this action translates into the absence of O-plane in the dual geometry. This is described in [37] where T-duality acts as a sort of Fourier transform: the O-planes of opposite charge are related to delta function whose transform are constant and opposite, cancelling each other. This interpretation nicely match the Gauss law analogy we presented earlier.

After one T-duality along x_7, the T-dual Type IIA construction is analogous to the ones studied in [38, 39, 40, 41, 42]. The relevant information is encoded in a cycle x_7' where D4-branes are suspended between two NS5-branes. As we explained before, the orientifold action acts now as a shift, rotating halfway the configuration, see fig. 37. This action is consistent with the mapping of gauge groups and matter fields on the dimer model.

Finally, if we further T-dualize along the direction spanned by NS5-branes x_9, we get to the tiling picture. After the last T-duality, the orientifold acts on x'_9 as a reflection[13]. Together with the shift on x'_7, these actions reproduce the glide reflection that we see on the tiling.

5.6 Involutions and Zig-Zag Paths

In this section, we first develop, in section 5.6.1, a condition the toric diagram (or equivalently, the ZZP's) of a singularity must satisfy to be compatible with the glide reflection. This enlarges the dictionary between orientifold projections of a given toric singularity and its ZZPs content, as initiated by [27]. Secondly, and with the help of ZZP techniques [24], we show in section 5.6.2 how to detect the presence of fractional branes in the orientifolded singularity. Finally, in section 5.7, we give a general proof that the "would be" shift orientifold projection is incompatible with the requirement to preserve SUSY.

5.6.1 Glide Orientifold from the Toric Diagram

A glide reflection can be seen as a combination of a shift and a reflection in the dimer model, even if each of them is not a symmetry per se. Starting from what we learned in our examples and using this simple observation, we can understand how this involution acts on the ZZP content of the toric diagram.

First of all, we notice that the shift and the reflection are performed along the same axis. Consider, for instance, a horizontal shift and axis of reflection as in fig. 38. The action of the glide reflection reverts the horizontal component of each ZZP. Actually, the glide reflection leaves no fixed ZZPs, since even those perpendicular to the axis are mapped among themselves because of the shift part of the glide reflection.

Putting the two observations together we can say that: if the glide reflection is composed by a *horizontal shift and a reflection axis*, directed as $(1, 0)$ in the dimer, ZZPs are mapped as follows: (p, q) is sent to $(-p, q)$ when $p \neq 0$, while all other ZZPs of the form $(0, \pm 1)$ are mapped to one another, preserving the orientation, meaning that they come in even numbers. In our example of fig. 39, the orange $(1, 1)$ and purple $(-1, 1)$ ZZPs are interchanged. The same is true for the blue and green ZZPs of the $(0, -1)$ type.

Similarly, in order to construct a Klein bottle with a *vertical shift and reflection axis*, the toric diagram should have ZZPs $(1, 0)$ and $(-1, 0)$ in even numbers, possibly different, and ZZPs (p, q) with $q \neq 0$ paired with ZZPs $(p, -q)$.

[13]This is a standard fact of orientifolds. Upon T-duality along a direction spanned by the O-plane, an Op-plane is mapped to an O$(p-1)$-plane, with action $\theta \to -\theta$ on the dual cycle.

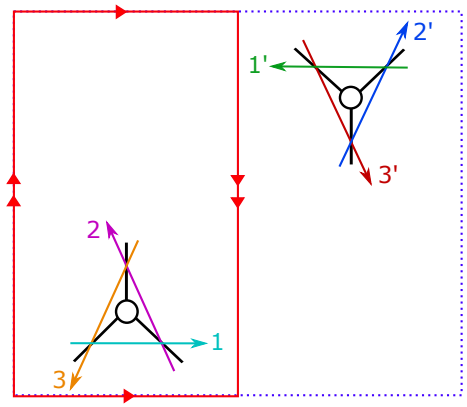

Figure 38: The glide orientifold maps together nodes of the same color. The dashed blue line delineates the unit cell of the parent theory, while the red frame represents the orientifold. The ZZPs $1, 2, 3$ are mapped to $1', 2', 3'$ respectively.

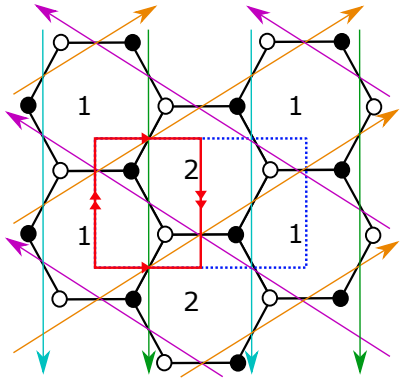

Figure 39: The Klein bottle obtained from the dimer of $\mathbb{C}^2/\mathbb{Z}_2 \times \mathbb{C}$ and the corresponding ZZPs.

These statements can be summarized by saying that the toric diagram should be symmetric with respect to a vertical or horizontal axis. Moreover, each ZZP has to be mapped to another one, imposing that each kind of ZZP parallel to the axis of reflection in the toric plane should come in even numbers. We show in fig. 40 that our examples of section 5.2 satisfy this criterion.

Lastly, an important remark is that this condition may not be satisfied in some of the $SL(2,\mathbb{Z})$ "frames" of the toric diagram, or equivalently, the unit cell in the dimer model may not be symmetric with respect to the glide reflection. Thus, we should state that a generic toric diagram can admit a glide orientifold if it satisfies the conditions above *up to a* $SL(2,\mathbb{Z})$ *action* that can bring its unit cell

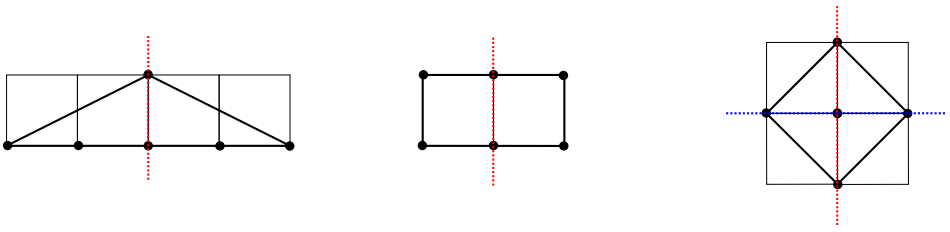

(a) (b) (c)

Figure 40: Toric diagrams for singularities that satisfy our necessary criterion to admit one (with an axis of reflection in red) or two (with the second axis of reflection in blue) glide projections: (a) orbifold $\mathbb{C}^2/\mathbb{Z}_4$, (b) conifold-like $\mathcal{C}/\mathbb{Z}_2$, and (c) zeroth Hirzebruch surface F_0.

to a symmetric form with respect to the glide.

5.6.2 Fractional branes

As already mentioned in section 5.4, these orientifolded theories may admit non-trivial rank assignments, i.e. fractional branes. Their presence can be deduced from the symmetries of the toric diagram and they can be seen as inherited from the "parent" theory. Following [24, 3], in what we dub "Butti's Algorithm", we can assign a value v_Γ to each of the n ZZPs of the toric diagram. These values give rise to anomaly free rank assignments, given that they satisfy the following constraints,

$$\begin{cases} \sum_\Gamma v_\Gamma p_\Gamma = 0 \\ \sum_\Gamma v_\Gamma q_\Gamma = 0 \end{cases} , \tag{157}$$

where the (p_Γ, q_Γ) are the winding numbers of the ZZP associated to v_Γ.

Since we know how the glide reflection acts on the ZZPs, we may follow the procedure of [3] to see which fractional branes survive the projection. As explained there, only *symmetric* fractional branes survive, in the sense that, given two ZZPs v_α and $v_{\bar\alpha}$ mapped to each other under the glide reflection, only rank assignments satisfying the following identification survive,

$$v_\alpha = v_{\bar\alpha} \,. \tag{158}$$

The orientifold projection thus reduces the number of variables v_Γ to the subset of v_α. Moreover, one can check that eq. (157) leaves only one non-trivial relation:

$$\sum_\alpha v_\alpha q_\alpha = 0 \,. \tag{159}$$

Butti's algorithm has a redundancy that allows to perform a global shift on the v_α without affecting the ranks of the gauge groups. Hence, we end up with

$$\#\text{fractional branes} = n/2 - 2 \tag{160}$$

in the orientifolded theory.

Butti's algorithm also tells how to construct different kind of fractional branes in the parent theory by specifying a set of v_Γ. We now apply this method to theories with a glide reflection orientifold to see when may $\mathcal{N} = 2$ and deformation fractional branes arise.

- $\mathcal{N} = 2$ fractional branes: The parent theory admits such fractional branes whenever the toric diagram hosts $k > 1$ ZZPs with the same winding numbers, say (p_μ, q_μ). They are turned on whenever only some of these v_μ, among the whole set of ZZPs $\{v_\Gamma\}$, are non-vanishing. Following eq. (157), one has

$$\sum_{i=1}^{k} v_{\mu_i} = 0\,, \qquad \text{and } \; v_\nu = 0 \;\text{ if }\; (p_\nu, q_\nu) \neq (p_\mu, q_\mu)\,. \tag{161}$$

  This condition is compatible with eq. (158) only if the k ZZPs are sent to ZZPs with the same winding numbers by the glide reflection, restricting to $(0, 1)$ or $(0, -1)$ when (p, q) is mapped to $(-p, q)$. Moreover, k should be a multiple of 4, since for each couple of ZZPs with a symmetric assignment v, we need a second couple with assignment $-v$ in order to satisfy the sum in eq. (161). In the examples of section 5.2, we found that the singularity $\mathbb{C}^2/\mathbb{Z}_4$ satisfies this criterion, see fig. 41a.

- Deformation fractional branes: The parent theory will have a deformation fractional brane if there is a subset of m ZZPs in equilibrium $\{v_\sigma\} \subset \{v_\Gamma\}$:

$$\sum_{i=1}^{m} (p_{\sigma_i}, q_{\sigma_i}) = 0\,. \tag{162}$$

  The deformation brane is turned on whenever all v_σ have the same non-zero value and all other $v_\tau \notin \{v_\sigma\}$ are vanishing. A glide reflection orientifold theory will have a deformation brane if there is a subset of m ZZPs in equilibrium where each ZZP is accompanied by its image under the glide action, and where m is smaller than n. In the examples of section 5.2, we found that $\mathcal{C}/\mathbb{Z}_2$ satisfies this criterion while the zeroth Hirzebruch surface F_0 does not, see fig. 41b and fig. 41c.

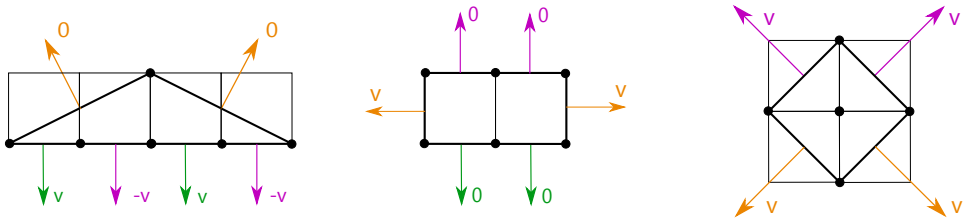

(a) (b) (c)

Figure 41: Symmetric fractional branes in the parent theory lead to fractional branes in its glide orientifolded version. Couples of ZZPs paired by the glide action are drawn in the same color. (a) $\mathcal{N} = 2$ fractional brane in $\mathbb{C}^2/\mathbb{Z}_4$, (b) deformation fractional brane in $\mathcal{C}/\mathbb{Z}_2$, and (c) the zeroth Hirzebruch surface F_0 admits only the regular brane as a symmetric fractional brane.

5.7 Shift Orientifolds

So far we have only considered orientifolds acting as glide reflections on the dimer. Now we address those acting as a simple shift. We have not discussed these orientifolds earlier because they always break supersymmetry, as we show in the following. In particular, we will see that the holomorphic 3-form Ω_3 is even under such an orientifold action, contradicting the rule of thumb that it should be odd.

As we observed in Section 5.1, the shift involution must identify nodes of opposite colors on the dimer, in order to be consistent with the orientifold identification rules. Under such a shift, each ZZP is mapped to a ZZP of opposite winding numbers, $(p, q) \to (-p, -q)$. This can be easily deduced from Figure 42.

From the toric diagram, it is possible to obtain the equations defining associated toric variety probed by the D-branes. To do so we need to compute the integer generators of the dual cone to the toric diagram. This procedure is standard in toric geometry and we refer to [43] for all the details. From the lattice vertices on the boundary of the toric diagram (r_i, s_i), we obtain the generators of the cone given by $m_i = (r_i, s_i, 1)$. The dual cone is then given by

$$S^\vee = \{n \in \mathbb{R}^3 | m_i \cdot n \geq 0\}\,, \tag{163}$$

from which it is easy to see that the vectors n are of the form (p, q, a), where (p, q) are the windings of the ZZPs and a is an integer. Indeed, the generators of the dual cone are nothing but the inward pointing vectors, normal to the faces of the cone generated by the m_i. We now need to add the extra generators to span the dual integer cone, $\sigma^\vee = S^\vee \cap \mathbb{Z}^3$. This is achieved by computing linear combinations of the generators with positive rational coefficient and adding all integer vectors we obtain this way. Finally, the equations defining our singularity are given by

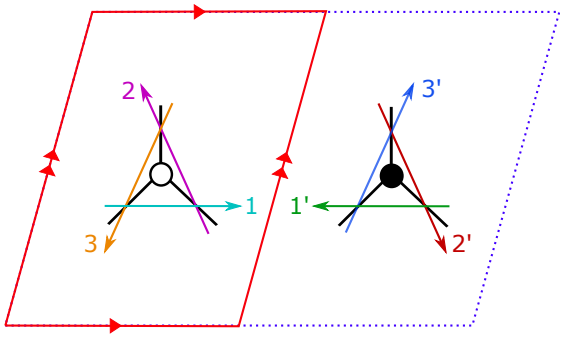

Figure 42: The shift orientifold maps white nodes to black nodes, and vice-versa. The dashed blue line delineates the unit cell of the parent theory, while the red frame represents the orientifold. The ZZPs $1, 2, 3$ are mapped to $1', 2', 3'$ respectively.

associating complex coordinates to the generators of the integer dual cone and the relations among them are obtained with the following identification,

$$n_1 + n_2 + \cdots = n_4 + n_5 + \cdots \quad \rightarrow \quad z_1 z_2 \cdots = z_4 z_5 \cdots . \tag{164}$$

For example, let us consider the toric diagram of the conifold, which we place in $\mathbb{Z}^2$ as the square with vertices $(0,0), (0,1), (1,1), (0,1)$. The associated cone is

$$\sigma = \left\langle \begin{pmatrix} 0 \\ 0 \\ 1 \end{pmatrix}, \begin{pmatrix} 0 \\ 1 \\ 1 \end{pmatrix}, \begin{pmatrix} 1 \\ 1 \\ 1 \end{pmatrix}, \begin{pmatrix} 1 \\ 0 \\ 1 \end{pmatrix} \right\rangle \subset \mathbb{R}^3 , \tag{165}$$

and its dual is

$$\sigma^\vee = \langle n_1 = (1,0,0), n_2 = (0,1,0), n_3 = (-1,0,1), n_4 = (0,-1,1) \rangle \subset (\mathbb{R}^3)^* , \tag{166}$$

from which it is easy to read the equation defining the singularity:

$$n_1 + n_3 = n_2 + n_4 \quad \rightarrow \quad z_1 z_3 = z_2 z_4 . \tag{167}$$

As a second example let us consider the toric diagram of dP_3 and the cone it generates:

$$\sigma = \left\langle \begin{pmatrix} 0 \\ -1 \\ 1 \end{pmatrix}, \begin{pmatrix} 1 \\ -1 \\ 1 \end{pmatrix}, \begin{pmatrix} 1 \\ 0 \\ 1 \end{pmatrix}, \begin{pmatrix} 0 \\ 1 \\ 1 \end{pmatrix}, \begin{pmatrix} -1 \\ 1 \\ 1 \end{pmatrix}, \begin{pmatrix} -1 \\ 0 \\ 1 \end{pmatrix} \right\rangle \subset \mathbb{R}^3 . \tag{168}$$

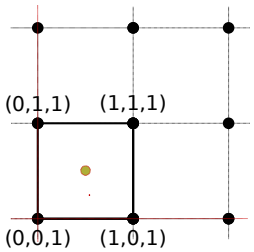

Figure 43: The toric diagram of the conifold.

It is dual to $\sigma^\vee$ which is the cone:

$$\langle n_1 = (0,1,1), n_2 = (-1,0,1), n_3 = (-1,-1,1), n_4 = (0,-1,1), \\ n_5 = (1,0,1), n_6 = (1,1,1), n_0 = (0,0,1) \rangle \ , \quad (169)$$

where we added the vector $n_0 = (0,0,1)$ since $n_1 + n_4 = 2n_0$, meaning that we where missing an integer generator. The equations of the variety are

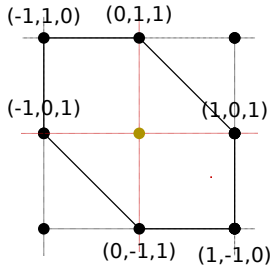

Figure 44: The toric diagram of dP_3.

$$z_1 z_4 = z_2 z_5 = z_3 z_6 = z_0^2 \\ z_1 z_3 z_5 = z_2 z_4 z_6 \, . \quad (170)$$

We can use the fact that under the shift involution each ZZP is mapped to a ZZP of opposite winding, hence the corresponding toric diagram must be symmetric under the reflection about its center of mass. Such center of mass has, in general, half-integer coordinates (α, β). Under such a reflection, a generic point in the lattice with coordinates $(r,s) \in \mathbb{Z}^2$ is sent to $(2\alpha - r, 2\beta - s)$. Under this

operation, the generators of the cone are mapped according to

$$m' = \begin{pmatrix} -1 & 0 & 2\alpha \\ 0 & -1 & 2\beta \\ 0 & 0 & 1 \end{pmatrix} \cdot m \tag{171}$$

which maps a generator $m = (a, b, 1)$ to $m' = (2\alpha - r, 2\beta - s, 1)$. The dual cone $S^\vee$ is in turn invariant under the (right) action of that matrix, which acts as

$$n' = \begin{pmatrix} -1 & 0 & 0 \\ 0 & -1 & 0 \\ 2\alpha & 2\beta & 1 \end{pmatrix} \cdot n\,, \tag{172}$$

or simply,

$$n = (p, q, a) \quad \to \quad n' = (-p, -q, 2\alpha p + 2\beta q + a)\,. \tag{173}$$

From these observations, we deduce the following properties:

1. All generators of the dual cone, obtained via eq. (163), $n_i = (p_i, q_i, a)$, come paired with another generator $n_i' = (-p_i, -q_i, a')$, for some integer a while a' is obtained via eq. (173).

2. Given a generator $n_i = (p_i, q_i, a)$ and its shift image $n_i' = (-p_i, -q_i, a')$, we see that a new integer generator that we were missing can be added $n_0 = (0, 0, 1)$, since
$$n_i + n_i' = (a + a')n_0\,. \tag{174}$$
This generator is invariant under the shift.

3. All other extra generators come in pairs. Given an extra generator n_l such that
$$n_i + \cdots + n_j' + \cdots = b\, n_l\,, \tag{175}$$
with b integer, by a symmetry argument, we also need to add n_l', since we have[14]
$$n_i' + \cdots + n_j + \cdots = b\, n_l'\,. \tag{176}$$

We now rearrange the generators into two sets: the set of n_i with $i = 1, ..., k$ and the set $n_{i+k} = n_i'$ of their images under the shift. Moreover we have n_0 which is the invariant generator. To each generator n_i we associate a complex coordinate z_i. We have $2k+1$ of them, related by $2k-2$ relations, that define the toric 3-fold. We divide these relations in two kinds. The k first kind relations are of the form

$$z_i z_{i+k} - z_0^{a+a'} = 0\,, \tag{177}$$

[14]The transformation law in eq. (173) acts linearly on eq. (175) such that we obtain eq. (176).

and come from eq. (174). We use it to relate every image z_{i+k} to its partner z_i and to z_0. The second kind relations relate all remaining z_i and z_0 together. For example, they may look like

$$z_i z_j z_h^b - z_l z_m z_0^c = 0\,, \tag{178}$$

for some integers b and c.

Under the shift, relations of the first kind are invariant, those of the second kind are not. However, we can build more symmetric expressions for the latter. As we did when going from eq. (175) to eq. (176), eq. (178) becomes, under the shift,

$$z_{i+k} z_{j+k} z_{h+k}^b - z_{l+k} z_{m+k} z_0^c = 0\,. \tag{179}$$

We can now multiply eq. (178) by a term $(z_{i+k} z_{j+k} z_{h+k}^b)$ and use the last equation to find

$$(z_i z_j z_h^b)(z_{l+k} z_{m+k}) z_0^c - (z_l z_m)(z_{i+k} z_{j+k} z_{h+k}^b) z_0^c = 0\,, \tag{180}$$

which is now symmetric up to a sign under the shift. We dub these relations the symmetrized second kind relations.

To describe our Calabi-Yau 3-fold, we start with $2k+1$ variables. From the equations of the first kind we can express all the z_{i+k} in terms of the z_i and z_0, fixing k variables. Then we can use the symmetrized second kind relations to fix $k-2$ equations, leaving us with only 3 independent variables. Now, the non-vanishing holomorphic 3-form Ω_3 is obtained as the Poincaré residue along the CY_3 of the meromorphic $(2k+1)$-form in the ambient space $\mathbb{C}^{2k+1}$:

$$\Omega_3 = \mathrm{Res}\, \frac{\mathrm{d}z_1 \wedge ... \wedge \mathrm{d}z_k \wedge ... \wedge \mathrm{d}z_{2k} \wedge \mathrm{d}z_0}{\left(\prod_{i=1}^{k} P_i \prod_{i=1}^{k-2} Q_i \right)}\,, \tag{181}$$

where the P_i are equations of the first kind, while Q_i are of the symmetrized second one.

Under the action of the shift, the numerator of the 3-form is multiplied by $(-1)^k$, since the shift acts on the coordinates exchanging them in pairs. From the denominator we get a factor $(-1)^{k-2}$ coming from the symmetrized second kind equations, cancelling the factor at the numerator and leaving the 3-form invariant. This means that such orientifold projection does not preserve the same supersymmetry as the D3-branes.

Let us finish this section working out an explicit example. In the case of dP_3, one has $k=3$, and the holomorphic 3-form is the residue of the meromorphic 7-form.

$$\Omega_3 = \mathrm{Res}\, \frac{\mathrm{d}z_1 \wedge ... \wedge \mathrm{d}z_6 \wedge \mathrm{d}z_0}{(z_1 z_4 - z_0^2)(z_2 z_5 - z_0^2)(z_3 z_6 - z_0^2)(z_1 z_3 z_5 - z_2 z_4 z_6)}\,. \tag{182}$$

Under the involution, the numerator is multiplied by $(-1)^3$. The first three relations are invariants while for the fourth one takes a minus sign. In the end, Ω_3 is even under the symmetry, and hence there cannot be any supersymmetric shift orientifold of dP_3.

5.8 Conclusion

In this section we have studied orientifolds on D3-branes at toric CY_3 singularities using dimer models. We established a classification in terms of smooth involutions of the dimer torus, which allowed us to find the last supersymmetric possibility, the glide reflection orientifold. This possibility may also be reached by directly performing the orientifold projection on the open string spectrum. A last possibility existed, a shift orientifold, but it breaks all supersymmetries, as explicitly argued by studying its action on the holomorphic 3-form. Note that these two cases, not considered before, leave no fixed loci. This exhausts the possible orientifolds acting smoothly on the dimer torus.

Given a toric gauge theory and its associated dimer, one may find the projected theory with the same dictionary as orientifolds with fixed loci. The resulting theories have properties strikingly similar to non-orientifolded theories.

- Unlike orientifold theories with fixed loci, glide reflection orientifolds are guaranteed to satisfy the anomaly cancellation conditions for some rank assignment. In fact, these theories are non-chiral. This fact is non-trivial, see [3], and granted by the absence of fixed loci in the glide orientifold that would give raise to tensor matter that could spoil the ACC. From the geometric point of view this boils down to the absence of net RR fluxes sourced by these orientifolds, as there are no fixed loci that can be interpreted as an O-plane. T-duality sheds further light, since the glide orientifold turns to a pair of oppositely charged O-planes on a circle, in the sense of [36, 37].

- Again, contrary to intuition, these theories are conformal, as shown by explicit computation of the one loop β-function, that vanishes identically.

- Some of these theories admit $\mathcal{N} = 2$ or deformation fractional branes. The latter trigger a cascade of dualities à la Klebanov-Strassler, with a constant step that allows for a UV completion purely in terms of field theory. This is unlike the orientifolds with fixed loci in the literature [44] and opens up the possibility of a simple supergravity dual.

- The glide reflection orientifold may be understood in the T-dual and mirror picture, at least for $\mathbb{C}^2/\mathbb{Z}_2$, providing a unifying picture.

The results of this section close the analysis of orientifolds of brane tilings, or at least those acting as smooth involutions on the torus. However, one may consider other kinds of involutions. For example, involutions not respecting the color mapping presented in section 5.1 or non smooth involutions, can lead to new projections of the tiling, different from the usual orientifold. One may also look for quotients of higher order, in the spirit of what has been done with S-folds [45, 46], and their connection with dimer models. These directions are yet to be explored.

Orientifolds have found extensive use in phenomenological applications by allowing for non-perturbatively generated superpotentials or opening the door to SUSY breaking, for instance. We hope our results may shed light in these and related issues.

Part III
Orientifolds in Dimer Models: applications

6 The quest for a DSB model

As we already reviewed, D3-branes probing a non compact toric CY geometry have, on their world sheet, degrees of freedom describing, in general, an $\mathcal{N} = 1$ SCFT. The introduction of fractional branes has the property of breaking conformal invariance, triggering a non trivial RG flow. The low energy effective dynamics depends on the nature of the fractional branes, as explained in section 1.2.

Using fractional branes, of the DSB kind, it was possible to construct theories admitting supersymmetry breaking behavior at the end of the RG flow. However, the DSB model is of the runaway type, [47, 15, 48].

This instability issue was addressed and overcome with the use of orientifold projections. As opposed to purely geometric backgrounds, orientifolds are known to allow for a variety of non-generic dynamical effects (see [49] for a review), including the possibility of lifting massless moduli [50, 51]. Indeed, in [25] two instances of fractional brane configurations at orientifold singularities reproducing exactly the matter content of the so-called uncalculable $SU(5)$ DSB model [52] were provided.

These models stood out as the only D-brane constructions leading to a reliable stable DSB vacuum, until in [14] it was shown that these DSB vacua were actually not stable. This happens as one tries to embed the supersymmetry breaking configuration in a decoupled, UV complete D-brane system (which is realized as a cascade or, more generally, a large-N gauge theory). Adding N regular D3-branes to the supersymmetry breaking configuration one can see that a Coulomb branch runaway direction opens up and the vacuum energy is set to zero, *i.e.* the lowest energy state is a supersymmetric vacuum.

The problem of finding stable supersymmetry breaking states in well-defined string theory set-ups is of course of the utmost importance, both in the context of string compactifications, in which such configurations arise as warped throats, as well as in the gauge/gravity duality framework. The evidence provided in [14] was taken as a negative result and an indication in favor of a new swampland conjecture, dubbed locally AdS weak gravity conjecture.[15]

In this section, we aim at understanding how generic is the situation analyzed

[15] See [9] for the original idea about the swampland and [10, 11] for recent reviews, plus references therein.

in [14], by finding more set-ups with a putative DSB vacuum, and then checking whether they also display some instability towards a supersymmetric vacuum. We will restrict to toric singularities with an orientifold projection which is necessary, as argued above, to allow for DSB models on fractional brane configurations.

6.1 DSB vacua and their instability

It is natural to ask first which DSB models have a chance of being engineered with D3-branes at orientifolded toric CY. Known DSB models are rather specific gauge theories, and we have to match their properties to the ones of the gauge theories one can engineer with branes.

We now briefly revise the models discussed in section 3:

SU(5) one family model This model [52] has an $SU(5)$ gauge group and one GUT-like chiral family $\square \oplus \overline{\square}$ (or in other words $\mathbf{10} \oplus \bar{\mathbf{5}}$). No chiral gauge invariant can be written, hence it has no superpotential and no classical flat directions. From arguments based on 't Hooft anomaly matching, its vacuum is believed to break supersymmetry in a purely strongly coupled fashion. The supersymmetry breaking vacuum energy density is given in terms of its dynamical scale, $E_{\rm vac} \sim \Lambda^4_{SU(5)}$.

3-2 model This other model [53] involves two gauge groups, $SU(3)$ and $SU(2)$ respectively, and one chiral family, resembling the ones of the Standard Model: under $SU(3)\times SU(2)$ matter fields transform as $(\mathbf{3},\mathbf{2})\oplus(\bar{\mathbf{3}},1)\oplus(\bar{\mathbf{3}},1)\oplus(1,\mathbf{2})$. This model has a number of flat directions, but a cubic superpotential lifts them all. After taking into account non-perturbatively generated contributions to the superpotential, it turns out there is a conflict between F-terms and D-terms so that no supersymmetric vacuum can be found. The actual minimum breaks supersymmetry dynamically, where now $E_{\rm vac} \sim \Lambda^4_{SU(3)}$ or $\Lambda^4_{SU(2)}$, depending on which group confines first.

The $SU(5)$ model has a matter field in the anti-symmetric representation, hence to recover it an orientifold projection is necessary. It turns out that also for recovering the 3-2 model an orientifold is needed. This is related to the fact that the two matter fields in the $(\bar{\mathbf{3}},1)$ representation are set apart by the superpotential. While in non-orientifolded quivers such pairs of similar fields always come in doublets of a global symmetry, in an orientifolded theory they can simply be taken apart by identifying one of the anti-fundamentals of $SU(3)$ as being in the anti-symmetric representation. Hence, we conclude that in order to recover the basic features of both the $SU(5)$ and the 3-2 models we need to have an orientifold projection.

After the orientifold projection, it turns out that, generically, the anomaly cancellation conditions result in constraints on the various ranks of the form

$$\sum_i N_i = \sum_{j'} N_{j'} + 4 \ , \tag{183}$$

where the two sums run on two different sets of gauge theory nodes, and strictly speaking the Ns are not the ranks but the dimensions of the fundamental representation of $SU(N)$,[16] $SO(N)$ or $USp(N)$ groups (the latter two possibilities being possible only after the orientifold projection). The imbalance of 4 units in eq. (183) is due to the orientifold charge, which contributes to tadpole cancellations.

Two simple ways to satisfy eq. (183) are the following. We can take one $N_i = 5$, one $N_{j'} = 1$ and all other ranks to vanish, so that the remaining gauge group is $SU(5) \times SU(1)$ or $SU(5) \times SO(1)$. The trivial factor actually allows for a bifundamental between the two nodes to be interpreted as a (anti)fundamental of $SU(5)$. If the latter also has an anti-symmetric matter field, then the field content is exactly the one of the $SU(5)$ DSB model.

The other simple solution to eq. (183) is to take one $N_i = 3$, another one $N_{j\neq i} = 2$, one $N_{j'} = 1$, and again all other factors to vanish, leading to the gauge group $SU(3) \times SU(2)/USp(2) \times SU(1)/SO(1)$. The 3-2 model is recovered if there are bifundamentals linking the three gauge groups, together with a cubic superpotential term, and in addition an antisymmetric of $SU(3)$ which provides for the remaining (anti)triplet, necessary for anomaly cancellation.

In some of the examples that we will review below, some additional decoupled gauge singlets will be present, or even additional decoupled gauge sectors, which themselves do not break supersymmetry. We will even encounter an example with two decoupled $SU(5)$ models.

The conclusion we will draw is that there is a sizable number of orientifold singularities that allow for configurations with a small number of fractional branes reproducing a gauge theory with a stable DSB vacuum.

After building the DSB model, we will address the problem of its stability after considering their stringy UV completions. This is achieved adding regular D3-branes at the CY singularity. This corresponds to increasing by a common factor N the ranks of all gauge groups. As one can check, the anomaly cancellation conditions eq. (183) are still satisfied. It is then easy to show that because of the underlying superconformal fixed point of the parent (non-orientifolded) theory, if one performs scale matching on the node that eventually drives supersymmetry breaking in the IR, one finds that

$$\Lambda_{IR} = \Lambda_{UV} \ . \tag{184}$$

[16] As usual in quiver gauge theories derived from branes at singularities, we assume that all the $U(1)$ factors have become free at low enough energies, hence acting as global symmetries.

In other words, moving the regular D3-branes out of the singularity is still a flat direction, even in the presence of the fractional branes generating the DSB vacuum energy. Note that adding regular D3-branes can also be related, in the models that allow for it, to a duality cascade, though the analysis in the presence of an orientifold can be subtle, see [44] for a discussion. The upshot is that regular D3-branes do not destabilize the DSB vacuum.

On the other hand, we anticipate that in all examples of DSB we have found, a mechanism similar to the one discussed in [14] takes place. I turns out that in all singularities we will discuss in this section, every time a DSB model can be constructed, the geometry allow for D3-branes to split into two complementary fractional branes of the $\mathcal{N} = 2$ kind. The latter have a one-dimensional Coulomb branch that takes them out of the singularity. One can then see what happens when higgsing the quiver in two steps, putting the two sets of $\mathcal{N} = 2$ branes on their Coulomb branches one after the other. In the partially higgsed configuration, the scale matching depends on the VEV v related to the position of the first set of branes. The second VEV v', related to the position of the second set of branes, will then compensate the first so that the final scale matching reads

$$\Lambda_{IR} = \left(\frac{v'}{v}\right)^{\alpha} \Lambda_{UV} \ , \tag{185}$$

where α is some model-dependent non-vanishing number. If the two sets of branes move together as a regular brane, $v = v'$ and we recover eq. (184). But if the two sets split, then we see that for α positive there is a runaway towards a supersymmetric vacuum with zero energy at $v' = 0$ or equivalently $v = \infty$, viceversa for α negative. We thus conclude that the models are unstable in their UV completion, because the vacuum energy can be brought to zero by moving in (or out) the singularity some $\mathcal{N} = 2$ fractional branes.

In the rest of the section we analyze a series of singularities, showing how the general pattern described above emerges. We also provide a proof that the decay mechanism related to the presence of $\mathcal{N} = 2$ fractional branes is general and does not depend on the specific CY realizing the model.

6.2 The $\mathbb{C}^3/\mathbb{Z}_6$ singularity

As a warm-up, let us start considering the (fixed point) orientifold of the orbifold $\mathbb{C}^3/\mathbb{Z}_6$, already analyzed in [14]. The orbifold action is defined by the $\mathbb{Z}_6$ acting on the complex coordinates of $\mathbb{C}^3$ as

$$\theta \ : \quad z_i \to e^{2\pi i v_i} z_i \ , \tag{186}$$

with $i = 1, 2, 3$ and $v = (1, 2, 3)/6$. The dimer associated to the $\mathbb{C}^3/\mathbb{Z}_6$ orbifold singularity is reported in fig. 45, including the fixed points with respect to which

we will eventually take the orientifold projection.

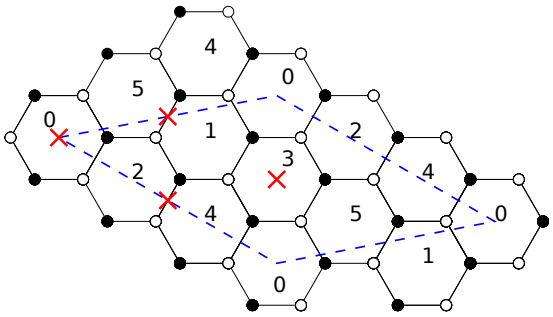

Figure 45: The $\mathbb{C}^3/\mathbb{Z}_6$ dimer. The theory is chiral, with 6 gauge factors and 18 bifundamental chiral superfields X_{ij}. The parallelogram is a possible choice of unit cell. Red crosses represent fixed points under the orientifold action.

From the dimer one can read the field content of the theory as well as the superpotential which is

$$\begin{aligned} W &= X_{152} + X_{143} + X_{032} + X_{053} + X_{254} + X_{104} \\ &\quad -X_{052} - X_{031} - X_{142} - X_{043} - X_{253} - X_{154} \ , \end{aligned} \tag{187}$$

where, for the ease of notation, we have defined $X_{lmn} \equiv X_{lm}X_{mn}X_{nl}$, and X_{lm} is in the $(\overline{\square}_l, \square_m)$ representation, where $l, m, n = 0, 1, ..., 5$. Following the general rules summarized in section 2.4.1, one can see that there do not exist deformation fractional branes, but only $\mathcal{N} = 2$ fractional branes. For instance, the strip 0-2-4 and its complement 1-3-5, are $\mathcal{N} = 2$ fractional branes.

We now perform an orientifold projection via point reflection. The unit cell has an even number of white nodes hence, following section 2.4.2, we have to choose orientifold charges with an even number of + signs. A convenient choice is $(+, +, -, -)$ starting from the fixed point on face 0 and going clockwise. The orientifold projection gives the following identifications between faces

$$0 \iff 0 \qquad 1 \iff 5 \qquad 2 \iff 4 \qquad 3 \iff 3. \tag{188}$$

The daughter theory has hence gauge group

$$SO(N_0) \times SU(N_1) \times SU(N_2) \times USp(N_3) \ , \tag{189}$$

and matter in the following representations

$$\begin{aligned} &X_1 = (\square_0, \overline{\square}_1) \quad , \quad X_2 = (\square_0, \overline{\square}_2) \quad , \quad X_3 = (\square_0, \square_3), \\ &Y_1 = (\square_1, \square_3) \quad , \quad Y_2 = (\square_2, \square_3) \quad , \quad Z_1 = (\square_1, \square_2) \\ &Z_2 = (\overline{\square}_1, \overline{\square}_2) \quad , \quad W = (\square_1, \overline{\square}_2) \quad , \quad A = \begin{smallmatrix}\square\\\square\end{smallmatrix}_2 \quad , \quad S = \overline{\square\square}_1 \ , \end{aligned} \tag{190}$$

where the subscript indicates under which gauge group the fields are charged.

Imposing anomaly cancellation condition on the two SU factors we get

$$\begin{cases} N_0 + N_1 - N_2 - N_3 + 4 = 0 & SU(N_1) \\ N_0 + N_1 - N_2 - N_3 + 4 = 0 & SU(N_2) \end{cases}$$

which is one and the same condition, that is

$$N_0 + N_1 - N_2 - N_3 + 4 = 0 \ . \tag{191}$$

SU(5) model

An interesting choice of ranks compatible with the constraint eq. 191 is $N_0 = 1, N_1 = 0, N_2 = 5, N_3 = 0$. With this choice, the theory becomes exactly the one describing the uncalculable $SU(5)$ DSB model (the $SO(1)$ becomes a flavor index), which breaks supersymmetry dynamically in a stable vacuum. The corresponding quiver is reported in fig. 46.

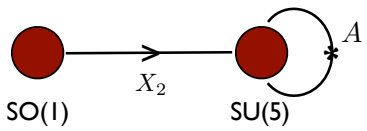

Figure 46: The quiver of the $SU(5)$ model at the $\mathbb{C}^3/\mathbb{Z}_6$ orbifold singularity. Matter fields follow the definitions in eq. 190. The asterisk refers to the anti-symmetric representation.

As recently argued in [14], in the decoupling limit this DSB vacuum becomes actually unstable. In such limit the effective matter-coupled gauge theory becomes

$$SO(N+1) \times SU(N) \times SU(N+5) \times USp(N) \ , \tag{192}$$

which actually corresponds to adding N regular D3-branes at the singularity. This is a much richer theory than $SO(1) \times SU(5)$ and it might have, possibly, many vacua. One should then ask whether in the larger moduli space of 192 there are instabilities which make the supersymmetry breaking vacuum unstable. This can be easily understood by scale matching.

The vacuum energy of the putative supersymmetry breaking vacuum will be $\sim \Lambda^4$, with Λ the intrinsic scale of the $SU(5)$ model. The higgsing of the N regular

branes can be obtained giving a VEV of scale v to the gauge invariant operator[17]

$$\Phi = \mathrm{Tr}(X_1 W Y_2 X_3^t) \ . \tag{193}$$

This makes the theory 192 flow to $SO(1) \times SU(5)$, namely the DSB $SU(5)$ model.

We can match the UV and IR scales evaluating the β functions of the relevant SU factor above and below the scale v.[18] Note that because the orbifold theory is a projection of $\mathcal{N} = 4$ SYM, fundamental fields do not acquire anomalous dimensions (equivalently, all superpotential terms are cubic). With obvious notation, we have (here, and in similar formulas thereafter, we omit a factor of $8\pi^2$ for clarity of exposition)

$$\begin{aligned} \frac{1}{g^2_{SU(5+N)}} &= \left[3(N+5) - \frac{1}{2}(6N+4)\right] \ln\left(\frac{\mu}{\Lambda_{UV}}\right) = 13 \ln\left(\frac{\mu}{\Lambda_{UV}}\right) \\ \frac{1}{g^2_{SU(5)}} &= \left[15 - \left(\frac{1}{2}+\frac{3}{2}\right)\right] \ln\left(\frac{\mu}{\Lambda}\right) = 13 \ln\left(\frac{\mu}{\Lambda}\right) \ . \end{aligned}$$

Matching the gauge coupling at $\mu = v$ we get

$$\Lambda = \Lambda_{UV} \ . \tag{194}$$

This shows that the effective potential does not depend on the VEV of Φ, meaning that regular brane dynamics does not change the nature of the supersymmetry breaking vacuum and its stability (there is no force acting on the N regular branes).

In fact, it turns out that there exists a different instability channel. This has to do with moduli associated to $\mathcal{N} = 2$ fractional branes, which are massless classically, but become runaway once non-perturbative corrections are taken into account. From the dimer in figure 45 we see that a regular brane can be seen as a bound state of two $\mathcal{N} = 2$ fractional branes corresponding to the strips 0-2-4 and 1-3-5, respectively. The classical flat directions correspond to the z_2 fixed line that is left invariant by θ^3, see eq. (186). Locally, this is a $\mathbb{C}^2/\mathbb{Z}_2$ singularity. Both these fractional branes survive the orientifold projection, becoming 0-2 and 1-3

[17] Hereafter, we assume that all fields appearing in the gauge invariants have a rank N piece in the upper left part, to ensure the correct higgsing pattern. If the rank N pieces are all proportional to the identity, then an $SU(N)$ diagonal gauge group is preserved. It can be checked to have $\mathcal{N} = 4$ SUSY to a good approximation, and to decouple from the rest of the quiver. We will not consider it further.

[18] The exact β function of $SU(N_c)$ supersymmetric gauge theory coupled to chiral matter fields Φ_i with anomalous dimensions γ_i is $\beta(8\pi^2/g^2) = 3N_c - \sum_i N_i T(\rho_i)(1-\gamma_i)$, where N_i is the number of fields in the representation ρ_i, and $T(\square) = \frac{1}{2}$ and $T(\begin{smallmatrix}\square\\\square\end{smallmatrix}) = \frac{1}{2}(N_c - 2)$. The absence of the denominator with respect to the usual NSVZ expression [54] is due to a choice of normalization for the vector superfield which differs from the canonical one by a factor of $1/g^2$, as usual in the framework of the gauge/gravity correspondence.

strips. Note that (135) and (024) are closed loops which represent operators not present in the superpotential. Hence, their VEVs represent motion along classical flat directions. In the daughter theory these directions are given by the operators[19]

$$\tilde{\Phi} = \mathrm{Tr}(X_2 A X_2^t)^2 \quad , \quad \tilde{\Phi}' = \mathrm{Tr}(J Y_1 S Y_1^t)^2 \ , \tag{195}$$

and we will denote the scale of their VEVs as v and v', respectively. The higgsing pattern is then[20]

$$\begin{aligned} &SO(N+1) \times SU(N) \times SU(N+5) \times USp(N) \stackrel{v}{\longrightarrow} \\ &SO(1) \times SU(N) \times SU(5) \times USp(N) \stackrel{v'}{\longrightarrow} SO(1) \times SU(5) \ . \end{aligned} \tag{196}$$

Above and below the scale v the gauge couplings run as

$$\begin{aligned} \frac{1}{g^2_{SU(5+N)}} &= \left[3(N+5) - \frac{1}{2}(6N+4)\right] \ln\left(\frac{\mu}{\Lambda_{UV}}\right) = 13 \ln\left(\frac{\mu}{\Lambda_{UV}}\right) \\ \frac{1}{g^2_{SU(5)_N}} &= \left[15 - \frac{1}{2}(4N+4)\right] \ln\left(\frac{\mu}{\Lambda_N}\right) = (13-2N) \ln\left(\frac{\mu}{\Lambda_N}\right) \ . \end{aligned}$$

Matching them at $\mu = v$ we get

$$\Lambda_N^{13-2N} = v^{-2N} \Lambda_{UV}^{13} \ . \tag{197}$$

Repeating the same computation above and below the scale v' we have

$$\begin{aligned} \frac{1}{g^2_{SU(5)_N}} &= \left[15 - \frac{1}{2}(4N+4)\right] \ln\left(\frac{\mu}{\Lambda_N}\right) = (13-2N) \ln\left(\frac{\mu}{\Lambda_N}\right) \\ \frac{1}{g^2_{SU(5)}} &= \left[15 - \left(\frac{1}{2}+\frac{3}{2}\right)\right] \ln\left(\frac{\mu}{\Lambda}\right) = 13 \ln\left(\frac{\mu}{\Lambda}\right) \ . \end{aligned}$$

and in turn $\Lambda_N^{13-2N} = v'^{-2N} \Lambda^{13}$. The end result is then

$$\Lambda^{13} = \left(\frac{v'}{v}\right)^{2N} \Lambda_{UV}^{13} \ . \tag{198}$$

The potential of the theory, V, is expected to be proportional to the strong coupling scale[21], since no superpotential is present nor can be generated. From this fact,

[19] As before, we assume that the fields in the gauge invariants have a rank N upper left piece, and we do not consider the decoupled effective $\mathcal{N} = 2$ diagonal gauge group. Note that the traces involve squares since $\mathrm{Tr}(X_2 A X_2^t) = 0$ because of antisymmetry of A, while $\mathrm{Tr}(J Y_1 S Y_1^t) = 0$ because of antisymmetry of the USp-invariant J.

[20] This pattern occurs for $v \gg v'$. One can check that the end result does not change when inverting the order of the two scales.

[21] It is expected to scale as $V = |\Lambda|^4$.

we see that the DSB vacuum is unstable. Indeed There exists a one-dimensional supersymmetric moduli space sitting at $v' = 0$ and parametrized by v. Indeed, one can estimate the minima of the potential in a (v, v') plane and check that any point at $v, v' \neq 0$ is driven to the $v' = 0$ axis. The gradient flow is reported in fig. 47.

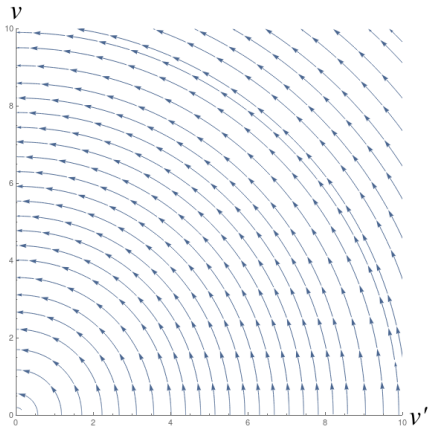

Figure 47: Plot of $-\text{Grad}(V)$ as a function of v and v'. The flow goes towards $v' = 0$, suggesting that the system, eventually, relaxes to a supersymmetry preserving vacuum at finite distance in field space.

In principle, one might try to obtain the $SU(5)$ by a different UV completion. For instance, one can add to the DSB configuration M fractional branes populating the second and fourth gauge factors only, corresponding to the strip 1-3-5 in the mother theory, which becomes 1-3 after orientifolding. The theory in this case has gauge group

$$SO(1) \times SU(M) \times SU(5) \times USp(M) \ . \tag{199}$$

This configuration does not change much the fate of the DSB vacuum. Previous analysis shows that, lacking one modulus, v in our conventions, the one-dimensional moduli space of supersymmetry preserving vacua becomes an isolated vacuum. This agrees with known field theory results [55]: the $SU(5)$ factor has extra vector-like matter and the theory does not lead to a supersymmetry breaking vacuum to start with.

If one instead populates nodes 0 and 2, $N_0 = M, N_1 = 0, N_2 = M + 4, N_3 = 0$ which in the mother theory corresponds to adding M $\mathcal{N} = 2$ fractional branes associated to the strip 0-2-4, the theory has a runaway direction associated to v. Note that this last system has the same gauge and matter content of a known, stable, DSB model [52, 55], but it lacks a crucial cubic term in the superpotential

whose effect is indeed to stop the runaway associated to v. The special case $M = 1$ is the only stable DSB model (our original brane construction, in fact).

To sum up, the $\mathbb{C}^3/\mathbb{Z}_6$ singularity does admit fractional brane configurations whose low energy open string dynamics enjoys stable DSB vacua. However, once coupled to regular branes, the supersymmetry breaking vacuum becomes unstable towards supersymmetry preserving ones. The $\mathbb{C}^3/\mathbb{Z}_6$ singularity can be embedded into a larger singularity which admits deformation branes [56] and, as such, a cascade (dual to a warped throat [57, 58, 59]). So the above analysis suggests that, at least within this construction, it is not possible to embed the $SU(5)$ DSB model into a warped throat keeping it stable [14].

3-2 model

Looking at eq. 191, one can see that another possible anomaly free rank assignment is given by $N_0 = 1, N_1 = 0, N_2 = 3, N_3 = 2$ which corresponds to the following gauge theory

$$SO(1) \times SU(3) \times USp(2) \ . \tag{200}$$

Using the fact that $USp(2) = SU(2)$ and that for $SU(3)$ $\begin{smallmatrix}\square\\\square\end{smallmatrix} = \overline{\square}$, from eq. 190 we see that the matter content is

$$\begin{aligned} X_2 &= (\square_0, \overline{\square}_2) = \overline{D}, \qquad & X_3 &= (\square_0, \square_3) = L, \\ Y_2 &= (\square_2, \square_3) = Q, \qquad & A &= \begin{smallmatrix}\square\\\square\end{smallmatrix}_2 = \overline{U} \ , \end{aligned} \tag{201}$$

with tree level superpotential

$$W = \overline{D}QL \ . \tag{202}$$

This reproduces exactly the DSB 3-2 model [53]! The corresponding quiver is reported in figure 48.

Again, one could ask what is the fate of this DSB vacuum in the full theory. In the present model, we have to perform the scale matchings on the gauge group that is most strongly coupled, since the DSB vacuum energy will be expressed in terms of its dynamical scale. We start by considering a regime where supersymmetry breaking is driven by the non-perturbative contributions in the $SU(3)$ gauge group [17].

As in the $SU(5)$ model, upon adding regular branes and higgsing them, the vacuum shows no instability. Indeed, giving a VEV to $\Phi = \mathrm{Tr}(X_1 W Y_2 X_3^t)$, the

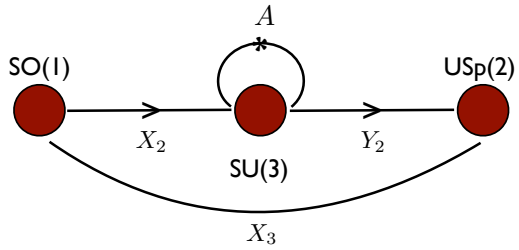

Figure 48: The quiver of the 3–2 model at the $\mathbb{C}^3/\mathbb{Z}_6$ orbifold singularity. Matter fields follow the definitions in eq. 190. Arrows are indicated only when needed (for $USp(2) = SU(2)$ the fundamental and anti-fundamental are equivalent representations). The asterisk refers to the anti-symmetric representation, as in fig. 46.

gauge coupling running above and below the matching scale is

$$\begin{aligned} \frac{1}{g^2_{SU(3+N)}} &= \left[3(N+3) - \frac{1}{2}(6N+4)\right] \ln\left(\frac{\mu}{\Lambda_{UV}}\right) = 7\ln\left(\frac{\mu}{\Lambda_{UV}}\right) \\ \frac{1}{g^2_{SU(3)}} &= \left[9 - \left(\frac{1}{2}+\frac{1}{2}+1\right)\right] \ln\left(\frac{\mu}{\Lambda_3}\right) = 7\ln\left(\frac{\mu}{\Lambda_3}\right) \ , \end{aligned}$$

and hence $\Lambda = \Lambda_{UV}$.

However, the theory has $\mathcal{N} = 2$ fractional branes, and following the same two-steps higgsing pattern as before, namely

$$\begin{aligned} SO(N+1) \times SU(N) \times SU(N+3) \times USp(N+2) \xrightarrow{v} \\ SO(1) \times SU(N) \times SU(3) \times USp(N+2) \xrightarrow{v'} SO(1) \times SU(3) \times USp(2) \end{aligned} \quad (203)$$

we get, above and below the scale v

$$\begin{aligned} \frac{1}{g^2_{SU(3+N)}} &= \left[3(N+3) - \frac{1}{2}(6N+4)\right] \ln\left(\frac{\mu}{\Lambda_{UV}}\right) = 7\ln\left(\frac{\mu}{\Lambda_{UV}}\right) \\ \frac{1}{g^2_{SU(3)_N}} &= \left[9 - \frac{1}{2}(4N+4)\right] \ln\left(\frac{\mu}{\Lambda_N}\right) = (7-2N)\ln\left(\frac{\mu}{\Lambda_N}\right) \ , \end{aligned}$$

and, at scale v'

$$\begin{aligned} \frac{1}{g^2_{SU(3)_N}} &= \left[9 - \frac{1}{2}(4N+4)\right] \ln\left(\frac{\mu}{\Lambda_N}\right) = (7-2N)\ln\left(\frac{\mu}{\Lambda_N}\right) \\ \frac{1}{g^2_{SU(3)}} &= \left[9 - \left(\frac{1}{2}+\frac{1}{2}+1\right)\right] \ln\left(\frac{\mu}{\Lambda_3}\right) = 7\ln\left(\frac{\mu}{\Lambda_3}\right) \ , \end{aligned}$$

which gives in the end

$$\Lambda_3^7 = \left(\frac{v'}{v}\right)^{2N} \Lambda_{UV}^7 \ . \tag{204}$$

We can now repeat the analysis when the supersymmetry breaking dynamics is driven by the strong coupling scale of $SU(2)$. We have

$$\begin{aligned} \frac{1}{g^2_{USp(N+2)}} &= \left[3\frac{(N+4)}{2} - \frac{1}{2}(3N+4)\right] \ln\left(\frac{\mu}{\Lambda_{UV}}\right) = 4\ln\left(\frac{\mu}{\Lambda_{UV}}\right) \\ \frac{1}{g^2_{USp(2)}} &= \left[6 - \left(\frac{1}{2}+\frac{3}{2}\right)\right] \ln\left(\frac{\mu}{\Lambda_2}\right) = 4\ln\left(\frac{\mu}{\Lambda_2}\right) \ , \end{aligned}$$

and hence $\Lambda_2 = \Lambda_{UV}$ by higgsing the N regular branes. Along the $\mathcal{N}=2$ directions we get instead the matching

$$\begin{aligned} \frac{1}{g^2_{USp(2+N)}} &= \left[3\frac{(N+4)}{2} - \frac{1}{2}(3N+4)\right] \ln\left(\frac{\mu}{\Lambda_{UV}}\right) = 4\ln\left(\frac{\mu}{\Lambda_{UV}}\right) \\ \frac{1}{g^2_{USp(2+N)_N}} &= \left[3\frac{(N+4)}{2} - \frac{1}{2}(N+4)\right] \ln\left(\frac{\mu}{\Lambda_N}\right) = (4+N)\ln\left(\frac{\mu}{\Lambda_N}\right) \end{aligned}$$

at scale v and

$$\begin{aligned} \frac{1}{g^2_{USp(2+N)_N}} &= \left[3\frac{(N+4)}{2} - \frac{1}{2}(N+4)\right] \ln\left(\frac{\mu}{\Lambda_N}\right) = (4+N)\ln\left(\frac{\mu}{\Lambda_N}\right) \\ \frac{1}{g^2_{USp(2)}} &= \left[6 - \left(\frac{1}{2}+\frac{3}{2}\right)\right] \ln\left(\frac{\mu}{\Lambda_2}\right) = 4\ln\left(\frac{\mu}{\Lambda_2}\right) \ , \end{aligned}$$

at scale v'. The final relation one gets between the UV and IR scale is now

$$\Lambda_2^4 = \left(\frac{v}{v'}\right)^{N} \Lambda_{UV}^4 \ . \tag{205}$$

This result is analogous to the one obtained before (even though the roles of v and v' are exchanged). We conclude that the Coulomb branch is unstable and it is so independently of the regime in which the 3-2 model finds itself.

6.3 The PdP4 singularity

We now want to consider a different model, based on the pseudo del Pezzo 4 singularity, $PdP4$ for short. We choose, for definiteness, the phase I, following the conventions of [60], where pseudo del Pezzo singularities were introduced. The dimer is depicted in figure fig. 49.

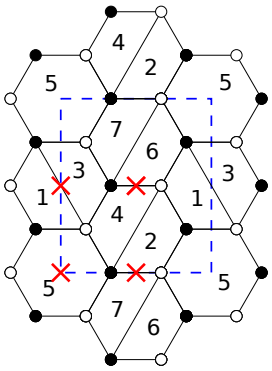

Figure 49: $PdP4$ dimer. Red crosses represent fixed points under the orientifold action.

As for the orbifold model, from the dimer one can extract the field theory content and the corresponding superpotential, which now reads

$$W = X_{1543} + X_{375} + X_{1642} + X_{5276} - X_{152} - X_{7643} - X_{5427} - X_{5316} \ , \qquad (206)$$

with by now familiar index conventions. Note that the superpotential admits also quartic terms now, implying that (some) fundamental fields have large anomalous dimensions. This is related to an important qualitative difference with respect to the previous example. In this model there exist deformation fractional branes, together with $\mathcal{N} = 2$ ones. For instance, the strip 1-3-5 is a $\mathcal{N} = 2$ brane, while 2-6 and 1-2-5 are two different kinds of deformation branes.

Upon point reflection with charges $(+,-,+,-)$ starting on the fixed point on face 5 and going clockwise, we get the following identifications between faces

$$1 \iff 3 \qquad 2 \iff 7 \qquad 4 \iff 6 \qquad 5 \iff 5 \ . \qquad (207)$$

The daughter theory has hence gauge group

$$SO(N_5) \times SU(N_1) \times SU(N_2) \times SU(N_4) \ , \qquad (208)$$

and matter in the following representations

$$\begin{array}{lll} X_1 = (\overline{\square}_1, \square_5), & X_2 = (\square_5, \square_2), & X_4 = (\square_5, \square_4), \\ Y_1 = (\overline{\square}_4, \overline{\square}_1), & Y_2 = (\overline{\square}_4, \square_2), & Z = (\overline{\square}_2, \square_1), \\ A_1 = \begin{smallmatrix}\square\\\square\end{smallmatrix}_1, & A_2 = \overline{\begin{smallmatrix}\square\\\square\end{smallmatrix}}_2, & S_4 = \square\square_4 \ . \end{array} \qquad (209)$$

The anomaly cancellation conditions for the three SU factors are

$$\begin{cases} N_2 + N_1 - N_5 - N_4 - 4 = 0 & SU(N_1) \\ N_5 + N_4 - N_2 - N_1 + 4 = 0 & SU(N_2) \\ N_5 - N_1 - N_2 + N_4 + 4 = 0 & SU(N_4) \end{cases} ,$$

which is the unique condition

$$N_1 + N_2 - N_4 - N_5 - 4 = 0 \ . \tag{210}$$

SU(5) model

The constraint eq. 210 allows to obtain an effective $SU(5)$ DSB model, as for the theory studied in the previous section, by choosing $N_5 = 1, N_1 = 5, N_2 = N_4 = 0$.[22]

We can now proceed as for the orbifold $\mathbb{C}^3/\mathbb{Z}_6$ and add to the aforementioned DSB brane configuration N regular D3-branes, which change the theory to $SO(N+1) \times SU(N+5) \times SU(N) \times SU(N)$ (with the corresponding matter and superpotential terms).

As already noticed, differently from the orbifold case, where the tree level potential of the parent theory contains only cubic terms, and hence the anomalous dimensions of all fields are zero, in this model we have both cubic and quartic terms, and so we have to take into account non-trivial anomalous dimensions. We can compute such anomalous dimensions in the parent theory. They are fixed by populating the dimer with regular branes and imposing vanishing β functions and R-charge equal 2 to all superpotential terms (in the present case this corresponds to 7+8=15 equations).

The symmetries of the dimer help in simplifying the system one has to solve. In particular there exist three $\mathbb{Z}_2$ symmetries acting on faces as $2 \leftrightarrow 3$, $1 \leftrightarrow 7$ and $(4,1,2) \leftrightarrow (6,3,7)$, respectively. Using these symmetries the number of independent anomalous dimensions is just 5 which gives back only 4 independent equations one has to solve, implying in the end a solution with one unfixed modulus. This can be fixed by a-maximization [61] giving finally, for the fields eq. 209, the following result

$$\begin{aligned}
&\gamma_{X_1} = \frac{2}{5}, \qquad \gamma_{X_2} = \frac{2}{5}, \qquad \gamma_{X_4} = -\frac{4}{5}, \\
&\gamma_{Y_1} = -\frac{4}{5}, \qquad \gamma_{Y_2} = -\frac{4}{5}, \qquad \gamma_Z = -\frac{4}{5}, \\
&\gamma_{A_1} = -\frac{4}{5}, \qquad \gamma_{A_2} = -\frac{4}{5}, \qquad \gamma_{S_4} = \frac{2}{5} \ ,
\end{aligned} \tag{211}$$

where $\Delta_i = 1 + \frac{1}{2}\gamma_i$. The orientifold projection may provide $1/N$ corrections to these anomalous dimensions, as fractional branes similarly do. Here and in the following, we will consistently neglect both of them.

We can now proceed as in the previous example by adding N regular branes to the DSB system, higgsing and doing scale matching. The gauge coupling associated

[22] We note that there is also the configuration $N_4 = 1, N_1 = 5, N_2 = N_5 = 0$ that leads to a $SU(5)$ DSB model, with the extra decoupled singlet S_4. The analysis goes through very similarly. Further interchanging the roles of nodes 1 and 2 provides two more trivially equal examples.

to face 1 above and below the scale v of the VEV of the gauge invariant operator $\Phi = \mathrm{Tr}(X_4 Y_2 Z X_1)$ runs as

$$\begin{aligned}\frac{1}{g^2_{SU(5+N)}} &= \left[3(N+5) - \left(\frac{N+1}{2}\left(1-\frac{2}{5}\right) + \frac{N}{2}\left(1+\frac{4}{5}\right) + \frac{N}{2}\left(1+\frac{4}{5}\right) + \right.\right. \\ &\left.\left. \frac{N+3}{2}\left(1+\frac{4}{5}\right)\right)\right] \ln\left(\frac{\mu}{\Lambda_{UV}}\right) = 12\ln\left(\frac{\mu}{\Lambda_{UV}}\right) \\ \frac{1}{g^2_{SU(5)}} &= \left[15 - \left(\frac{3}{10}+\frac{27}{10}\right)\right]\ln\left(\frac{\mu}{\Lambda}\right) = 12\ln\left(\frac{\mu}{\Lambda}\right) \ .\end{aligned}$$

Matching the scale at $\mu = v$ we get

$$\Lambda = \Lambda_{UV} \ . \tag{212}$$

Again, the matching of the two scales is exact, *i.e.* Λ does not depend on v.

Let us now investigate other possible decay channels. In the parent theory, a regular brane can be seen as a bound state of a $\mathcal{N}=2$ brane associated to the strip 1-3-5 and its complement, 2-4-6-7. Upon orientifolding these two fractional branes become a 1-5 and a 2-4 strips, respectively. We can see that also in this theory, after the orientifold projection, the two types of $\mathcal{N}=2$ fractional branes behave differently, one leading to a supersymmetric vacuum and the other triggering supersymmetry breaking into runaway. The details are similar to the orbifold case, and we refrain to repeat the analysis here. The end result, after scale matching, is

$$\Lambda^{12} = \left(\frac{v'}{v}\right)^{\frac{9}{5}N} \Lambda_{UV}^{12} \ . \tag{213}$$

The dynamics is qualitatively the same as for the $\mathbb{C}^3/\mathbb{Z}_6$ case. The theory enjoys a one-dimensional moduli space of supersymmetry preserving vacua at $v' = 0$, parametrized by v.

3-2 model

Also this orientifold admits a 3-2 DSB model. Indeed, a different rank assignment which satisfies the anomaly cancellation condition is $N_5 = 1, N_1 = 3, N_2 = 2, N_4 = 0$ which gives a $SU(3) \times SU(2) \times SO(1)$ gauge theory with matter content

$$\begin{aligned} X_1 = (\overline{\square}_1, \square_5) = \overline{D}, \qquad & X_2 = (\square_5, \square_2) = L, \qquad , \qquad Z = (\overline{\square}_2, \square_1) = Q, \\ A_1 = \begin{smallmatrix}\square\\\square\end{smallmatrix}_1 = \overline{U}, \qquad & A_2 = \begin{smallmatrix}\overline{\square}\\\overline{\square}\end{smallmatrix}_2 = S \ , \end{aligned} \tag{214}$$

where we used again that the two index antisymmetric representation of $SU(3)$ is equal to the antifundamental, and that the two index antisymmetric of $SU(2)$ is

actually the singlet representation. The matter content is precisely the one of the 3-2 model (up to a decoupled singlet S) and, from eq. 206, one can also see that the only term surviving in the superpotential is precisely

$$W = \overline{D}QL \ . \tag{215}$$

As for the $SU(5)$ model, the addition of regular branes does not destabilize the DSB vacuum. As before, however, the theory has $\mathcal{N} = 2$ fractional branes, which eventually do destabilze the vacuum, as in the orbifold case. In particular, it is possible to show, by scale matching, that the strong coupling scale which controls the DSB vacuum energy (Λ_3 of the $SU(3)$ factor or Λ_2 of the $SU(2)$ factor) is affected by the higgsing procedure and the vacuum energy relaxes to zero. The scale matchings give, in the two cases

$$\Lambda_3^6 = \left(\frac{v'}{v}\right)^{\frac{9}{5}N} \Lambda_{UV}^6 \ , \qquad \Lambda_2^3 = \left(\frac{v}{v'}\right)^{\frac{6}{5}N} \Lambda_{UV}^3 \tag{216}$$

which, again, show that the vacuum is unstable, eventually.

The $PdP4$ case is different from the previous orbifold case in that it has a natural warped throat UV completion. Indeed, it contains deformation fractional branes, so that the parent theory admits a cascade of Seiberg dualities. For instance, in the conformal case, $N_i = N$ for any i, it is straightforward to show that starting from node 1 and following the sequence $1 \to 2 \to 4 \to 5 \to 6 \to 7 \to 3$ we get back to the starting point. Then, if we add M (deformation) fractional branes on nodes 1-2-5, we trigger a cascade. Performing the previous sequence six times, we find that the number of regular branes is diminished by seven times the number of fractional ones

$$\begin{gathered} SU_1(N'+M) \times SU_2(N'+M) \times SU_3(N') \times \\ SU_4(N') \times SU_5(N'+M) \times SU_6(N') \times SU_7(N') \end{gathered}$$

where $N' = N - 7M$. Upon orientifolding,[23] the fractional brane configuration that could give rise to the one containing the 3-2 model discussed above should in fact be

$$N_5 = 1 + 2M \quad N_1 = 3 + M \quad N_2 = 2 + M \quad N_4 = 0 \ , \tag{217}$$

which is indeed compatible with the anomaly condition eq. 210. This can be seen in the parent theory as a bound state of M fractional branes 1-2-5 and M fractional branes 3-5-7, both of deformation type, one mirror of the other through the orientifold projection. Now, however, this superposition of deformation branes

[23] See again [44] for the subtleties of performing a duality cascade in an orientifolded theory.

can be alternatively seen as being composed of two sets of $\mathcal{N} = 2$ fractional branes, 1-3-5 and 2-5-7, whose Coulomb branch survives the orientifold projection. A straightforward repetition of the scale matchings previously discussed shows that even this different UV completion has a Coulomb branch instability, eventually.

6.4 Other DSB set-ups

In this section we want to generalize the previous analysis and show that the DSB $SU(5)$ and 3-2 models arise in a large class of CY orientifold singularities, either $\mathbb{C}^3$ orbifolds or Pseudo del Pezzo's, of which previous examples are protoypes. As we will see, in all these models the same instability channel displayed above emerges.

6.4.1 del Pezzo singularities

We start focusing on non-orbifold singularities, like the one discussed in section 6.3, and limit ourselves to toric CY's whose dual gauge theories admit at most eight gauge factors. The complete list of corresponding toric diagrams and dimers can be found in [62], to which we refer for details.

Most of these singularities are obtained as blow ups of del Pezzo singularities. Toric CYs at del Pezzo singularities are complex cones over del Pezzo surfaces dPn with $n = 0, \ldots, 3$ [21]. By blowing up at smooth points of the del Pezzo one obtains larger CY singularities, dubbed Pseudo del Pezzo's, following the terminolgy of [60]. The blow up corresponds to unhiggsing in the dual field theory.

Within this class, we list below those singularities which, after suitable orientifold projection, admit an anomaly free rank assignment giving a $SU(5)$ or 3–2 dynamical supersymmetry breaking model.

For each singularity we present the dimer, including the unit cell and the orientifold action. Orientifold charges are reported as a string of plus and minus signs with the following conventions. For point reflection, by starting from the bottom left corner of the unit cell and going clockwise. For lines, the first sign is for the central line and the second for the one on the edge of the fundamental cell. We also present the gauge group and the matter content of the orientifolded theory, the anomaly cancellation conditions (ACC) for the SU gauge factors and the rank assignment leading to interesting DSB configurations (as far as the 3–2 model, it is understood that also the correct cubic superpotential term is reproduced). Finally, for each singularity, we indicate the Coulomb branch directions whose quantum dynamics we have analyzed, following the two-steps Higgsing pattern discussed in previous sections. For the sake of clarity, these are indicated in terms of faces of the dimer after the orientifold action has been taken into account. Our end results are summarized in the table below.

	$SU(5)$ model	3-2 model
$PdP3_c$	○	○
$PdP3_b$(line)	○	×
$PdP3_b$(point)	○	×
$PdP4_b$	○	○
$PdP5$	○	×
$PdP5_b$	○	×
$PdP5'_a$	○	×
$PdP5'_b$	○	×

- $PdP3_c$ $(+,-,+,-)$

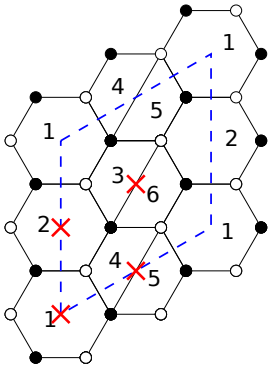

Figure 50: $PdP3_c$ dimer with orientifold points.

- Gauge group:

$$SO(N_1) \times USp(N_2) \times SU(N_3) \times SU(N_4) \tag{218}$$

- Matter content:

$$\begin{array}{lll} X_1 = (\square_1, \overline{\square}_3), & X_2 = (\square_3, \square_2), & Z = (\square_3, \square_4) \\ Y_1 = (\square_4, \square_1), & Y_2 = (\square_2, \overline{\square}_4), & V = (\square_2, \square_1), \\ \overline{A}_4 = \overline{\square\!\square}_4, & \overline{S}_3 = \overline{\square\!\square}_3. & \end{array} \tag{219}$$

- ACC:

$$\Big\{ N_4 - N_1 + N_2 - N_3 - 4 = 0 \qquad SU(N_3) \text{ and } SU(N_4) \tag{220}$$

- DSB configurations:

$SU(5)$ model: $N_1 = 1$, $N_4 = 5$; $N_3 = 1$, $N_4 = 5$ gives an additional singlet, $\overline{S}_3$.

3-2 model: $N_1 = 1$, $N_2 = 2$ and $N_4 = 3$.

- Coulomb branch directions:

$$1 - 4 \quad , \quad 2 - 3 \tag{221}$$

- $PdP3_b$ $(+,-)$

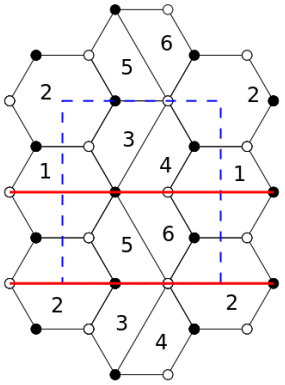

Figure 51: $PdP3_b$ dimer with orientifold lines.

- Gauge group:

$$SO(N_1) \times USp(N_2) \times SU(N_3) \times SU(N_4) \tag{222}$$

- Matter content:

$$\begin{array}{lll} Z = (\square_1, \square_2), & X_1 = (\square_1, \square_3), & X_2 = (\overline{\square}_3, \square_2) \\ V = (\overline{\square}_3, \square_4), & Y_2 = (\overline{\square}_4, \square_2), & Y_1 = (\square_1, \square_4), \\ \overline{S}_4 = \overline{\square\square}_4, & A_3 = \begin{smallmatrix}\square\\\square\end{smallmatrix}_3. & \end{array} \tag{223}$$

- ACC:

$$\Big\{ N_1 - N_2 + N_3 - N_4 - 4 = 0 \qquad SU(N_3) \text{ and } SU(N_4) \tag{224}$$

- DSB configurations:

$SU(5)$ model: $N_3 = 5$ and $N_4 = 1$. This model has an extra singlet due to the symmetric tensor of $SU(N_4)$, $\overline{S}_4$.[24]

[24] $N_3 = 5$ and $N_2 = 1$ is not a valid configuration since N_2, being related to a USp group, has to be even.

- Coulomb branch directions:

$$3-4 \quad , \quad 1-2 \tag{225}$$

Note that this is the only example we found of a *line* orientifold admitting an anomaly free rank assignment leading to a DSB configuration.

- $PdP3_b$ $(+,-,+,-)$

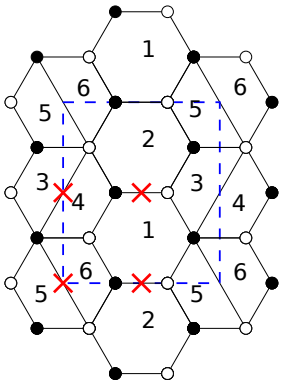

Figure 52: $PdP3_b$ dimer with orientifold points.

- Gauge group:

$$SU(N_1) \times SU(N_3) \times SU(N_5) \tag{226}$$

- Matter content:

$$\begin{array}{lll} Z = (\overline{\square}_5, \square_3), & X_1 = (\overline{\square}_1, \square_3), & X_2 = (\square_1, \square_5) \\ Y_1 = (\overline{\square}_3, \overline{\square}_1), & Y_2 = (\overline{\square}_5, \square_1), & \\ \overline{S}_1 = \overline{\square\square}_1, & A_1 = \begin{smallmatrix}\square\\\square\end{smallmatrix}_1, & \\ S_5 = \square\square_5, & \overline{A}_3 = \overline{\begin{smallmatrix}\square\\\square\end{smallmatrix}}_3. & \end{array} \tag{227}$$

- ACC:

$$\left\{ N_3 - N_5 - 4 = 0 \qquad SU(N_1)\,,\ SU(N_3) \text{ and } SU(N_5) \right. \tag{228}$$

- DSB configurations:

$SU(5)$ model: $N_3 = 5$ and $N_5 = 1$. This model has an extra singlet due to the symmetric tensor of $SU(N_5)$, S_5.

- Coulomb branch directions:

$$3-5 \quad , \quad 1 \tag{229}$$

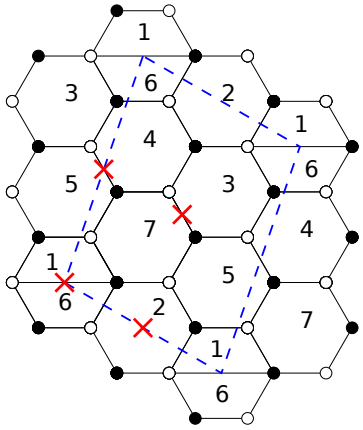

Figure 53: $PdP4_b$ dimer with orientifold points.

- $PdP4_b$ $(-,-,+,+)$

  - Gauge group:

$$SU(N_1) \times SO(N_2) \times SU(N_3) \times SU(N_4) \tag{230}$$

  Matter content:

$$\begin{array}{lll} X_1 = (\square_2, \square_1), & X_3 = (\square_2, \square_3), & X_4 = (\overline{\square}_4, \square_2) \\ Y_1 = (\overline{\square}_3, \square_1), & Y_2 = (\overline{\square}_1, \square_4), & Z_1 = (\overline{\square}_3, \square_4), \\ Z_2 = (\overline{\square}_4, \square_3), & Z_3 = (\overline{\square}_4, \overline{\square}_3), & \\ \overline{A}_1 = \overline{\square\!\square}_1, & S_3 = \square\square_3, & A_4 = \square\!\square_4. \end{array} \tag{231}$$

  - ACC:

$$\Big\{ N_1 - N_2 - N_3 + N_4 - 4 = 0 \qquad SU(N_1)\,,\, SU(N_3) \text{ and } SU(N_4) \tag{232}$$

  - DSB configurations:

  $SU(5)$ model I: $N_1 = 5$ and $N_2 = 1$; equivalently $N_4 = 5$ and $N_2 = 1$.

  $SU(5)$ model II: $N_1 = 5$ and $N_3 = 1$. This model has an extra singlet due to the symmetric tensor of $SU(N_3)$, S_3.

  3-2 model: $N_1 = 3$, $N_2 = 1$ and $N_4 = 2$. There is again an extra singlet due to the antisymmetric tensor of $SU(N_4)$, A_4. The roles of nodes 1 and 4 can be interchanged, providing another equivalent model.

  - Coulomb branch directions:

$$1 - 2 \quad , \quad 3 - 4 \tag{233}$$

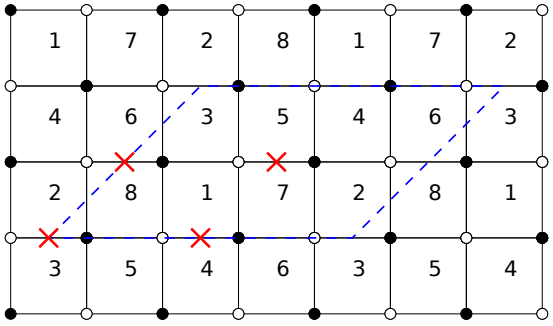

Figure 54: $PdP5$ dimer with orientifold points.

- $PdP5$ $(-,+,+,-)$

  - Gauge group:

$$SU(N_1) \times SU(N_2) \times SU(N_5) \times SU(N_6) \tag{234}$$

  - Matter content:

$$\begin{aligned} &X_1 = (\overline{\square}_1, \overline{\square}_5), \qquad X_2 = (\square_5, \square_6), \qquad X_3 = (\overline{\square}_1, \overline{\square}_6) \\ &X_4 = (\square_2, \square_1), \qquad X_5 = (\overline{\square}_2, \overline{\square}_5), \qquad X_6 = (\overline{\square}_2, \overline{\square}_6), \\ &A_2 = \begin{smallmatrix}\square\\\square\end{smallmatrix}_2, \qquad S_6 = \square\square_6, \qquad S_5 = \square\square_5, \qquad A_1 = \begin{smallmatrix}\square\\\square\end{smallmatrix}_1 \ , \end{aligned} \tag{235}$$

  - ACC:

$$N_1 + N_2 - N_5 - N_6 - 4 = 0 \quad SU(N_1)\,,\, SU(N_2)\,,\, SU(N_5) \text{ and } SU(N_6) \tag{236}$$

  - DSB configurations:

  $SU(5)$ models: $N_1 = 5$ or $N_2 = 5$ and $N_5 = 1$ or $N_6 = 1$. In all configurations there is an additional singlet arising from the symmetric representation at nodes 5 or 6.

  Note also that in this model it is straightforward to exclude the existence of a 3-2 model, since the superpotential is purely quartic.

  - Coulomb branch directions:

$$1 - 5 \ \ , \ \ 2 - 6 \tag{237}$$

As a side remark, note that $PdP5$ is actually an orbifold of the conifold, hence it inherits some of its features, such as all anomalous dimensions being equal to $\gamma = -1/2$. This makes the scale matching simpler to check.

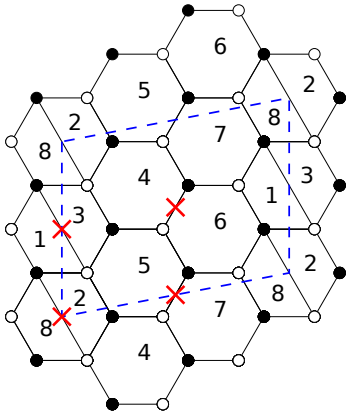

Figure 55: $PdP5_b$ dimer with orientifold points.

- $PdP5_b$ $(+,-,-,+)$

  - Gauge group:

$$SU(N_1) \times SU(N_2) \times SU(N_4) \times SU(N_5) \tag{238}$$

  - Matter content:

$$\begin{aligned} &X_1 = (\overline{\square}_1, \square_2), \qquad X_2 = (\square_1, \square_4), \qquad X_3 = (\overline{\square}_1, \overline{\square}_5), \\ &Y_1 = (\overline{\square}_4, \square_2), \qquad Y_2 = (\overline{\square}_2, \square_5), \qquad Z_1 = (\overline{\square}_4, \square_5), \\ &Z_2 = (\overline{\square}_5, \square_4), \qquad Z_3 = (\overline{\square}_4, \overline{\square}_5), \\ &A_1 = \begin{smallmatrix}\square\\\square\end{smallmatrix}_1, \qquad S_5 = \square\square_5, \qquad \overline{S}_2 = \overline{\square\square}_2, \qquad A_4 = \begin{smallmatrix}\square\\\square\end{smallmatrix}_4 \ . \end{aligned} \tag{239}$$

  - ACC:

$$\begin{cases} N_1 - N_2 - N_5 + N_4 - 4 = 0 \end{cases} \qquad SU(N_1)\,,\, SU(N_2)\,,\, SU(N_4) \text{ and } SU(N_5) \tag{240}$$

  - DSB configurations:

  $SU(5)$ models: $N_1 = 5$ and $N_2 = 1$, or $N_1 = 5$ and $N_5 = 1$, or $N_4 = 5$ and $N_2 = 1$. They all include a singlet related to the symmetric of the $SU(1)$ node.

  - Coulomb branch directions:

$$1 - 2 \quad , \quad 4 - 5 \tag{241}$$

This exhausts Pseudo del Pezzo's properly defined. Below we consider two more models in the list reported in [62] (corresponding to the toric diagrams 15 and 16 of their table 6, respectively).

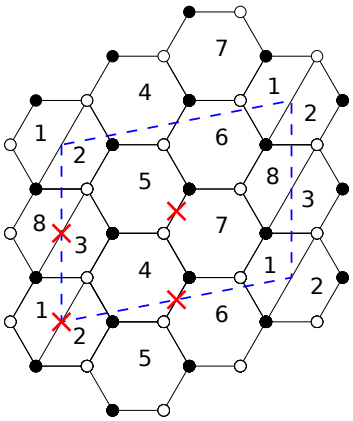

Figure 56: $PdP5'_a$ dimer with orientifold points.

- $PdP5'_a$ $(-,+,+,-)$

  This singularity can be obtained by unhiggsing $PdP3_c$.

  - Gauge group:

$$SU(N_1) \times SU(N_3) \times SU(N_4) \times SU(N_5) \tag{242}$$

  - Matter content:

$$\begin{array}{lll} X_1 = (\overline{\square}_3, \square_1), & X_2 = (\square_4, \square_1), & X_3 = (\overline{\square}_5, \overline{\square}_1) \\ Y_1 = (\overline{\square}_3, \square_5), & Y_2 = (\overline{\square}_4, \square_3), & Z_1 = (\overline{\square}_5, \square_4), \\ Z_2 = (\overline{\square}_4, \overline{\square}_5), & Z_3 = (\overline{\square}_4, \square_5) & \\ \overline{A}_1 = \overline{\square\!\square}_1, & S_5 = \square\!\square_5, & S_3 = \square\!\square_3, \qquad A_4 = \begin{smallmatrix}\square\\\square\end{smallmatrix}_4 \ , \end{array} \tag{243}$$

  - ACC:

$$\begin{cases} N_1 - N_3 - N_4 + N_5 - 4 = 0 & SU(N_1) \text{ and } SU(N_3) \\ N_1 - N_3 + N_4 - N_5 - 4 = 0 & SU(N_4) \text{ and } SU(N_5) \end{cases} \tag{244}$$

  leading to $N_1 = N_3 + 4$, $N_4 = N_5$.

  - DSB configurations:

  $SU(5)$ model: $N_1 = 5$ and $N_3 = 1$. There is an additional singlet given by S_3.

  - Coulomb branch directions:

$$1 - 3 \ , \ \ 4 - 5 \tag{245}$$

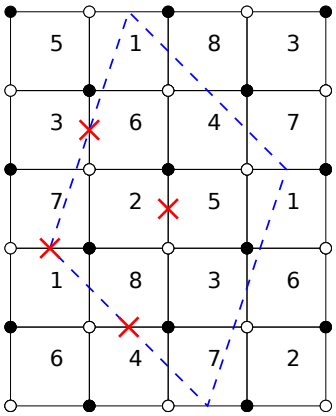

Figure 57: $PdP5'_b$ dimer with orientifold points.

- $PdP5'_b$ $(-,+,-,+)$

  This singularity is again an unhiggsing of $PdP3_c$.

  - Gauge group:

$$SU(N_1) \times SU(N_2) \times SU(N_3) \times SU(N_4) \tag{246}$$

  - Matter content:

$$\begin{array}{llll} X_1 = (\square_1, \square_2), & X_2 = (\square_4, \square_1), & X_3 = (\overline{\square}_1, \overline{\square}_3) & \\ Y_1 = (\overline{\square}_2, \overline{\square}_3), & Y_2 = (\overline{\square}_4, \overline{\square}_2), & Z = (\square_4, \square_3), & \\ \overline{A}_1 = \overline{\square\!\square}_1, & A_2 = \square\!\square_2, & S_3 = \square\!\square_3, & \overline{S}_4 = \overline{\square\!\square}_4 \ , \end{array} \tag{247}$$

  - ACC:

$$\begin{cases} N_1 - N_2 + N_3 - N_4 - 4 = 0 & SU(N_1) \text{ and } SU(N_4) \\ N_1 + N_2 - N_3 - N_4 - 4 = 0 & SU(N_2) \text{ and } SU(N_3) \end{cases} \tag{248}$$

  leading to $N_1 = N_4 + 4$, $N_2 = N_3$.

  - DSB configurations:

  $SU(5)$ model: $N_1 = 5$ and $N_4 = 1$. We have again the additional singlet $\overline{S}_4$.

  - Coulomb branch directions:

$$1 - 4 \quad , \quad 2 - 3 \tag{249}$$

One can continue the unhiggsing process and look for more and more singularities admitting fractional brane configurations described by $SU(5)$ or 3–2 DSB

models at low energy. The procedure is easy to understand from the point of view of toric diagrams and we refer the interested reader to [62].

The above analysis shows that the DSB $SU(5)$ and the 3–2 models are not specific to the $PdP4$ example discussed in section 6.3, but actually arise in a large (in principle infinite, see above comment) class of (blown-up) del Pezzo singularities, sensibly enlarging the landscape of D-brane configurations enjoying a stable DSB vacuum at low energy.

Similarly to the $PdP4$ case, one can then ask what is the fate of these vacua in a large N completion. As anticipated, one can show that the Coulomb branch directions we have indicated and that all these singularities possess, become runaway at the quantum level, and the true vacua are in fact supersymmetric.

6.5 Orbifolds

In this subsection we want to generalize the analysis of section 6.2 and present other instances of (orientifolds of) $\mathbb{C}^3$ orbifold singularities displaying DSB models. The corresponding dimers can be obtained from the hexagonal tiling of $\mathbb{C}^3$ with algorithms that can be found in [63]. We report below a scan of both $\mathbb{C}^3/\mathbb{Z}_n$ and $\mathbb{C}^3/\mathbb{Z}_p \times \mathbb{Z}_q$ orbifolds.

6.5.1 Orbifolds $\mathbb{C}^3/\mathbb{Z}_n$

Following the same logic of the $\mathbb{C}^3/\mathbb{Z}_{6'}$ case, we extended our analysis to higher orders of the cyclic group $\mathbb{Z}_n$. DSB models can again be found for some orientifold projections. Interestingly, no DSB models were found for n odd. We summarize our scan for n as large as 30 in the table below.

	Action on $\mathbb{C}_3$	$SU(5)$ model	3-2 model
$\mathbb{Z}_8$	(1,2,5)	$\circ$	$\times$
$\mathbb{Z}_{12}$	(1,4,7)	$\circ$	$\times$
$\mathbb{Z}_{30}$	(1,10,19)	$\circ$	$\times$

In the above table, a triplet (i, j, k) refers to an orbifold action defined as

$$\theta \ : \quad z_i \to e^{2\pi i w_i} z_i \tag{250}$$

with $w = (a, b, c)/n$, where $a + b + c = n$. It turns out that a necessary condition for allowing interesting DSB models is to focus on orientifold point reflection with two points on top a face. This has the effect of giving an orientifoled theory with two SO/USp gauge factors and $(n-2)/2$ SU factors as

$$SO/USp \times SU \times \cdots \times SU \times SO/USp \ . \tag{251}$$

Let us summarize the specific features of each case.

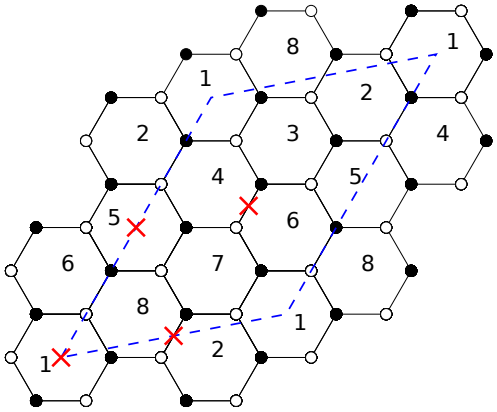

Figure 58: $\mathbb{C}^3/\mathbb{Z}_8$ dimer with orientifold points.

- $\mathbb{Z}_8$ $(+,-,+,-)$

  - Gauge group:

$$SO(N_1) \times SU(N_2) \times SU(N_3) \times SU(N_4) \times USp(N_5) \tag{252}$$

  - Matter content:

$$\begin{array}{llll} (\square_1, \overline{\square}_2), & (\square_1, \overline{\square}_3), & (\square_1, \square_4), & (\square_2, \overline{\square}_3) \\ (\square_2, \overline{\square}_4), & (\overline{\square}_2, \square_5), & (\square_2, \square_3), & (\square_3, \overline{\square}_4) \\ (\square_3, \square_5), & (\overline{\square}_3, \overline{\square}_4), & (\square_4, \square_5), & \overline{\square\!\square}_2, \quad \square\!\square_4, \end{array} \tag{253}$$

  - ACC:

$$\begin{cases} N_1 + N_2 - 2N_3 - N_4 + N_5 - 4 = 0 & SU(N_2) \\ N_1 - N_5 = 0 & SU(N_3) \\ N_1 - N_2 - 2N_3 + N_4 + N_5 + 4 = 0 & SU(N_4) \end{cases} \tag{254}$$

  leading to $N_2 = N_4 + 4$, $N_1 = N_3 = N_5$.

  - DSB configurations:

  $SU(5)$ model: $N_2 = 5$ and $N_4 = 1$, with an additional singlet at node 4.

  - Coulomb branch directions:

$$2 - 4 \quad , \quad 1 - 3 - 5 \tag{255}$$

- $\mathbb{Z}_{12}$ $(-,+,-,+)$

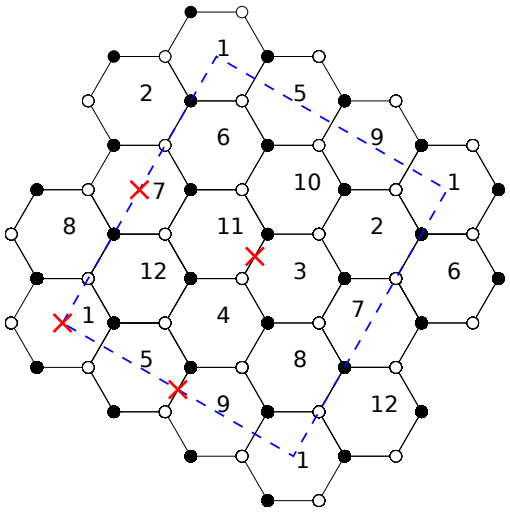

Figure 59: $\mathbb{C}^3/\mathbb{Z}_{12}$ dimer with orientifold points.

- Gauge group:

$$USp(N_1) \times SU(N_2) \times SU(N_3) \times SU(N_4) \times SU(N_5) \times SU(N_6) \times SO(N_7) \tag{256}$$

- Matter content:

$$\begin{array}{llll} (\square_1, \square_2), & (\square_1, \square_5), & (\square_1, \overline{\square}_6), & (\square_2, \square_4) \\ (\overline{\square}_2, \overline{\square}_5), & (\square_2, \square_7), & (\overline{\square}_2, \square_6), & (\overline{\square}_2, \square_3) \\ (\overline{\square}_3, \overline{\square}_4), & (\square_3, \square_6), & (\overline{\square}_3, \square_7), & (\overline{\square}_3, \square_4) \\ (\square_4, \square_5), & (\overline{\square}_4, \overline{\square}_6), & (\overline{\square}_4, \square_5), & (\overline{\square}_5, \square_6) \\ (\overline{\square}_6, \square_7), & \begin{array}{|c|}\hline \\ \hline \square \\ \hline \end{array}_3, & \begin{array}{|c|c|}\hline \square & \square \\ \hline \end{array}_5. & \end{array} \tag{257}$$

- ACC:

$$\begin{cases} N_1 + N_4 - N_5 + N_7 - N_6 - N_3 = 0 & SU(N_2) \\ N_2 - 2N_4 + N_6 - N_7 + N_3 - 4 = 0 & SU(N_3) \\ N_2 - N_6 = 0 & SU(N_4) \\ N_1 - N_2 + 2N_4 - N_6 - N_5 - 4 = 0 & SU(N_5) \\ N_1 - N_2 - N_3 + N_4 - N_5 + N_7 = 0 & SU(N_6) \end{cases} \tag{258}$$

leading to $N_2 = N_4 = N_6$, $N_1 = N_5 + 4$, $N_3 = N_7 + 4$.

- DSB configurations:

$SU(5)$ model: $N_3 = 5$, $N_7 = 1$ and $N_1 = 4$. This is actually an anomaly-free $SU(5) \times USp(4)$ gauge theory, with matter charged under the $SU(5)$ factor only. The $USp(4)$ pure SYM condenses leaving exactly the uncalculable $SU(5)$ DSB model at low energy.

- Coulomb branch directions:

$$3-7 \quad , \quad 1-5 \quad , \quad 2-4-6 \tag{259}$$

- $\mathbb{Z}_{30}$

  Due to the large order of this orbifold, we will refrain from listing all its characteristics (and displaying the dimer), but just comment on the outcome.

  Upon orientifolding, the gauge group reduces to sixteen gauge groups and the ACC allows for the following choice of non-vanishing ranks

$$SO(1)_1 \times SU(5)_2 \times SU(4)_3 \times SU(4)_4 \times SU(4)_5 \times USp(4)_6 \ , \tag{260}$$

  with matter content

$$\begin{aligned} &Q = (\square_1, \overline{\square}_2), \qquad X = (\overline{\square}_4, \square_3), \qquad Y = (\square_5, \square_4), \\ &Z = (\overline{\square}_3, \overline{\square}_5), \qquad A = \begin{smallmatrix}\square\\\square\end{smallmatrix}_2 \ , \end{aligned} \tag{261}$$

  and tree level superpotential

$$W = YXZ \ . \tag{262}$$

  Each $SU(4)$ factor has four flavors and they all condense on the baryonic branch. Supposing that, say, $SU(4)_3$ condenses first, the superpotential becomes a mass term for the meson $M = XZ$ and the field Y, which can then be integrated out. The remaining two $SU(4)$s become pure SYM at low energy and condense, too, leaving again a DSB $SU(5)$ model at low energy.

The analysis for orbifolds of order higher than 30 is more complicated, hence we stop our scan at this level. We just mention that, for instance, a $\mathbb{Z}_{40}$ orbifold seems to possess an $SU(5)$ DSB model configuration, though it comes together with a decoupled sector involving 6 more gauge groups. A preliminary analysis suggests that the extra sector eventually confines in a supersymmetric vacuum, but a detailed analysis is clearly beyond the scope of the present scan.

All above examples have also the usual Coulomb branch instability that destabilizes the DSB vacua. Being orientifolds of orbifolds, all anomalous dimensions vanish and it is a simple exercise to check that the scale matchings lead to a dependency on the VEVs in the DSB vacuum energy.

6.5.2 Orbifolds $\mathbb{C}^3/\mathbb{Z}_p \times \mathbb{Z}_q$

One may also consider the product of cyclic groups, *i.e.* the $\mathbb{Z}_p \times \mathbb{Z}_q$ orbifold action.

Also within this class, at least within our scan, one can find DSB $SU(5)$ models as well as 3-2 models. The end results, for some of the cases we have analyzed, are summarized in the table below.

	Action on $\mathbb{C}_3$	$SU(5)$ model	3-2 model
$\mathbb{Z}_2 \times \mathbb{Z}_4$	[(0,1,1),(1,0,3)]	$\circ$	$\times$
$\mathbb{Z}_3 \times \mathbb{Z}_3$	[(0,1,2),(1,0,2)]	$\circ$	$\circ$
$\mathbb{Z}_2 \times \mathbb{Z}_6$	[(0,1,1),(1,0,5)]	$\circ\circ$	$\times$

Starting from $\mathbb{C}^3$, the orbifold action is now defined by two triplets, corresponding to $\mathbb{Z}_p$ and $\mathbb{Z}_q$ actions, respectively, both defined as eq. (250). Similarly, following the conventions of [63], to which we refer for details, faces in the dimer have a double-index notation associated to the two independent orbifold actions.

From the dimer one can look for suitable orientifold projections and DSB anomaly free rank assignments. Again, in all cases a Coulomb branch runaway direction is present as soon as one tries to embed the D-brane configurations in a large-N theory.

In the following we list the properties of each case.

- $\mathbb{Z}_2 \times \mathbb{Z}_4$ $(-,+,-,+)$

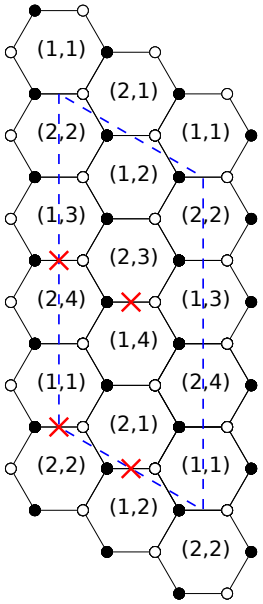

Figure 60: $\mathbb{C}^3/\mathbb{Z}_2 \times \mathbb{Z}_4$ dimer with orientifold points.

We denote the surviving faces by $i \equiv (1,i)$ with $i = 1 \ldots 4$.

- Gauge group:

$$SU(N_1) \times SU(N_2) \times SU(N_3) \times SU(N_4) \tag{263}$$

- Matter content:

$$\begin{array}{llll} (\Box_1, \overline{\Box}_2), & (\Box_1, \Box_3), & (\overline{\Box}_1, \Box_4), & (\Box_1, \Box_2) \\ (\overline{\Box}_1, \overline{\Box}_2), & (\Box_2, \overline{\Box}_3), & (\overline{\Box}_2, \overline{\Box}_4), & (\Box_3, \overline{\Box}_4) \\ (\Box_3, \Box_4), & (\overline{\Box}_3, \overline{\Box}_4), & \overline{\Box}_1, \quad \Box\Box_2, \quad \overline{\Box\Box}_3, & \Box_4 \ . \end{array} \tag{264}$$

- ACC:

$$N_1 + N_4 - N_2 - N_3 - 4 = 0 \quad SU(N_1)\,,\, SU(N_2)\,,\, SU(N_3) \text{ and } SU(N_4) \tag{265}$$

- DSB configurations:

$SU(5)$ model: $N_1 = 5$ and $N_3 = 1$, or $N_4 = 5$ and $N_2 = 1$. Both models have an additional singlet at nodes 3 or 2, respectively.

- Coulomb branch directions:

$$1 - 3 \quad , \quad 2 - 4 \tag{266}$$

- $\mathbb{Z}_3 \times \mathbb{Z}_3$ $(-,-,+,-)$

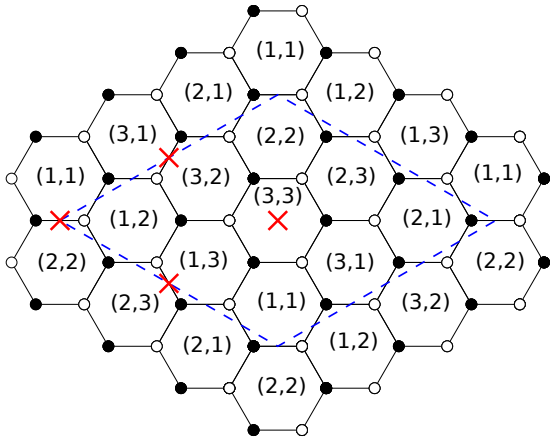

Figure 61: $\mathbb{C}^3/\mathbb{Z}_3 \times \mathbb{Z}_3$ dimer with orientifold points.

We denote the surviving faces as follows

$$\begin{array}{lll} 1 \equiv (1,1) \iff (2,2) & & 2 \equiv (1,2) \iff (2,1) \\ 3 \equiv (1,3) \iff (2,3) & & 4 \equiv (3,1) \iff (3,2) \\ & 5 \equiv (3,3) & \end{array} \tag{267}$$

- Gauge group:

$$SU(N_1) \times SU(N_2) \times SU(N_3) \times SU(N_4) \times SO(N_5) \tag{268}$$

- Matter content:

$$\begin{array}{llll} (\Box_1, \Box_2), & (\Box_1, \Box_5), & (\overline{\Box}_1, \Box_4), & (\overline{\Box}_1, \Box_3) \\ (\Box_1, \overline{\Box}_2), & (\overline{\Box}_2, \overline{\Box}_3), & (\overline{\Box}_2, \overline{\Box}_4), & (\Box_2, \overline{\Box}_4) \\ (\Box_2, \overline{\Box}_3), & (\Box_3, \Box_4), & (\overline{\Box}_3, \Box_5), & (\overline{\Box}_4, \Box_5), \\ \multicolumn{2}{r}{\begin{array}{|c|c|}\hline \overline{\Box} \\ \hline \Box \\ \hline \end{array}_1,} & \multicolumn{2}{l}{\begin{array}{|c|}\hline \Box \\ \hline \Box \\ \hline \end{array}_3, \qquad \begin{array}{|c|}\hline \Box \\ \hline \Box \\ \hline \end{array}_4 \ .} \end{array} \tag{269}$$

- ACC:

$$N_1 - 2N_2 + N_3 + N_4 - N_5 - 4 = 0 \quad SU(N_1)\,,\, SU(N_3) \text{ and } SU(N_4) \tag{270}$$

while the ACC on $SU(N_2)$ is trivially satisfied.

- DSB configurations:

$SU(5)$ models: $N_5 = 1$ and either $N_1 = 5$, $N_3 = 5$ or $N_4 = 5$.

3-2 models: $N_1 = 3$, $N_3 = 2$ and $N_5 = 1$, and any other permutation of nodes 1, 3 and 4. There is an additional decoupled singlet related to the antisymmetric at the $SU(2)$ node.

- Coulomb branch directions:

$$1 - 5 \ \ , \ \ 2 - 3 - 4 \tag{271}$$

- $\mathbb{Z}_2 \times \mathbb{Z}_6$ $(-,-,+,+)$

Upon the following face identifications

$$\begin{array}{lll} 1 \equiv (1,1) \iff (2,2) & & 2 \equiv (1,3) \iff (2,6) \\ 3 \equiv (1,5) \iff (2,4) & & 4 \equiv (1,2) \iff (2,1) \\ 5 \equiv (1,6) \iff (2,3) & & 6 \equiv (1,4) \iff (2,5) \end{array} \tag{272}$$

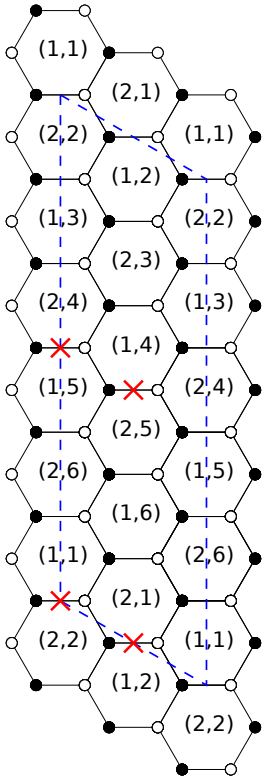

Figure 62: The dimer of the orbifold $\mathbb{C}^3/\mathbb{Z}_2 \times \mathbb{Z}_6$ with orientifold points.

the gauge group is $\prod_i^6 SU(N_i)$ with matter in the following representations

$$\begin{array}{llll} (\square_1, \square_2), & (\overline{\square}_2, \overline{\square}_3), & (\overline{\square}_4, \overline{\square}_5), & (\square_6, \square_5), \\ (\overline{\square}_1, \square_5), & (\overline{\square}_5, \square_3), & (\overline{\square}_3, \square_6), & (\overline{\square}_6, \square_2), \\ (\overline{\square}_2, \square_4), & (\overline{\square}_4, \square_1), & (\square_1, \square_4), & (\overline{\square}_1, \overline{\square}_4), \\ (\square_2, \square_5), & (\overline{\square}_2, \overline{\square}_5), & (\square_3, \square_6), & (\overline{\square}_3, \overline{\square}_6), \\ \overline{\square\!\square}_1, & \square\!\square_3, & \square\!\square_4, & \overline{\square\!\square}_6 \ . \end{array} \tag{273}$$

The ACC reads

$$\begin{cases} N_2 - N_5 + N_4 - N_1 + 4 = 0 & SU(N_1) \text{ and } SU(N_4) \\ N_2 - N_5 + N_6 - N_3 + 4 = 0 & SU(N_3) \text{ and } SU(N_6) \\ N_1 - N_3 - N_4 + N_6 = 0 & SU(N_2) \text{ and } SU(N_5) \end{cases} . \tag{274}$$

The solution to the ACC allows for a choice of ranks leaving a non-anomalous theory with gauge group

$$SU(5)_1 \times SU(1)_2 \times SU(5)_3 \tag{275}$$

and matter content given by

$$X = (\Box_1, \Box_3), \qquad A_1 = \overline{\Box}_1, \qquad Y = (\overline{\Box}_2, \overline{\Box}_3), \qquad A_2 = \Box_2 \quad (276)$$

We then end up with two decoupled $SU(5)$ DSB models. Since we now have two independent contributions to the vacuum energy, one could think that the different higgsing scales can conspire in a non-trivial way, possibly leading to a non-zero minimum.

Again, higgsing by regular branes does not destabilize the supersymmetry breaking vacua. Performing the following (three steps, now) $\mathcal{N} = 2$ brane higgsing pattern

$$\begin{aligned} & SU(5+N)_1 \times SU(1+N)_2 \times SU(5+N)_3 \times SU(N)_4 \times SU(N)_5 \times SU(N)_6 \\ & \xrightarrow{v} SU(5)_1 \times SU(1+N)_2 \times SU(5+N)_3 \times SU(N)_5 \times SU(N)_6 \\ & \xrightarrow{v'} SU(5)_1 \times SU(1+N)_2 \times SU(5)_3 \times SU(N)_5 \\ & \xrightarrow{v''} SU(5)_1 \times SU(1)_2 \times SU(5)_3 \ , \end{aligned}$$

we get instead the following scale matching

$$\Lambda^{13}_{1,\mathrm{IR}} = \left(\frac{v''}{v}\right)^N \Lambda^{13}_{1,\mathrm{UV}} \quad \text{and} \quad \Lambda^{13}_{3,\mathrm{IR}} = \left(\frac{v''}{v'}\right)^N \Lambda^{13}_{3,\mathrm{UV}} \ , \qquad (277)$$

for the two $SU(5)$ factors, respectively. The potential hence scales as

$$V \ \sim \ \left| \left(\frac{v''}{v}\right)^{N/13} \Lambda_{1,\mathrm{UV}} \right|^4 + \left| \left(\frac{v''}{v'}\right)^{N/13} \Lambda_{3,\mathrm{UV}} \right|^4 \ . \qquad (278)$$

When trying to minimize the potential with respect to v, v' and v'', the minimum is reached at $v'' = 0$, and it is a supersymmetry preserving one. In other words, there is no compensation between the two factors in the potential, as one could have in principle hoped for.

This ends the list of examples we wanted to present. As anticipated, in all orbifold models we have discussed, similarly to the models of section 6.4.1, the supersymmetry breaking vacua are destabilized once one tries to embed the DSB configurations in a large N theory. As one can easily check, the mechanism is again the same: while regular branes correspond to exact flat directions, $\mathcal{N} = 2$ fractional brane directions become runaway once the dependence of the vacuum energy on the Coulomb branch modulus is taken into account.

6.6 A no-go theorem and how to avoid it

In previous sections we presented several models which allow for brane configurations giving DSB vacua, both at orbifold and del Pezzo-like singularities. However, when properly UV completed, all models include runaway directions, associated to $\mathcal{N} = 2$ fractional branes, which destabilize the non-supersymmetric minima. One might wonder whether it is possible to get rid of such an ubiquitous instability channel.

The first question one could ask is under which conditions the dangerous Coulomb branch direction can remain flat at the quantum level. In order for this to hold it suffices that the coefficient α in eq. eq. (185) vanishes

$$\alpha = 0 \ . \tag{279}$$

Let us then see if this can happen. Let us start considering the gauge theory prior to the orientifold projection. Generically, if considering N regular D3-brane at the singularity the theory is a SCFT and all β functions vanish, that is for each gauge factor the following holds

$$\beta_{SU(N)} = 3N - \frac{N}{2}\sum_{i=1}^{n}(1-\gamma_i) = 0 \ , \tag{280}$$

where γ_i are the anomalous dimensions of the bi-fundamental fields charged under the given gauge group (recall that in the unorientifolded theory all matter fields are in bifundamental representations).

Let us now add M fractional branes to the N regular ones and focus on those gauge groups to which the fractional branes couple to. The corresponding β function changes as

$$\beta_{SU(N+M)} = 3(N+M) - \frac{N}{2}\sum_{i=1}^{j}(1-\gamma_i^{(0)}) - \frac{N+M}{2}\sum_{i=1}^{k}(1-\gamma_i^{(1)}) \ , \tag{281}$$

where $\gamma_i^{(0)}$ are the anomalous dimensions of bifundamental fields charged under groups not coupling to the fractional branes while $\gamma_i^{(1)}$ are those of fields charged under groups coupling to the fractional branes. Using eq. 280 and the identity $\sum_i^k(1-\gamma_i^{(1)}) + \sum_i^j(1-\gamma_i^{(0)}) = \sum_i^n(1-\gamma_i)$ the above expression can be re-written as

$$\beta_{SU(N+M)} = \frac{M}{2}\sum_{i=1}^{j}(1-\gamma_i^{(0)}) \ , \tag{282}$$

which does not vanish since fractional branes do not support a SCFT. Hence we conclude that

$$\sum_{i=1}^{j}(1-\gamma_i^{(0)}) \neq 0 \ . \tag{283}$$

Let us now consider the orientifold action and start with a configuration with regular D3-branes, only. One important point is that β functions are now affected by the fact that some ranks are finitely shifted to balance the O-plane charge. For example, in the $PdP4$ model discussed in section 6.3, the orientifolded theory with N regular branes has gauge group $SO(N+1) \times SU(N+5) \times SU(N) \times SU(N)$.

Compared to eq. 280, the expression for the β function becomes

$$3(N+c) - \sum_{i=1}^{n}(1-\gamma_i)\frac{N+b_i}{2} = 3c - \sum_{i=1}^{n}(1-\gamma_i)\frac{b_i}{2} \ , \tag{284}$$

where c is the extra coefficient of the gauge group we are considering and b_i those of the gauge groups under which bifundamental matter is charged (in our $PdP4$ example $c = 5$ for the $SU(N+5)$ group, and bifundamental matter charged also under the $SO(N+1)$ group has $b = 1$). Note that the β function is no longer vanishing, due to the O-plane charge, and its coefficient does not depend on N.

Let us now perform the two-steps Higgsing which $\mathcal{N} = 2$ fractional branes make possible, as in all models previously considered. Using the same conventions as in previous sections, the gauge coupling running at different scales is

- UV (above scale v)

$$\begin{aligned}\frac{1}{g^2_{SU(N+c)}} &= \left(3(N+c) - \sum_{i=1}^{n}(1-\gamma_i)\frac{N+b_i}{2}\right)\ln\left(\frac{\mu}{\Lambda_{UV}}\right) \\ &= \left(3c - \sum_{i=1}^{n}(1-\gamma_i)\frac{b_i}{2}\right)\ln\left(\frac{\mu}{\Lambda_{UV}}\right) \ . \end{aligned} \tag{285}$$

- Intermediate scale (below scale v and above scale v')

$$\begin{aligned}\frac{1}{g^2_{SU(c)_N}} &= \left(3c - \sum_{i=1}^{k}(1-\gamma_i^{(1)})\frac{b_i}{2} - \sum_{i=1}^{j}(1-\gamma_i^{(0)})\frac{N+b_i}{2}\right)\ln\left(\frac{\mu}{\Lambda_N}\right) \\ &= \left(3c - \sum_{i=1}^{n}(1-\gamma_i)\frac{b_i}{2} - \sum_{i=1}^{j}(1-\gamma_i^{(0)})\frac{N}{2}\right)\ln\left(\frac{\mu}{\Lambda_N}\right) \ . \end{aligned} \tag{286}$$

- IR (below scale v')

$$\frac{1}{g^2_{SU(c)}} = \left(3c - \sum_{i=1}^{n}(1-\gamma_i)\frac{b_i}{2}\right)\ln\left(\frac{\mu}{\Lambda}\right) \ . \tag{287}$$

Note that this pattern holds for all groups and all kinds of matter. Indeed, the presence of (anti)symmetric representations gives factors of the form $\frac{N+b}{2}$ in the β-function, the same as having fundamental matter charged under a $SU(N+b)$ flavor group.

Matching the scale at $\mu = v$ and $\mu = v'$ gives

$$\Lambda^{3c-\sum_{i=1}^{n}(1-\gamma_i)\frac{b_i}{2}} = \left(\frac{v'}{v}\right)^{\sum_{i=1}^{j}(1-\gamma_i^{(0)})\frac{N}{2}} \Lambda_{UV}^{3c-\sum_{i=1}^{n}(1-\gamma_i)\frac{b_i}{2}} \ , \tag{288}$$

which implies that

$$\alpha \propto \sum_{i=1}^{j}(1-\gamma_i^{(0)})\frac{N}{2} \ . \tag{289}$$

In order for α to vanish we need that $\sum_i^j(1-\gamma_i^{(0)}) = 0$, which is in contradiction with eq. eq. (283). This shows that whenever $\mathcal{N} = 2$ fractional branes couple to the DSB nodes, they inevitably become runaway and destabilize the otherwise stable DSB vacuum.

This result suggests that in order to avoid this instability channel one could try to look at singularities which, unlike those we have analyzed, admit deformations or DSB branes and no $\mathcal{N} = 2$ ones, and see whether there could be room for DSB models there.

A comprehensive survey of toric singularities up to eight gauge groups is provided in [62] and we have analyzed, in this finite class, all singularities having deformation and/or DSB fractional branes only (note that $\mathbb{C}^3$ orbifolds do not belong to this class, since at these singularities a basis of fractional branes, if there are any, always includes $\mathcal{N} = 2$ ones).

More specifically, following the list provided in [62], the singularities not admitting $\mathcal{N} = 2$ fractional branes are the following ones: for toric diagrams of area 2 (Table 1) singularity number 2; for toric diagrams of area 4 (Table 2) singularities number 6 and 7; for area 5 (Table 3) number 5, for area 6 (Table 4), number 8, 9, 10, 12 and 13; for area 7 (Table 5), number 7, 8 and 9; for area 8 (Table 6), number 1, 3, 4, 5, 7, 8, 13 and 17. In order to obtain the dimer, we used the techniques of [23].

Starting from these singularities, one has to see which do admit orientifold point or line projections. This can be done using the criteria spelled out in [27]. If

an orientifold projection is admitted, one performs it and then checks the anomaly cancellation conditions. The latter often do not have any solutions (barring the addition of flavors). If they do have solutions, instead, one has then to see if the corresponding orientifold admits a configuration reproducing a DSB model.

The upshot of our scan is that there exist several possible point and line reflections and in some cases one can also satisfy anomaly cancellation conditions without the addition of extra flavors. When this is the case, however, it turns out that there do not exist configurations leading to any known DSB model and in fact all solutions lead to supersymmetric vacua. This result seems to suggest that the presence of line singularities (*i.e.* $\mathcal{N} = 2$ fractional branes) is a key property a CY singularity should have to allow for DSB low energy dynamics but, at the same time, the one that eventually makes the vacua unstable. In the next section we will elaborate further on this point.

7 Octagon, you are my only hope

As discussed in the previous section, the presence on $\mathcal{N} = 2$ fractional branes can lead to instability in DSB models. These kind of fractional branes are present when the singularity has more than one ZZP with the same winding number. Figure 63 shows an example, based on the PdP_3 geometry [60, 1]. The collection of phases shaded in blue defines an $\mathcal{N} = 2$ fractional brane (its complement is obviously also an $\mathcal{N} = 2$ fractional brane). These faces stretch between the parallel red and green ZZP.

Using this simple observation, we will see how one can to put constraints on the geometry in order to find the minimal requirements for a stable DSB model.

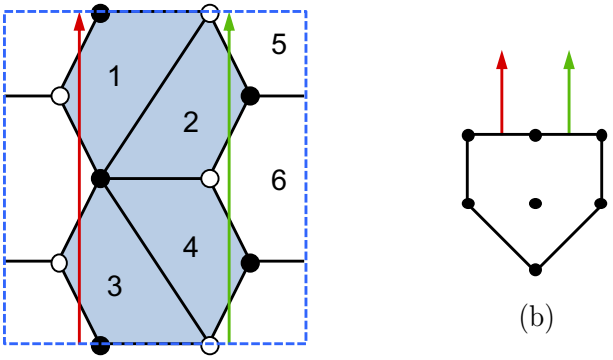

(a)

(b)

Figure 63: a) Dimer model for phase b of PdP_3. b) Toric diagram for PdP_3 showing the two parallel legs of the (p, q)-web associated to the ZZP under consideration.

7.1 $SU(5)$ Models

Let us first consider the $SU(5)$ model. This theory has an $SU(5)$ gauge group and one GUT-like chiral family $\square \oplus \overline{\square}$. The presence of the antisymmetric representation implies that if one wants to engineer such a model by D-branes at a CY singularity, an orientifold projection is necessary. Moreover, one has to consider two gauge groups in order to get the antifundamental representation $\overline{\square}$, which can be generated by either an $SU(1)$ or an $SO(1)$ flavor group [1].

Using the dimer formalism, there are two classes of orientifolds, depending on whether they have *fixed points* or *fixed lines* [25]. We will analyze them in turn.

7.1.1 Fixed Point Orientifolds

Let us remind that fixed point orientifolds are associated to dimers which enjoy a point reflection. It is always possible to choose the unit cell of the dimer in such a way that its corners coincide with a fixed point. Additionally, due to the dimer's toroidal periodicity, there will also be fixed points at the center of the boundaries of the unit cell, and in the center of the unit cell itself, see fig. 64.

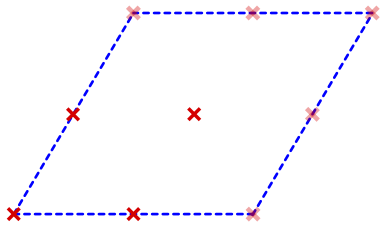

Figure 64: A schematic representation of a dimer unit cell with orientifold fixed points. The shaded points are the periodic images of the four basic ones.

As we now review, we not only need a fixed point on one edge of the $SU(5)$ face, but a second fixed point is needed to avoid anomalies in the face providing the (anti)fundamental matter field.

The first possibility is to directly avoid the anomaly in the flavor group by having it SO or USp. USp is ruled out since it would give always an even number of antifundamentals, hence more than one. We are then left with $SO(1)$.

- SO flavor group

  Figure 65 shows the generic structure of a local configuration of a dimer leading to the $SU(5)$ model, including the signs for the two relevant fixed points. The dotted lines and nodes represent a completely general configuration for the rest of the dimer, only constrained by its compatibility with the point reflections. The blue dotted line indicates that it is possible to choose the unit cell such that the two fixed points live on one of the four segments that form its boundary. This comment will be relevant later.

  Assigning arbitrary ranks to the gauge groups, N_i for face i in the dimer, the anomaly cancellation conditions (ACC) have a solution in which $N_1 = N_{1'} = 5$, $N_2 = 1$ and the rest of the faces are empty.[25] This choice leads exactly to the $SU(5)$ model. Face 1 becomes the $SU(5)_1$ gauge group. Since face 2 has a fixed point with a positive sign on top of it, becomes the $SO(1)_2$ flavor group.

[25] Of course whether the ACC of the empty nodes are also satisfied depends on the details of the boundary of the cluster of faces under consideration. This observation also applies to the examples that follow.

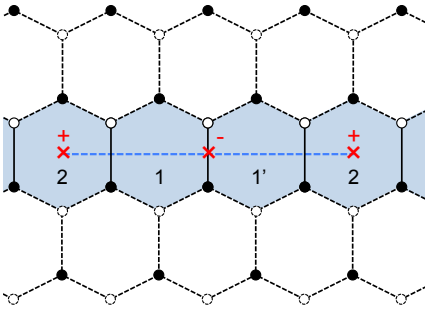

Figure 65: Fixed point orientifold realizing the $SU(5)$ model with $SO(1)$ flavor group. The dotted part of the graph indicates the rest of the dimer, which is completely general and not necessarily hexagonal as shown.

A second possibility is that the flavor group is of SU type, with its anomaly (when regular branes are added) being canceled by the presence of symmetric matter on a different edge of the face.

- SU flavor group with symmetric

  Figure 66 shows the local configuration of a dimer leading to another realization of the $SU(5)$ model in a fixed point orientifold. Once again, the ACC have a solution in which $N_1 = N_{1'} = 5$, $N_2 = N_{2'} = 1$ and the rest of the faces are empty. The resulting theory is the $SU(5)$ model, plus a decoupled singlet corresponding to the symmetric associated to the edge between face 2 and its image.

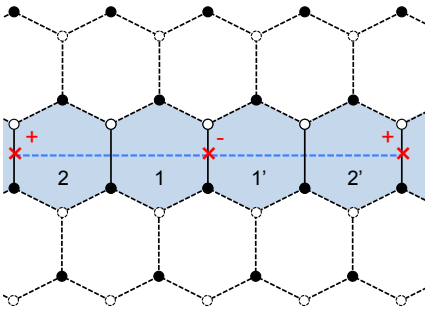

Figure 66: Fixed point orientifold realizing the $SU(5)$ model with $SU(1)$ flavor group.

  Note that the $SU(1)$ group has no anomaly, but the symmetric is necessary to cancel the anomaly when all the ranks are increased by N (corresponding to the addition of N regular D3-branes which populate the dimer democratically). By construction, the additional (white) faces with rank N will not

contribute to the anomaly. In order to cancel the $N+5$ antifundamentals coming from face 1, we need to have a symmetric of $SU(N+1)$ at face 2. It reduces to a decoupled singlet when $N=0$.

A third possibility is that the flavor group is of SU type, and its anomaly (when regular branes are added) is canceled by 5 fundamentals attached to an $SO(5)$ group. This configuration is shown in fig. 67. The low-energy theory of this configuration is an $SU(5)$ model together with a decoupled $SO(5)$ SQCD with one flavor. The latter theory develops an ADS superpotential [53], so that we have a runaway behavior (on top of the DSB of the $SU(5)$ model), and hence no true vacuum. We thus discard this possibility since it is already unstable at this low-energy field theory level.

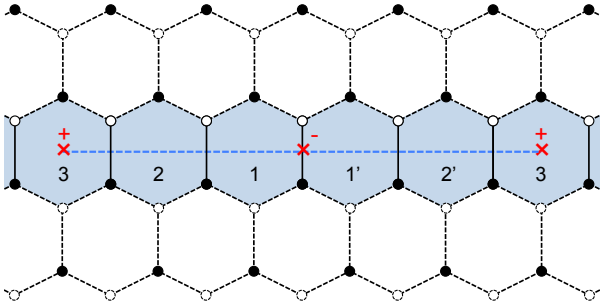

Figure 67: Fixed point orientifold realizing the $SU(5)_1$ model with $SU(1)_2$ flavor group and an additional $SO(5)_3$ factor. $SO(5)_3$ develops an ADS superpotential and leads to a runaway behavior.

A fourth possibility is that the flavor group is again of SU type, but now its anomaly is canceled by the presence of a replica of the $SU(5)$ group with its own antisymmetric. We will call this possibility *twin* $SU(5)$ *model*.

- SU flavor group with twin $SU(5)$

  Figure 68 shows the local configuration of a dimer leading to yet another realization of the $SU(5)$ model in a fixed point orientifold. The ACC have a solution in which $N_1 = N_{1'} = 5$, $N_2 = N_{2'} = 1$, $N_3 = N_{3'} = 5$ and the rest of the faces are empty. The resulting theory corresponds to two $SU(5)$ models sharing one and the same $SU(1)$ flavor group which provides their (anti)fundamentals. Since $SU(1)$ is actually empty, and in any case no chiral gauge invariants can be written for each $SU(5)$ model, the twins are effectively decoupled and thus their low-energy dynamics is completely independent.

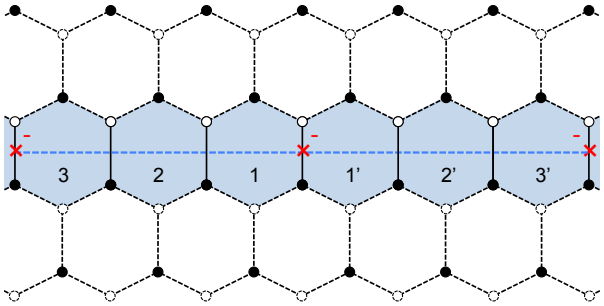

Figure 68: Fixed point orientifold realizing the twin $SU(5)$ model.

In principle, we could go on with further possibilities. Indeed, the anomaly of the second $SU(5)$ gauge group at face 3 can be canceled with a fundamental, instead of an antisymmetric. The simplest possibility is that the fundamental is attached to an $SO(1)$ face, however it could also be an $SU(1)$ with a symmetric, or further an $SU(1)$ with 5 antifundamentals given by an $SO(5)$, or another $SU(5)$. The possibilities already discussed above repeat themselves. What is important to notice is that the gauge theory on face 3 would always be an $SU(5)$ with one flavor, hence developing an ADS superpotential and leading to runaway behavior.

We thus conclude that the only possibilities to engineer an $SU(5)$ model, which is stable at low-energies, in a dimer with fixed points are the three bullets above: SO flavor group, SU flavor group with a symmetric and SU flavor group with twin $SU(5)$.

An important remark is that in all the examples above the following holds: there can be a long chain of gauge groups to eventually cancel the anomaly of the initial $SU(5)$ gauge group, but it always ends with an orientifold fixed point.[26] As a consequence, we do not have to look far in order to identify an $\mathcal{N} = 2$ fractional brane in these dimers. Remarkably, in all cases the $SU(5)$ model is fully supported on a set of faces that corresponds to an $\mathcal{N} = 2$ fractional brane in the parent (i.e., non-orientifolded) theory. From fig. 65, fig. 66 and fig. 68 we see that in all cases the $SU(5)$ model indeed lives on a stripe that gives rise to a gauge invariant not contained in the superpotential. The expectation value of such operator parametrizes the corresponding Coulomb branch.

We conclude that an $SU(5)$ model cannot be obtained for this class of orientifolds if the parent theory does not contain line singularities, i.e. $\mathcal{N} = 2$ fractional

[26] We are ignoring more ramified possibilities. For instance, for an $SU(1)$ flavor at face 2, we could imagine providing the 5 fundamentals from more than one SO gauge group. That would lead to the need of more than one extra fixed point. The other cases can be treated similarly. Thus a more precise statement is that we always need *at least* another fixed point to cancel the anomaly of the $SU(5)$ at face 1.

branes.[27] The previous discussion implies that the no-go theorem in [1] cannot be avoided for this class of orientifolds.

Let us discuss how the instability is realized in these models in more detail. We start with the model with SO flavor, fig. 65. After adding N regular D3-branes, the relevant gauge group becomes

$$SU(N+5)_1 \times SO(N+1)_2 \ . \tag{290}$$

Let us denote

$$A = \begin{array}{|c|}\hline \ \ \\ \hline \ \ \end{array}_1 \quad , \quad \overline{Q} = (\overline{\square}_1, \square_2) \tag{291}$$

where A corresponds to the edge in the dimer between face 1 and its orientifold image and $\overline{Q}$ corresponds to the edge between faces 1 and 2. The Coulomb branch is parametrized by the expectation value of the gauge invariant going around the stripe. In principle we can build an $SU(N+5)_1$ gauge invariant as

$$\phi^{SO}_{ab} = \overline{Q}^i_a \overline{Q}^j_b A_{ij} \ , \tag{292}$$

where i, j are fundamental indices of $SU(N+5)_1$ and a, b are fundamental indices of $SO(N+1)_2$. Note that it is in the antisymmetric representation of $SO(N+1)_2$, hence it does not exist for $N = 0$, and it has vanishing trace for $N \geq 1$.

As discussed in [1], we actually need to go twice around the stripe in order to have a non-vanishing gauge invariant given by

$$\langle \delta^{ac} \delta^{bd} \phi^{SO}_{ab} \phi^{SO}_{cd} \rangle \ , \tag{293}$$

parametrizing the Coulomb branch. That the gauge invariant still vanishes automatically for $N = 0$, is consistent with the fact that the $SU(5)$ model does not have a moduli space and that the additional regular branes are necessary for the instability.

We now consider the case with SU flavor and a symmetric, fig. 66. After adding N regular D3-branes, the gauge group becomes

$$SU(N+5)_1 \times SU(N+1)_2 \ . \tag{294}$$

We denote

$$A = \begin{array}{|c|}\hline \ \ \\ \hline \ \ \end{array}_1 \quad , \quad \overline{Q} = (\overline{\square}_1, \square_2) \quad , \quad \overline{S} = \overline{\square\square}_2 \tag{295}$$

[27] This result is consistent with an observation made in [27], namely that singularities with deformation branes are incompatible with point projections.

where now $\overline{S}$ corresponds to the edge between face 2 and its image under the second fixed point. The $SU(N+5)_1$ gauge invariant is

$$\phi^{SU}_{ab} = \overline{Q}^i_a \overline{Q}^j_b A_{ij} \ , \tag{296}$$

where now a, b are fundamental indices of $SU(N+1)_2$. It is in the antisymmetric representation of $SU(N+1)_2$, hence again it does not exist for $N = 0$, and for $N \geq 1$ it cannot be contracted with $\overline{S}^{ab}$ which is symmetric. A non-vanishing gauge invariant is given by

$$\langle \overline{S}^{ac} \overline{S}^{bd} \phi^{SU}_{ab} \phi^{SU}_{cd} \rangle \ , \tag{297}$$

which now parametrizes the Coulomb branch. The same remarks as in the previous case apply.

Finally, let us discuss the last case of the twin $SU(5)$, where the gauge group becomes

$$SU(N+5)_1 \times SU(N+1)_2 \times SU(N+5)_3 \ . \tag{298}$$

We denote

$$A = \square_1 \quad , \quad \overline{Q} = (\overline{\square}_1, \square_2) \quad , \quad \overline{P} = (\overline{\square}_2, \square_3) \quad , \quad \overline{A} = \overline{\square}_3 \tag{299}$$

where now $\overline{P}$ corresponds to the edge between faces 2 and 3, and $\overline{A}$ to the edge between face 3 and its image under the second fixed point. The $SU(N+5)_1$ and $SU(N+5)_3$ gauge invariants are

$$\phi_{ab} = \overline{Q}^i_a \overline{Q}^j_b A_{ij} \quad , \quad \overline{\phi}^{ab} = \overline{P}^a_\alpha \overline{P}^b_\beta \overline{A}^{\alpha\beta} \ , \tag{300}$$

where α, β are fundamental indices of $SU(N+5)_3$. They are in the antisymmetric and conjugate antisymmetric representation of $SU(N+1)_2$, respectively. They do not exist for $N = 0$, but for $N \geq 1$ the simplest gauge invariant is given by

$$\langle \phi_{ab} \overline{\phi}^{ab} \rangle \ , \tag{301}$$

which parametrizes the Coulomb branch in this case. The same remarks as in the previous cases apply. Further, note that this last case allows for a simpler gauge invariant parametrization of the Coulomb branch because it is the only one where the two fixed points (giving rise to A and $\overline{A}$) have the same sign, see fig. 68. In the two previous cases the fixed points have opposite signs, and we have to take the loop twice.

Double $SU(5)$ Models

In some cases, the structure of the dimer is such that it could be possible to use all four fixed points to generate a pair of $SU(5)$ models. Figure 69 shows the general structure for a dimer giving rise to two $SU(5)$ models with $SO(1)$ flavor nodes. Other possibilities, for instance two models with $SU(1)$ flavor nodes, an $SU(1)/SO(1)$ combination or two twin $SU(5)$ models, are also feasible. The same logic of previous examples applies to each of the two stripes of blue faces, so we conclude that each of these models contain $\mathcal{N} = 2$ fractional branes and hence are not stable.

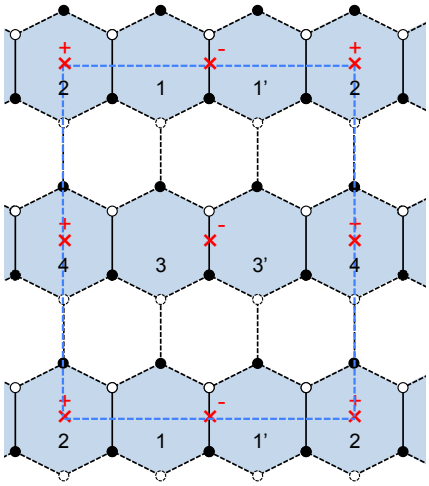

Figure 69: General structure of a fixed point orientifold realizing a double $SU(5)$ with $SO(1)$ flavor group model.

The different cases considered so far illustrate the general strategy that we will apply to most of the other models we will be considering. While the DSB models under consideration are relatively simple, we are considering here their embedding into arbitrarily complicated toric singularities. Therefore, establishing the existence of $\mathcal{N} = 2$ fractional branes (which implies the instability of the DSB model) might naively seem an intractable problem since, generically, the majority of the dimer model will be unknown. However, as it occurred in the previous examples, the necessary interplay between the region of the dimer that makes up the DSB model and the orientifold fixed points (or fixed lines, as we will see shortly), implies that we fully know the dimer model along a "short direction" of the unit cell. This is sufficient to identify an $\mathcal{N} = 2$ fractional brane. In even simpler terms, in these cases the DSB models are actually supported on faces of the dimer that define an $\mathcal{N} = 2$ fractional brane. We will see that there is only one specific way to circumvent this argument.

7.1.2 Fixed Line Orientifolds

A second possibility is that dimers admit line reflection. We can have orientifolds with either two independent fixed lines or a single diagonal fixed line.

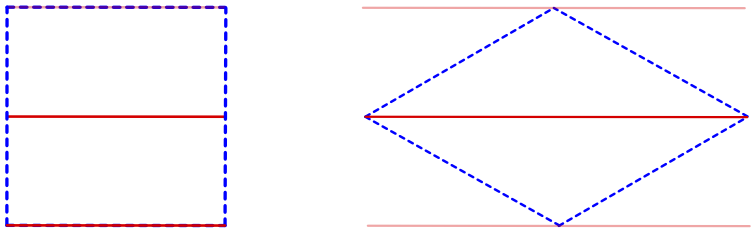

Figure 70: A schematic representation of orientifold fixed lines going through the dimer unit cell: two fixed lines on the left, a single fixed line on the right.

An orientifold with two fixed lines is such that the unit cell of the dimer can be taken to be rectangular, and the dimer is further invariant under a reflection leaving fixed the lines going along one of the boundaries of the unit cell. By the periodicity of the dimer, there must be a second fixed line parallel to the first one, and going through the middle of the unit cell. Vertical and horizontal fixed lines will be considered on the same footing here.

Orientifolds with a single fixed line are such that the unit cell can be taken to have the shape of a rhombus, and the dimer is invariant under reflections about a fixed line which goes along one of the diagonals of the rhombus. The periodicity of the dimer does not imply the presence of other fixed lines in the unit cell. Again, we will not make the distinction between the two diagonals. Both situations are depicted in fig. 70. In the following, we will use the two nomenclatures "double and single" or "horizontal/vertical and diagonal fixed lines" interchangeably.

DSB Models between Two Fixed Lines

The cases with two fixed lines are basically identical to the orientifolds considered in the previous section, with the exchange of fixed points for fixed lines. We therefore present them succinctly.

- *SO* flavor group

  Figure 71 shows the local configuration realizing the $SU(5)$ model with $SO(1)$ flavor group, including the signs of the fixed lines. This is achieved by setting $N_1 = N_{1'} = 5$, $N_2 = 1$ and vanishing ranks for all other faces. Since the two lines have opposite signs, this configuration is only possible in orientifolds with two independent fixed lines.

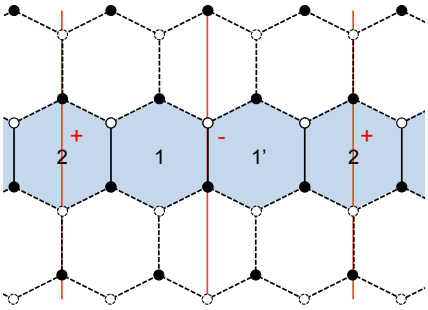

Figure 71: Two fixed lines orientifold realizing the $SU(5)$ model with $SO(1)$ flavor group.

- *SU* flavor group with symmetric

  Figure 72 shows the local configuration realizing the $SU(5)$ model with $SU(1)$ flavor group and a symmetric. This corresponds to $N_1 = N_{1'} = 5$, $N_2 = N_{2'} = 1$ and vanishing ranks for all other faces. Since the two lines have opposite signs, this configuration is only possible in orientifolds with two independent fixed lines.

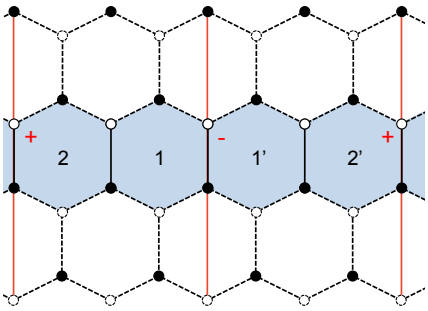

Figure 72: Two fixed lines orientifold realizing the $SU(5)$ model with $SU(1)$ flavor group.

- *SU* flavor group with twin $SU(5)$

  Figure 73 shows the local configuration realizing the $SU(5)$ model with $SU(1)$ flavor group and a twin $SU(5)$ model. This corresponds to $N_1 = N_{1'} = 5$, $N_2 = N_{2'} = 1$, $N_3 = N_{3'} = 5$ and vanishing ranks for all other faces. In this case the two lines have the same sign, hence it is possible to find this configuration both in orientifolds with two independent fixed lines or with a single diagonal fixed line. Note that in the latter case, we have to consider the situation in which the strip goes from one line to a second one, in a contiguous unit cell.

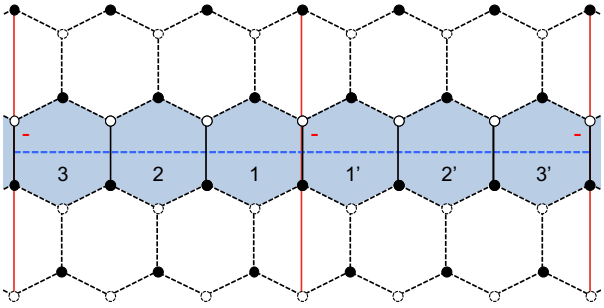

Figure 73: Two fixed lines orientifold realizing the twin $SU(5)$ model.

Using the same arguments as for the fixed point orientifolds in section 7.1.1, we conclude that in all these cases the models are supported on a stripe of faces of the dimer that define an $\mathcal{N} = 2$ fractional brane.

Multiple $SU(5)$ Models

We previously saw that fixed point orientifolds can give rise to double $SU(5)$ models. Similarly, orientifolds with fixed lines can produce multiple $SU(5)$ models, as shown in fig. 74. In this case, the number of models is not restricted to two. It is important to note that, unlike in the example shown in the Figure, it is possible for different stripes to use the two fixed lines in different ways, for instance simultaneously leading to models with both $SO(1)$ and $SU(1)$ flavor groups, when the two lines have opposite signs. Once again, our general discussion applies to each individual stripe of blue faces, so we conclude that $\mathcal{N} = 2$ fractional branes exist for each individual stripe and hence the models are not stable.

DSB Models on a Single Fixed Line: the Twin $SU(5)$

There is one additional way in which an $SU(5)$ model could be engineered. This is when both the projection needed for the antisymmetric of $SU(5)$ and the one for canceling the anomaly due to the antifundamental, are provided by the same fixed line. This could be realized both in orientifolds with a diagonal fixed line, and in orientifolds with two fixed lines. What is important is that only one line is needed to define the relevant cluster of faces.

Importantly, since the orientifold line cannot change sign along the dimer, this possibility is effective only when the two projections have the same sign. Then the only case that fits the bill is the twin $SU(5)$ model, as the one in fig. 73.

Basically, the chain of gauge groups represented by faces 1, 2 and 3 has to bend and end on the same line. There are now two possibilities. Either all the black nodes at the bottom of the edges between faces 1, 2 and 3 are one and the same,

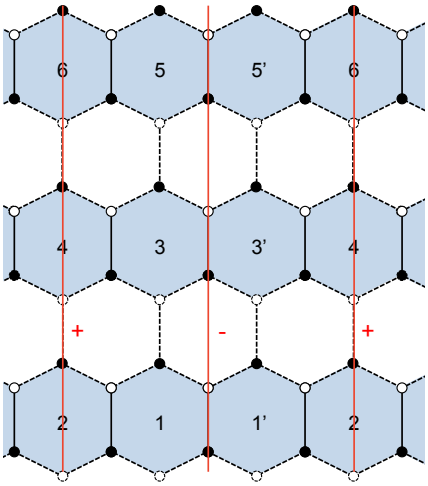

Figure 74: An example of the general structure of a portion of a dimer with two fixed lines giving rise to multiple $SU(5)$ models.

or the chain 1-2-3 and their images enclose some (unoccupied) faces of the dimer. The latter case is inconsistent from the dimer point of view: such a chain cannot be a fractional brane in the parent theory. We are thus left with the former case, which in the dimer corresponds to a hexagonal cluster of faces around a node, as depicted in fig. 75.

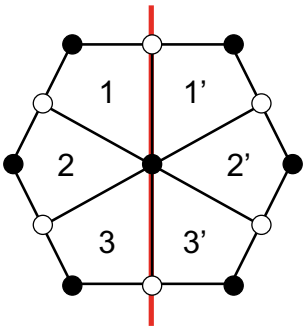

Figure 75: The hexagonal cluster with six faces on an orientifold line. All faces are here depicted with four edges, but some of them could have more.

Interestingly, such a collection of faces surrounding a node corresponds to a deformation fractional brane in the classification of [15]. It is reassuring that unlike in the cases with fixed points, deformation branes are compatible with line orientifolds [27].

The analysis of this case is similar to what we carried out for the twin $SU(5)$

model previously, leading to a gauge group

$$SU(N+5)_1 \times SU(N+1)_2 \times SU(N+5)_3 \ . \tag{302}$$

The difference is that now the node at the center of the hexagonal cluster corresponds to a sextic superpotential term. Using the same notation as in eq. (299), we have

$$W = \mathrm{tr} A \overline{QPAP}^t \overline{Q}^t = \mathrm{tr} \phi \overline{\phi} \ . \tag{303}$$

For $N = 0$, the superpotential vanishes and we are left with two $SU(5)$ models sharing an $SU(1)$ flavor node, in which both surviving $SU(5)$ factors break supersymmetry dynamically into a stable vacuum. Unlike the other realizations of the twin $SU(5)$ model, in the present one there is no indication that the dimer must contain an $\mathcal{N} = 2$ fractional brane.

Combining the analysis in section 7.1.1 and section 7.1.2, we conclude that engineering a single $SU(5)$ DSB model without instabilities at an orientifold of a toric singularity is impossible. Conversely, our analysis implies that engineering a minimal $SU(5)$ model requires non-isolated singularities with curves of $\mathbb{C}^2/\mathbb{Z}_n$ singularities passing through the origin, which in turn result in the instability. This means that, the toric diagram must contain internal points on its boundary edges. On the other hand, our analysis shows that an instance of a DSB model, the twin $SU(5)$ model, actually exists which is compatible with an orientifold projection with fixed line(s). We should now understand whether such sub-dimer can actually be embedded into a consistent dimer and, if so, whether such dimer can be free of $\mathcal{N} = 2$ fractional branes. We investigate these questions in section 7.3.

7.2 3-2 Models

Let us now turn to the 3-2 model, another prominent example of DSB that was recovered within brane setups at orientifold singularities in [1]. The model has gauge group $SU(3) \times SU(2)$. Its matter content is reminiscent of one SM generation

$$Q = (\square_3, \overline{\square}_2) \ , \ \overline{U} = \overline{\square}_3 \ , \ \overline{D} = \overline{\square}_3 \ , \ L = \square_2 \ , \tag{304}$$

where the subindices indicate the corresponding gauge group in an obvious way. In addition, the theory has the following superpotential

$$W = \overline{D} Q L \ . \tag{305}$$

In principle, the above field content (SU gauge groups, (bi)fundamental matter, together with a cubic superpotential) does not seem to require an orientifold projection. As it will become clear in the following, such a projection is nevertheless necessary in order to allow for a fractional brane (i.e. an anomaly free configuration) with the desired ranks for the gauge groups.

7.2.1 General Features

Let us think more carefully about the basic features of the D-brane realization of this model. In this subsection we enumerate all different ways to recover the 3-2 model from fractional branes at an orientifold singularity. The structure of these models is more intricate than that of the $SU(5)$ model, so it is convenient to draw the corresponding quivers.

The candidate models are presented in fig. 76. In the figure, we have kept the ranks of the gauge group general by introducing N_i, $i = 1, \ldots, 4$. These additional integers account for more general configurations of D-branes at the singularity, e.g. the addition of regular or fractional D3-branes, and we posit that anomaly cancellation must hold even in those cases. The 3-2 model arises when all N_i and the ranks of additional gauge groups, which depend on the specific singularity and are not shown in these quivers, vanish.

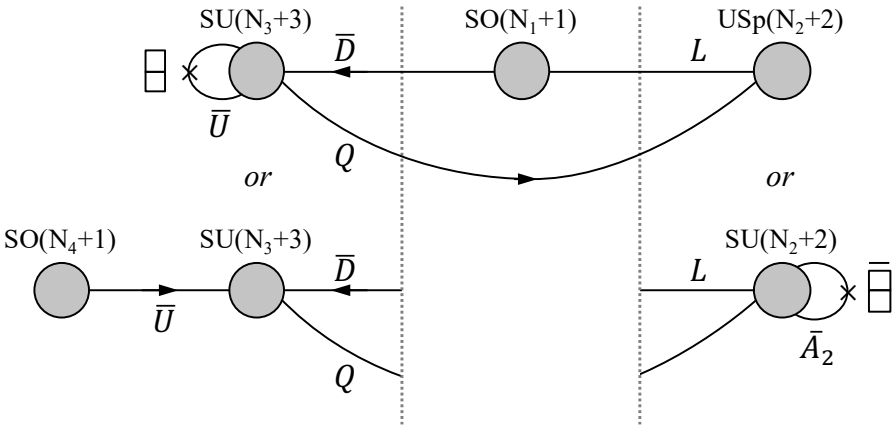

Figure 76: Four quivers giving rise to the 3-2 model when all $N_i = 0$. All these models use three orientifold fixed loci.

For similar reasons as in the case of the $SU(5)$ model, we need at least an additional gauge group factor, which we will call node 1, to serve as a flavor group providing the $\overline{D}$ and L fields. Both $\overline{D}$ and L should be connected to the same node for the superpotential eq. (305) to be possible. In dimer terminology, we identify the smallest building block of a 3-2 model as three faces connected by a trivalent vertex. In this sense 3-2 model realizations are necessarily more involved than $SU(5)$ model realizations, since the latter only required a building block of two faces.

The quivers in fig. 76 should be interpreted as follows. For each of the two endpoints of the quiver, we have presented two possibilities. The two options on the left correspond to realizing $\overline{U}$ as an antisymmetric of node $SU(3)$ or via a fourth

gauge group acting as a flavor node. The two options on the right correspond to the fact that node 2 can be either $USp(2)$ or $SU(2)$. All possible combinations of these endpoints realize the desired 3-2 model, therefore fig. 76 accounts for four models.

In principle, the flavor nodes 1 and 4 in fig. 76 could be SU or SO. However, if these nodes were of SU type, their ACC in the case of general ranks would require additional nodes, that come to life when regular D-branes are added. Generically, these gauge groups will give rise to new matter fields charged under the nodes of the original quiver. Such fields would contribute to and potentially help in the cancellation of anomalies. However, for N regular D3-branes, it is easy to show that for neither node the anomaly would cancel, as there would still be an imbalance of one or three units for nodes 1 and 4, respectively. In order to cancel the anomalies there are then only two options. The first is to introduce an orientifold projection. It turns out that setting both nodes to be SO is the simplest such option, and without loss of generality we will stick to it in the following. The second option is to compensate the anomaly by a mirror construction. We defer the treatment of the latter possibility to the last subsection.

It is worth noting that in two of the four models described by fig. 76, those for which the second gauge group is $SU(N_2 + 2)$, we have also introduced an antisymmetric tensor $\bar{A}_2$. This field is necessary for satisfying the ACC for the more general ranks that arise when regular D3-branes are added (see appendix C). It becomes a singlet when $N_2 = 0$, so it decouples and does not affect the IR physics.

A final option is to get the two antifundamentals of the $SU(3)$, $\overline{U}$ and $\overline{D}$ from the same flavor $SO(1)$ group. However, in order to realize the 3-2 model, the structure of the dimer model should be such that a $\overline{U}QL$ term is not present in the superpotential. This possibility is then obtained by simply identifying nodes 1 and 4 in fig. 76.

We thus reach the conclusion that we need no less than three orientifold projections to realize a 3-2 model: one for the $SO(1)$ flavor group (thus with a $+$ sign), one for node 2 which is either $USp(2)$ or $SU(2)$ with an antisymmetric (in both cases, with a $-$ sign), and one for node 3, either with an antisymmetric ($-$ sign) or with the $SO(1)$ flavor node 4 ($+$ sign). Of course some of these projections can be given by the same object, in the case of an orientifold line, provided they require the same sign.[28]

All quivers described by fig. 76 are viable as stand-alone gauge theories. However, as for the $SU(5)$ model, we need to verify whether the theories remain

[28]It is worth noting that in all the realizations of the 3-2 model found in [1], node 3 has an antisymmetric, node 1 is of SO type, while node 2 is $USp(2)$ in the $\mathbb{Z}_6$ orbifold and in PdP_4, and $SU(2)$ with an antisymmetric in PdP_{3c}, PdP_{4b} and the $\mathbb{Z}_3 \times \mathbb{Z}_3$ orbifold.

anomaly free upon the addition of regular and/or fractional D3-branes. It turns out that the $SO(N_1+1) \times SU(N_2+2) \times SU(N_3+3) \times SO(N_4+1)$ model does not pass this test, as shown in appendix C.

Below we investigate the realization of these models in terms of fixed point and fixed line orientifolds.

7.2.2 Fixed Point Orientifolds

Interestingly, for the purpose of establishing the existence of an $\mathcal{N}=2$ fractional brane, and hence the instability of the supersymmetry breaking vacuum, it is sufficient to focus on a very small part of all these theories. In particular, all of them contain one of the following two subsectors:

- $SO(N_1+1) \times USp(N_2+2)$.
- $SO(N_1+1) \times SU(N_2+2)$ with the tensor $\overline{A}_2$.

Knowledge of the dimer around gauge groups 1 and 2 will be enough for our purposes. Let us consider the general structure of the dimers associated to these two possibilities.

- $SO(N_1+1) \times USp(N_2+2) \subset$ 3-2 model

  fig. 77 shows the general structure of the relevant part of the dimer model. The edge between faces 1 and 2 represents the L field. Clearly, faces 1 and 2 define a stripe that winds around the unit cell of the parent dimer, giving rise to a gauge invariant that is not in the superpotential. Therefore, they correspond to an $\mathcal{N}=2$ fractional brane.

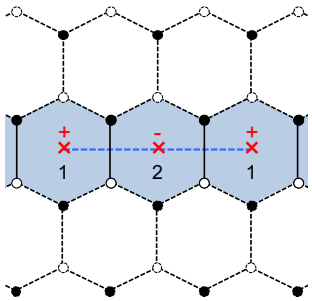

Figure 77: A piece of the dimer for a fixed point orientifold realizing the 3-2 model with an $SO(N_1+1) \times USp(N_2+2)$ subsector.

- $SO(N_1+1) \times SU(N_2+2)$ with $\overline{A}_2 \subset$ 3-2 model

fig. 78 shows the part of the dimer that we are interested in. The edge between faces 1 and 2 corresponds to L, while the one between face 2 and its image gives rise to $\overline{A}_2$. Once again, we see that faces 1, 2 and 2' define an $\mathcal{N}=2$ fractional brane in the parent dimer. It is interesting to note that this picture is identical to fig. 65 for the $SU(5)$ model.

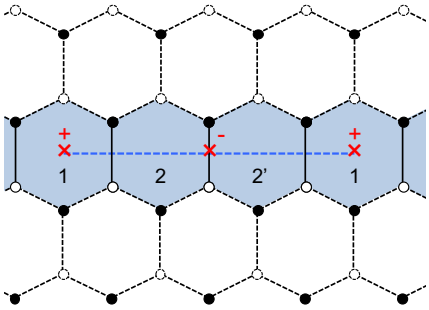

Figure 78: A piece of the dimer for a fixed point orientifold realizing the 3-2 model with an $SO(N_1+1)\times SU(N_2+2)$ with $\overline{A}_2$ subsector.

From the previous discussion, we conclude that all realizations of the 3-2 model at fixed point orientifolds suffer from an $\mathcal{N}=2$ fractional brane instability.

Models with more than one type of $\mathcal{N}=2$ fractional branes

Before moving on, let us consider the models in Figures 77 and 78 in further detail. As we have already mentioned, in all these cases the portion of the dimer realizing the 3-2 model involves three fixed points. For concreteness, let us focus on the case in which $\overline{U}$ is an antisymmetric of node 3 and node 2 if of USp type. All other combinations are analogous and lead to the same conclusions. fig. 79 shows the general structure of the dimer model. Interestingly, in this case we can identify yet another $\mathcal{N}=2$ fractional brane, in addition to the one covered by our previous analysis. This new fractional brane corresponds to faces 1, 3 and 3' in the parent dimer and is shown in pink in fig. 79. We conclude that when sub-dimers as in Figures 77 and 78 are embedded in a complete dimer model, the corresponding toric singularity has at least two different types of $\mathcal{N}=2$ fractional branes. Explicit models illustrating this phenomenon were constructed in [1].

Another interesting fact we would like to notice has to do with the intertwining between $SU(5)$ and 3-2 models realizations. fig. 79 shows that in any such configuration realizing a 3-2 model, an $SU(5)$ model can also be realized, by simply turning off the rank of node 2, while pumping up the rank of node 3 to $SU(5)$. Even more, 3-2 model realizations like the one of fig. 78 allow for two alternative $SU(5)$ model realizations, the other one being by turning off node 3 and setting

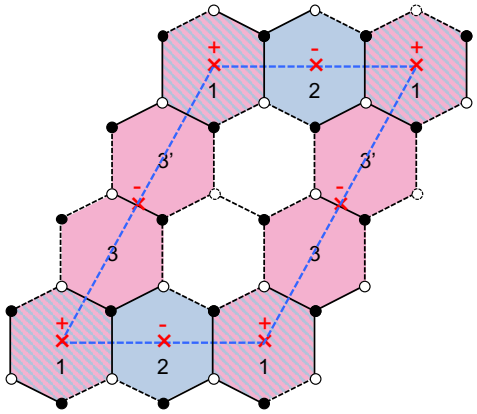

Figure 79: General structure of the dimer model for one of the models in fig. 76. This model contains two different $\mathcal{N} = 2$ fractional branes. They are shown in blue and pink, with the striped face belonging to both of them.

node 2 to $SU(5)$, as already noticed when commenting the figure. Multiple explicit examples of this connection can be found in [1]. The only realization of a 3-2 model that does not lead directly to a realization of the $SU(5)$ model would be one with $USp(2)$ at node 2 and a node 4 to compensate the anomaly of node 3. Unfortunately, no examples of this exist in the literature, and it is beyond our scope to find one here, as we have in any case shown that it would be afflicted by an $\mathcal{N} = 2$ fractional brane instability.

Double 3-2 Models

It is natural to ask whether fixed point orientifolds can lead to a pair of 3-2 models. In this case, each of the models should use two of the four fixed points. However, all the models of fig. 76 need three different projections, and thus three different fixed points. One could still think about the case where nodes 1 and 4 are identified, where only two identifications are actually required. However in order for node 3 to have two different connections with node 1, the faces corresponding to this 3-2 model realization end up being spread across all the unit cell, so that again two such models cannot coexist.[29]

7.2.3 Fixed Line Orientifolds

We now consider the realization of the 3-2 models in orientifolds with fixed lines.

[29]It would be interesting to investigate whether such model can actually be engineered in terms of dimers. Again, since we have already proven that all realizations of the 3-2 models at fixed point orientifolds are unstable, we do not pursue this challenging question any further.

The analysis in the case in which the 3-2 model uses two different orientifold fixed lines is identical to the one for fixed points. In particular, it is sufficient to focus on faces 1 and 2. We simply need to replace fixed points by fixed lines in the previous discussion.

- $SO(N_1+1) \times USp(N_2+2) \subset$ 3-2 model

  Figure 80 shows the relevant part of the dimer. We immediately identify an $\mathcal{N}=2$ fractional brane in the parent dimer consisting of faces 1 and 2.

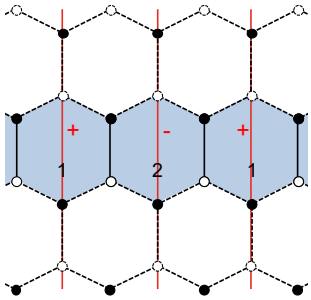

Figure 80: A piece of the dimer for an orientifold with two fixed lines realizing the 3-2 model with an $SO(N_1+1) \times USp(N_2+2)$ subsector.

- $SO(N_1+1) \times SU(N_2+2)$ with $\overline{A}_2 \subset$ 3-2 model

  Figure 81 shows the part of the dimer that we focus on. Faces 1, 2 and 2' form an $\mathcal{N}=2$ fractional brane in the parent dimer.

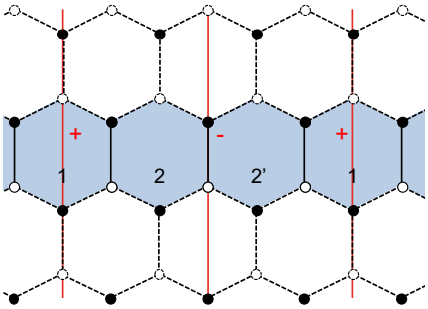

Figure 81: A piece of the dimer for an orientifold with two fixed lines realizing the 3-2 model with an $SO(N_1+1) \times SU(N_2+2)$ with $\overline{A}_2$ subsector.

Multiple 3-2 Models

Orientifolds with fixed lines can in principle give rise to multiple 3-2 models, stacking them as we did in fig. 74 for $SU(5)$. In this case, the projection needed for node

3 can be provided either by the line with a $-$ sign, in case of an antisymmetric, or by the line with a $+$ sign, in case of a flavor node 4. Our previous arguments show that each of these models contain (at least) an $\mathcal{N} = 2$ fractional brane and are hence unstable.

SU(5) - 3-2 Mixed Models

At this point it is interesting to point out that our arguments for multiple models, in the case of fixed lines, indicate that we can also have models that realize a combination of $SU(5)$ and 3-2 models. Once again, our arguments from section 7.1 and this section show that each DSB sector would be independently unstable.

Twin 3-2 models?

We are now left to investigate the possibility that the anomalies of the 3-2 model are cancelled in a twin realization, along the lines of what was done for the $SU(5)$ model in Figures 68 and 73. Further, we would like to know if there is a realization similar to the one of fig. 75, i.e. on a *single* fixed line, which would not automatically imply the presence of $\mathcal{N} = 2$ fractional branes.

As already alluded to, we can cancel the anomalies of a node 1 of SU nature, and/or node 4, if in the configuration there is a twin copy of the 3-2 model sharing the $SU(1)$ node. Note that in compensating the anomaly with a twin, it is important that the two models are decoupled. If we were to use the same mechanism to compensate the anomaly of node 2, the non-zero coupling of node 2 itself would couple the twins and alter the low-energy physics of the models (typically destroying the stable supersymmetry breaking dynamics). Hence whatever we do, node 2 will always require a projection. As a consequence, if such twin model is realized in a way that it extends between two different fixed points or fixed lines, by the same arguments used around fig. 68 and fig. 73, there will be $\mathcal{N} = 2$ fractional branes that render the DSB model eventually unstable. We will thus refrain from investigating further the feasibility of such a configuration.

Finally, we would like to see if it is possible to realize a twin 3-2 model on a single fixed line. Given that node 2 and its twin require a $-$ sign, in principle we have two options. Either both node 3 and its twin have an antisymmetric by ending-up on the same fixed line, or they compensate the anomaly by sharing an $SU(1)$ node 4. It is easy to draw the minimal requirements for the portion of the dimer that would translate these properties, see respectively fig. 82 and fig. 83.

Naively, these configurations look consistent and one can find a choice of ranks satisfying the ACC. These are the following. For fig. 82, $N_3 = N_{3'} = N_{\bar{3}} = N_{\bar{3}'} = M_3 + 3$, $N_2 = N_{2'} = N_{\bar{2}} = N_{\bar{2}'} = M_2 + 2$ and $N_1 = N_{1'} = M_2 + M_3 + 1$. For fig. 83, $N_3 = N_{3'} = N_{\bar{3}} = N_{\bar{3}'} = M_3 + 3$, $N_1 = N_{1'} = M_1 + 1$, $N_4 = N_{4'} = M_1' + 1$ and

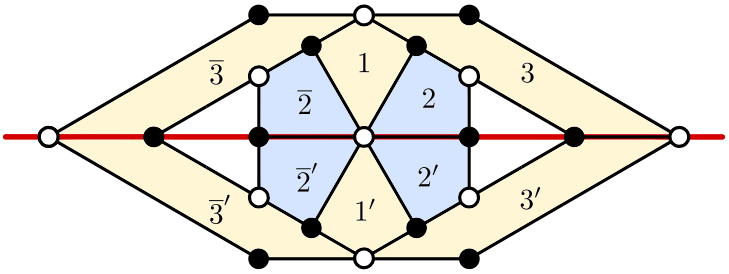

Figure 82: A tentative sub-dimer for a twin 3-2 model where the $SU(3)$ faces have an antisymmetric flavor.

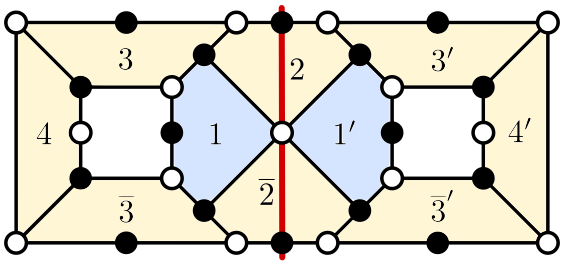

Figure 83: A tentative sub-dimer for a twin 3-2 model where the $SU(3)$ faces share a flavor $SU(1)_4$.

$N_2 = N_{\bar{2}} = M_1 + M_1' + 2$.

Assuming that in the parent theory every rank parameterizing the solutions above can be taken independently large, we observe that both situations would imply the existence of a fractional brane described by a ring of faces with equal ranks (up to the usual $\mathcal{O}(1)$ corrections) surrounding a hole. These are obtained by setting $M_2 = 0$ in fig. 82, and $M_1 = 0$, $M_1' = M_3$ in fig. 83. The ring-shaped would-be fractional brane is depicted in both figures by the yellow-shaded faces. As shown in appendix A, this is an inconsistent dimer. We conclude that unlike the $SU(5)$ model, there is no way to build a stable twin version of the 3-2 model on a single orientifold line.

7.3 The Rise of the Octagon

In section 7.1 and section 7.2 we have shown that the only alternative for an a priori consistent realization of a DSB model which does not automatically imply the presence of an $\mathcal{N} = 2$ fractional brane, and hence is potentially stable in the decoupling limit, is the twin $SU(5)$ living on a single fixed line of an orientifold. The twin $SU(5)$ model is described by the hexagonal cluster depicted in fig. 75. Now we want to understand if such cluster can be embedded in a fully consistent dimer and if such dimer can be free of $\mathcal{N} = 2$ fractional branes.

Let us first argue that in the full theory the hexagonal cluster is associated to a fractional brane. From fig. 75 we see that the ACC are satisfied for $N_1 = N_3 = N + 4$ and $N_2 = N$. Namely, we are free to choose any value of N while all other faces of the dimer sharing an edge with the faces of the hexagonal cluster have vanishing rank. This freedom is associated to the presence of a fractional brane. The twin $SU(5)$ is obtained for $N = 1$, i.e. a single fractional brane.

Now we can ask whether this fractional brane is of deformation or runaway DSB type, in the parent theory (we already know we do not want it to be of $\mathcal{N} = 2$ type). If it were a runaway DSB brane some other regions of the dimer, besides the hexagon, would be populated and the corresponding faces would have ranks with different multiples of N [15, 48]. This is the key ingredient to generate an ADS superpotential and hence a runaway behavior, and this will still be true after orientifolding. Thus a runaway DSB brane in the parent theory, if it survives the orientifold, will still be of runaway type. Populating the dimer with regular branes, the runaway sector will communicate with the twin $SU(5)$ sector, destabilizing the vacuum. The other possibility is that the hexagonal cluster corresponds to a deformation brane in the parent theory and that it survives the orientifold projection. This has no instability in the parent theory, and thus we expect it to remain stable also upon orientifolding.

It is known [15, 24] that deformation fractional branes are related to ZZP. We are looking for a dimer containing a six-valent node inside a cluster of faces. The corresponding toric diagram must contain at least 6 edges whose associated ZZP are ordered around the relevant node [64, 65]. Those edges need to be in equilibrium, and once removed the rest of the (p, q)-web must be in equilibrium, too. This implies that we need at least two extra ZZP in equilibrium, for a total of eight. Absence of $\mathcal{N} = 2$ fractional branes in the dimer further requires that there cannot be more than one ZZP with a given winding (p, q) of the unit cell. This corresponds to toric diagrams with no more than two consecutive points which are aligned on an external edge.

Since we are looking for a singularity admitting line orientifolds, we consider toric diagrams with line symmetry, either vertical/horizontal or diagonal.

- Diagonal line

  From fig. 75 we see that we need two antisymmetric fields, in $\square_1$ and $\overline{\square}_3$ representations, respectively. Even if dimer models containing the required deformation can be engineered, it turns out that there is no solution to the ACC of the full dimer, as it happens for all the theories (but a very special family, which however contains $\mathcal{N} = 2$ fractional branes) obtained as orientifolds of dimers with a diagonal fixed line, as proven in section 4. Thus, such cases are excluded.

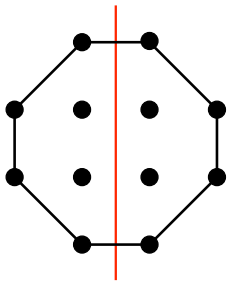

Figure 84: The toric diagram of the Octagon singularity.

- Vertical/horizontal lines

  As discussed in section 7.1, the freedom in choosing different charges for the two fixed lines is a crucial difference with respect to diagonal line orientifolds. In fact, it guarantees the existence of solutions to the ACC after orientifolding, exactly balancing the contribution from the different tensor fields. As discussed in section 4, this is ensured by noticing that tensor fields come in pairs in the dimer, one in each of the two lines. Assigning opposite signs to the two lines grants that the two contributions cancel, yielding an anomaly free theory. If the two signs are chosen the same, the situation is the same as with diagonal lines.

The upshot is that having vertical/horizontal lines, with opposite signs for the two orientifold lines, is the only option which can lead to viable twin $SU(5)$ models and it is what we are going to focus on in the following.

The need for two tensor fields is a stringent constraint on the ZZP, and therefore on the toric diagram. In particular, it implies that two couples of ZZP must have the correct intersection number among themselves and with the fixed lines, as computed from the toric diagram, see section 4.

Remarkably, the aforementioned necessary conditions provide substantial guidance for where to look for a model that works, as we now explain. The simplest example of a toric diagram with the required eight ZZP, with the correct intersection numbers, no $\mathcal{N} = 2$ fractional branes and the necessary horizontal symmetry is the toric diagram depicted in fig. 84, that we dub the Octagon.

Using standard techniques one can associate a dimer to a toric diagram, one for each different toric phase [21, 66]. A generic toric phase does not display the symmetry required to perform the orientifold projection. In the present case, however, one can find a symmetric toric phase where the vertical fixed lines are manifest and which realizes the twin $SU(5)$ model as described above. The corresponding dimer is depicted in fig. 85, where the hexagonal cluster is described by the white dot in the center of the unit cell. A quick and direct way to check that the dimer in

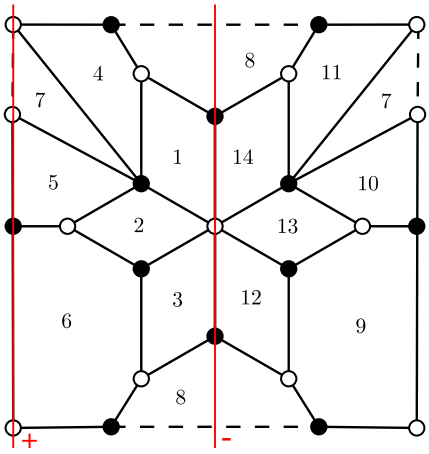

Figure 85: The (unit cell of the) dimer describing the symmetric phase of the Octagon. Orientifold lines are in red. Each orientifold line has a sign associated to it, which in this case needs to be opposite one another.

Figure 85 does correspond to the toric diagram in Figure 84 is by the Fast Forward Algorithm [21], as detailed in Appendix A.

Let us look at the orientifold gauge theory more closely. The orientifold projection identifies faces $(1, \ldots, 6)$ with faces $(14, \ldots, 9)$ while faces 7 and 8 are self-identified. Hence, D-branes at such orientifold singularity are described by a matter coupled supersymmetric gauge theory with six SU factors, one SO and one USp factors. The twin $SU(5)$ model is given by the rank assignment $SU(5)_1 \times SU(1)_2 \times SU(5)_3$ with all other faces being empty but face 7 which is a decoupled pure SYM with gauge group $SO(5)$ and hence confines on its own. ACC and self-consistency of such rank assignment follow the general discussion in section 7.1.

More details on the Octagon and its physical properties can be found in section 7.4. Here it suffices to say that this model represents a concrete example of an orientifold singularity which allows DSB by a D-brane bound state which is free of any known instability, in particular the $\mathcal{N} = 2$ fractional brane decay channel or the runaway behavior typical of DSB branes. The absence of $\mathcal{N} = 2$ fractional branes is clear from the toric diagram in fig. 84, which does not have internal points on boundary edges. This model therefore provides a realization (the first, to our knowledge) of stable DSB with D-branes at CY singularities and suggests for an extension of the string theory landscape as it is currently known.

7.4 Stability of the octagon

Let us now study the physics of the Octagon. We choose opposite signs as in fig. 85.For this sign configuration, there is a rank assignment which is anomaly free: $SU(N+M+4)$ for faces 1 and 3, $SU(N+M)$ for face 2, $SO(N+M+4)$ for face 7, $SU(N)$ for faces 4, 5 and 6, and $USp(N)$ for face 8. Setting $N=0$ we obtain a gauge theory with an isolated $SO(M+4)_7$ SYM theory, which confines on its own, together with a quiver gauge theory based on the group $SU(M+4)_1 \times SU(M)_2 \times SU(M+4)_3$ with matter fields and a superpotential that we proceed to analyze.

The theory gauge group is

$$SU(M+4)_1 \times SU(M)_2 \times SU(M+4)_3\,, \tag{306}$$

the matter content

$$A_1 = \square_1,\ X_{12} = (\overline{\square}_1, \square_2),\ X_{23} = (\overline{\square}_2, \square_3),\ A_3 = \overline{\square}_3\,, \tag{307}$$

with superpotential

$$W = A_1 X_{12} X_{23} A_3 X_{23}^t X_{12}^t\ . \tag{308}$$

The superpotential can be interpreted as follows. The gauge invariant $X_{12}^t A_1 X_{12}$ of group 1 and the gauge invariant $X_{23} A_3 X_{23}^t$ of group 3 are respectively in the $\square_2$ and $\overline{\square}_2$ of gauge group 2, with W above providing a bilinear in these two invariants, thus akin to a mass term. It is obvious that the antisymmetrics of $SU(M)_2$ can exist as such only if $M \geq 2$. In this case, one can show that strongly coupled dynamics generates superpotential terms that, together with the tree level one, eventually lead to supersymmetric vacua. For $M=0$ one gets instead two decoupled theories at faces 1 and 3 both having gauge group $SU(4)$ and one chiral superfield in the antisymmetric, which have a runaway behavior. The case of interest is $M=1$.

For $M=1$ node 2 becomes trivial ($SU(1)$ is empty) and, more importantly, the superpotential actually vanishes. Indeed, both nodes 1 and 3 are $SU(5)$ gauge theories with matter in the $\square \oplus \overline{\square}$ representations, and there is no chiral gauge invariant that can be written in this situation [52]. Hence the two gauge theories are effectively decoupled, and their IR behavior can be established independently. Both happen to be the $SU(5)$ model for stable DSB. Since the $SO(5)$ SYM on node 7 just confines, we thus determine that this configuration displays DSB in its vacuum. Quite interestingly, this DSB vacuum may then arise at the bottom of a duality cascade (possibly more complicated with respect to the simpler unorientifolded case, due to the orientifold projection which would modify it, see [44]), hence within a stringy UV completed theory.

Is this DSB vacuum stable? In principle, there can be different sources of potential instabilities.

First, one could be concerned about stringy instantons, whose presence may affect the low energy dynamics. Indeed, the D-brane configuration giving rise to the twin $SU(5)$ DSB model, $N = 0, M = 1$, contains both a $USp(0)$ and an $SU(1)$ factor coupling to the $SU(5)$ gauge groups. These are the two instances where contributions to the low-energy effective superpotential are allowed (see [50] and [67], respectively). However, no such contributions can be generated in our model simply because there are no chiral gauge invariants that can be written which can contribute to the superpotential. We thus conclude that stringy instantons cannot alter the DSB dynamics.

A second source of instability is the one discussed in [14, 1]. In fact, as can be readily seen from the toric diagram of fig. 84, this singularity does not admit $\mathcal{N} = 2$ fractional branes. The latter arise when the singularity can be partially resolved to display, locally, a non-isolated $\mathbb{C}^2/\mathbb{Z}_n$ singularity and a Coulomb-like branch associated to it. This translates into the presence of points inside some of the edges along the boundary of the toric diagram. The Octagon does not have this property. Hence, without the presence of $\mathcal{N} = 2$ fractional branes, there is no vacuum expectation value on which the energy of the DSB vacuum can depend on, or equivalently there is no Coulomb branch along which the energy can slide to zero value.

A third possible source of instability comes from the baryonic branch. It is indeed possible to build gauge invariant dibaryon operators from the bifundamental fields of our theory. The VEV of these operators parametrizes the baryonic branch of the theory's moduli space. Suitable values of these VEV can lead to partial resolutions of the CY manifold, effectively changing it and, in principle, opening the possibility for $\mathcal{N} = 2$ fractional branes in the resolved geometry. As we will discuss in appendix F, these resolutions are obstructed by the presence of both O-planes and fractional branes, thus preventing instabilities in the baryonic branch.

A final source of instability may come from the $\mathcal{N} = 4$ Coulomb branch represented by regular D3-branes. As in the previously analyzed cases [14, 1], one can easily show that this is a non-supersymmetric flat direction, essentially because of the conformality of the parent (non-orientifolded, large N) gauge theory. Therefore, there are no supersymmetric vacua along this branch [30].

[30] Flat directions are usually not expected in a non-supersymmetric vacuum. Subleading $1/N$ corrections to anomalous dimensions of matter fields, which could lift such flat direction, are not easily calculable, particularly in a complicated singularity such as the Octagon. However, they should neither change the number of supersymmetric vacua nor modify the behavior of the potential at infinity, at least for sufficiently large N.

7.5 Conclusions

In the third part of this thesis we studied possible realizations of DSB models in the framework of D-branes at toric CY singularities. In section 6, we reviewed known constructions of the $SU(5)$ model and provided new examples of singularity hosting it. Moreover, for the first time, we constructed the 3-2 model, the first example of a computable model built within this framework. We then studied the stability of these models under the decay mechanism introduced in [14]. We showed that all analysed models are affected by the same kind of instability and we provided the proof of a general no-go theorem, stating that DSB models engineered at non-isolated singularities are always unstable.

In section 7, we studied how to overcome such no-go theorem. We explored all possible embeddings of the $SU(5)$ a nd 3-2 models, proving that trivial realizations are always coupled to $\mathcal{N} = 2$ fractional branes and thus unstable. In order to avoid this decay mechanism we explored different realization of DSB models, proving that the *twin* $SU(5)$ model is the only possible configuration compatible with the stability requirements. Using the results of section 4, we were able to restrict the set of possible singularities that can contain the twin $SU(5)$ model, finding the simplest example in the singularity dubbed "the Octagon". Finally, we showed that a specific toric phase of the Octagon, compatible with orientifold projections, contains the twin $SU(5)$ model , which is the first instance, to our knowledge, of a stable DSB configuration of fractional branes. We discussed the main sources of instability that could affect the model and it avoids all of them.

With this example, we have shown, contrary to common lore, that stable DSB can be engineered by brane configurations at CY singularities. The Octagon is just the simplest example we could find satisfying all the requirements needed for stability. It is possible that similar models can be found in more complex singularities. Given the remarkable properties of this family of models, we consider it important to study them in further detail.

These models can be embedded into warped throat without instabilities, it would be thus of great interest to compute the gravity dual of such models, allowing the study of strong coupling phenomena, such as supersymmetry breaking and gauge group condensation, using a theory of gravity at weak coupling. Moreover, the study of compact versions of the same geometry, can be used to reproduce scenarios with supersymmetry breaking and hidden gravity sectors or put to the test swampland conjectures, such as the *Local AdS-Weak Gravity Conjecture* presented in [14].

A Holes in the Dimer and Zig-Zag Paths

In the following we present an argument forbidding the presence of holes of reduced rank inside a specific sub-dimer which appears in different twin models. We rely on ZZP techniques for anomaly cancellation developed in [3, 24]. One associates a value v_i to every ZZP in the dimer and then assigns an arbitrary rank to a given face in the dimer. The remaining ranks are set by requiring that the rank differences between two adjacent faces m, n obey $N_m - N_n = v_i - v_j$ where i, j are the ZZP separating them.

Consider a ring-shaped sub-dimer of rank $N + \mathcal{O}(1)$. We assume that as we go along it, from one of its faces to another, we only cross edges with identical orientation, see fig. 86a. We now show that the region inside the ring, the "hole", is inconsistent if of reduced rank.

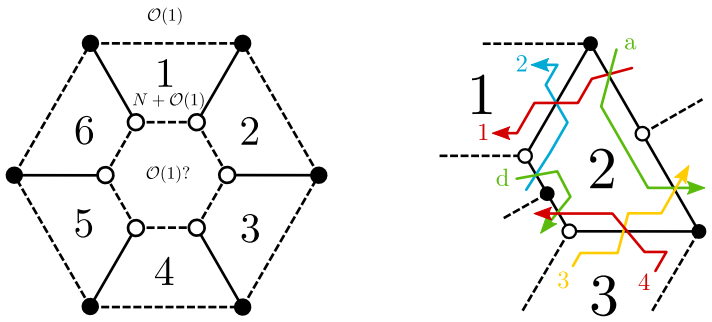

(a) (b)

Figure 86: (a) Generic ring of rank $N + \mathcal{O}(1)$ surrounded by faces of rank $\mathcal{O}(1)$ with a hole of rank $\mathcal{O}(1)$. (b) Face 2 edges with zig-zag paths.

Consider a face of the ring, as face 2 in fig. 86b. The intersections between the ZZP 1, 2, 3 and 4 yield

$$N_1 - N_2 = v_1 - v_2 \sim 0\,, \quad N_2 - N_3 = v_4 - v_3 \sim 0\,, \tag{309}$$

where $\sim$ means "equal up to $\mathcal{O}(1)$". Since the hole is supposed to be of rank $\mathcal{O}(1)$, the intersections with Zig-Zags that separate it from the ring give

$$N \sim v_2 - v_d, \quad -N \sim v_d - v_4, \quad \Rightarrow \quad v_2 \sim v_4\,. \tag{310}$$

Changing the number of edges between face 2 and the hole can only be done by adding/removing pairs of edges and will not change the fact that

$$v_1 \sim v_2 \sim v_3 \sim v_4 \qquad \text{and} \qquad v_d \sim v_1 - N\,, \tag{311}$$

where v_d is understood as any ZZP that comes with the pair of edges added between the hole and face 2. One can repeat the reasoning for every face of the

ring and find that its internal edges will be always produced by ZZP $\sim v_1$. This is in contradiction with the presence of ZZP $v_d \sim v_1 - N$ since there are only ZZP $\sim v_1$ entering the hole. It implies that v_d is circular or not present. The first option is forbidden in dimer models and the second spoils the presence of the hole itself. Hence the presence of an anomaly-free hole inside such a ring is inconsistent.

As a comment, let us notice that to reach this conclusion we did not assume anything about the exterior of the ring. If one does not look at the hole but asks that the exterior has a reduced rank, it implies that ZZP v_a on its border, see fig. 86b, will satisfy

$$v_a \sim v_1 + N \sim v_3 + N \,, \tag{312}$$

and thus we recover the result of eq. (310) using eq. (309). Again, it can be shown that this result does not depend on the number of edges in contact with the exterior of the ring. The cluster (hexagonal or otherwise) is now viable only with ranks $N + \mathcal{O}(1)$, because it is made only of ZZP $\sim v_1$.

B The Octagon and its Symmetric Phase

As discussed in [68, 69, 70], to any dimer model one can associate a weighted, signed adjacency matrix, known as the Kasteleyn matrix, whose determinant is the characteristic polynomial of the dimer model from which one can extract the toric data. This procedure is known as the Fast Forward Algorithm and is reviewed in [21].

To obtain the Kasteleyn matrix one assigns a sign to every edge such that for every face in the dimer the product of signs is $+1$ if its number of edges is $2 \bmod 4$ and -1 if its number of edges is $0 \bmod 4$. One then constructs two closed oriented (gauge invariant) paths γ_w, γ_z with holonomy $(0,1)$ and $(1,0)$. Every edge crossed by these paths is multiplied by w or $1/w$, depending on the relative orientation (respectively by z or $1/z$). The resulting graph for the Octagon is shown in fig. 87.

The adjacency matrix of the graph with such weights is the Kasteleyn Matrix and, for the Octagon, it reads

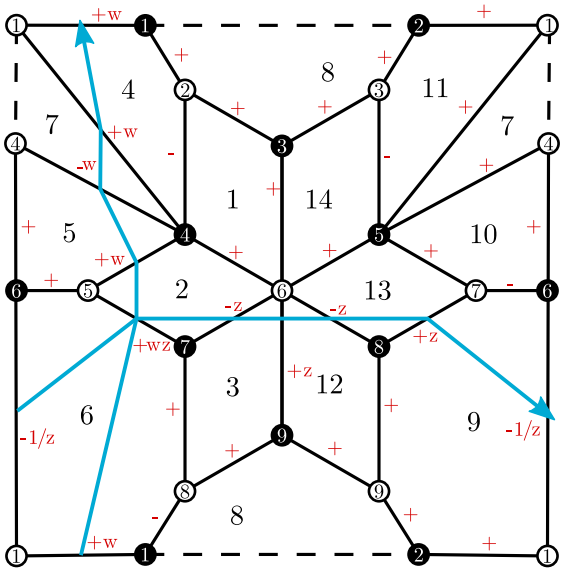

Figure 87: Dimer diagram of the Octagon with weights (in red) for building the Kasteleyn matrix. White and black nodes have been numbered. Two fundamental paths are shown in blue.

$$K = \left(\begin{array}{c|ccccccccc} & 1 & 2 & 3 & 4 & 5 & 6 & 7 & 8 & 9 \\ \hline 1 & w & 1 & 0 & w & 1 & -\frac{1}{z} & 0 & 0 & 0 \\ 2 & 1 & 0 & 1 & -1 & 0 & 0 & 0 & 0 & 0 \\ 3 & 0 & 1 & 1 & 0 & -1 & 0 & 0 & 0 & 0 \\ 4 & 0 & 0 & 0 & -w & 1 & 1 & 0 & 0 & 0 \\ 5 & 0 & 0 & 0 & w & 0 & 1 & wz & 0 & 0 \\ 6 & 0 & 0 & 1 & 1 & 1 & 0 & -z & -z & z \\ 7 & 0 & 0 & 0 & 0 & 1 & -1 & 0 & z & 0 \\ 8 & -1 & 0 & 0 & 0 & 0 & 0 & 1 & 0 & 1 \\ 9 & 0 & 1 & 0 & 0 & 0 & 0 & 0 & 1 & 1 \end{array}\right) \tag{313}$$

where rows and columns correspond to white and black nodes in the dimer, respectively. Its determinant is

$$\det(K) = w^3z^2+w^3z+w^2z^3-24w^2z^2+26w^2z-w^2+wz^3+24wz^2+26wz+w-z^2+z\,. \tag{314}$$

One may compute the Newton Polygon of the above expression and it should correspond to the toric diagram of the dimer one is dealing with [70]. For every monomial $a\ w^b z^c$ one draws a point in a $2d$ lattice with coordinates (b, c). As expected, one obtains the toric diagram depicted in fig. 84. Nicely, there is a

single perfect matching for each of its external points, thus ensuring that the dimer meets a necessary condition of minimality.

C ACC for 3-2 Quivers

Not all of the quivers presented in fig. 76 are free of anomalies when $N_i \neq 0$. In this appendix we check this explicitly. Our calculations also motivate the choice of the antisymmetric tensor $\overline{A}_2$ to satisfy the ACC. Below we summarize the ACC for each of these models. For completeness, we added here as different cases also the two models where node 1 and 4 are identified.

- $\underline{SO(N_1+1) \times USp(N_2+2) \times SU(N_3+3) \text{ with } \square\!\square_3}$:

$$\textbf{Node 3:} \quad (N_3+3-4) - (N_1+1) + (N_2+2) \;=\; 0\,. \tag{315}$$

- $\underline{SO(N_1+1) \times SU(N_2+2) \times SU(N_3+3) \text{ with } \square\!\square_3}$:

$$\begin{aligned} \textbf{Node 2:} \quad & -(N_2+2-4) + (N_1+1) - (N_3+3) \;=0\,, \\ \textbf{Node 3:} \quad & (N_3+3-4) - (N_1+1) + (N_2+2) \;=0\,. \end{aligned} \tag{316}$$

  Note that the choice of conjugate representation for the antisymmetric tensor of $SU(N_2+2)$ is fixed by the first equation, in order to satisfy it when all $N_i = 0$.

  For these two first models, the ACC reduce to

$$N_1 = N_2 + N_3\,. \tag{317}$$

- $\underline{SO(N_1+1) \times USp(N_2+2) \times SU(N_3+3) \times SO(N_4+1)}$:

$$\textbf{Node 3:} \quad -(N_1+1) + (N_2+2) - (N_4+1) = 0\,. \tag{318}$$

  In this case, N_3 is not constrained by the ACC, which can be rewritten as

$$N_2 = N_1 + N_4\,. \tag{319}$$

- $\underline{SO(N_1+1) \times SU(N_2+2) \times SU(N_3+3) \times SO(N_4+1)}$:

$$\begin{aligned} \textbf{Node 2:} \quad & -(N_2+2-4) + (N_1+1) - (N_3+3) \;=0\,, \\ \textbf{Node 3:} \quad & -(N_1+1) + (N_2+2) - (N_4+1) \;=0\,. \end{aligned} \tag{320}$$

This translates to the two conditions

$$\begin{aligned} N_1 = &\quad N_2 + N_3 \,, \\ N_2 = &\quad N_1 + N_4 \,, \end{aligned} \tag{321}$$

implying $N_3 = -N_4$. This in turn sets $N_3 = N_4 = 0$, since all N_i must be positive and potentially large. In principle this issue does not rule out the possible engineering of these models, since the corresponding dimers might give rise to additional gauge groups and fields when regular D3-branes are added, in a way that anomalies are cancelled. Assuming that at least some fractional branes are needed in order to turn on all the ranks of the 3-2 model (i.e. even for $N_i = 0$), then such models are excluded.

- $SO(N_1+1) \times USp(N_2+2) \times SU(N_3+3)$ with $2(\overline{\square}_3, \square_1)$:

$$-2(N_1+1) + (N_2+2) = 0 \,, \tag{322}$$

which is simply

$$N_2 = 2N_1 \,. \tag{323}$$

- $SO(N_1+1) \times SU(N_2+2) \times SU(N_3+3)$ with $2(\overline{\square}_3, \square_1)$:

$$\begin{aligned} \textbf{Node 2:} \quad -(N_2+2-4) + (N_1+1) - (N_3+3) &= 0 \,, \\ \textbf{Node 3:} \quad -2(N_1+1) + (N_2+2) &= 0 \,. \end{aligned} \tag{324}$$

This can be simplified into

$$\begin{aligned} N_2 = &\quad 2N_1 \,, \\ N_3 = &\quad -N_1 \,, \end{aligned} \tag{325}$$

which has no solution beyond $N_i = 0$ in the absence of additional ingredients coming from the full dimer.

The results of this appendix can be summarized in the following table:

Gauge groups	ACC
$SO(N_1+1) \times USp(N_2+2) \times SU(N_3+3)$ with $\square\!\square_3$	✓
$SO(N_1+1) \times SU(N_2+2) \times SU(N_3+3)$ with $\square\!\square_3$	✓
$SO(N_1+1) \times USp(N_2+2) \times SU(N_3+3) \times SO(N_4+4)$	✓
$SO(N_1+1) \times SU(N_2+2) \times SU(N_3+3) \times SO(N_4+4)$	✗
$SO(N_1+1) \times USp(N_2+2) \times SU(N_3+3)$ with $2(\overline{\square}_3, \square_1)$	✓
$SO(N_1+1) \times SU(N_2+2) \times SU(N_3+3)$ with $2(\overline{\square}_3, \square_1)$	✗

D Worldsheet analysis for the Klein bottle projection of $\mathbb{C}^2/\mathbb{Z}_4$

In this appendix, we present the worldsheet computations for the glide orientifold of $\mathbb{C}^2/\mathbb{Z}_4$ presented in Section 5.2.2.

The open sector of strings on the orbifold before the orientifold projection is obtained as follows:

$$\begin{aligned} A_\mu &= \begin{pmatrix} A_{1\mu} & 0 & 0 & 0 \\ 0 & A_{2\mu} & 0 & 0 \\ 0 & 0 & A_{3\mu} & 0 \\ 0 & 0 & 0 & A_{4\mu} \end{pmatrix}, \quad \Phi_1 = \begin{pmatrix} 0 & X_{12} & 0 & 0 \\ 0 & 0 & X_{23} & 0 \\ 0 & 0 & 0 & X_{34} \\ X_{41} & 0 & 0 & 0 \end{pmatrix}, \\ \Phi_2 &= \begin{pmatrix} 0 & 0 & 0 & Y_{14} \\ Y_{21} & 0 & 0 & 0 \\ 0 & Y_{32} & 0 & 0 \\ 0 & 0 & Y_{43} & 0 \end{pmatrix}, \quad \Phi_3 = \begin{pmatrix} Z_{11} & 0 & 0 & 0 \\ 0 & Z_{22} & 0 & 0 \\ 0 & 0 & Z_{33} & 0 \\ 0 & 0 & 0 & Z_{44} \end{pmatrix}. \end{aligned} \tag{326}$$

The appropriate orientifold projection, defined as in Equations section 5.2.1 and section 5.2.1, is given by

$$\gamma_\Omega = \begin{pmatrix} 0 & 0 & \mathbb{1}_N & 0 \\ 0 & 0 & 0 & \mathbb{1}_N \\ \mathbb{1}_N & 0 & 0 & 0 \\ 0 & \mathbb{1}_N & 0 & 0 \end{pmatrix}, \quad \text{and} \quad R = \begin{pmatrix} 0 & 1 & 0 \\ 1 & 0 & 0 \\ 0 & 0 & 1 \end{pmatrix}. \tag{327}$$

It gives the following identification of gauge bosons

$$A_{1\,\mu} = -A_{3\,\mu}^T \quad \text{and} \quad A_{2\,\mu} = -A_{4\,\mu}^T\,, \tag{328}$$

the resulting gauge group is $SU(N)_1 \times SU(N)_2$. The matter content follows from

$$\begin{array}{rcccl} X_{12} & = & Y_{43}^T & \equiv & \mathcal{X}_{12} \in (\,\overline{\square}_1,\,\square_2\,)\,, \\ X_{23} & = & Y_{14}^T & \equiv & \mathcal{X}_{21} \in (\,\overline{\square}_2,\,\overline{\square}_1\,)\,, \\ Y_{21} & = & X_{34}^T & \equiv & \mathcal{Y}_{21} \in (\,\overline{\square}_2,\,\square_1\,)\,, \\ Y_{32} & = & X_{41}^T & \equiv & \mathcal{Y}_{12} \in (\,\square_1,\,\square_2\,)\,, \\ Z_{11} & = & Z_{33}^T & \equiv & \mathcal{Z}_{11} \in \mathrm{Adj}_1\,, \\ Z_{22} & = & Z_{44}^T & \equiv & \mathcal{Z}_{22} \in \mathrm{Adj}_2\,. \end{array} \tag{329}$$

One can check that the superpotential is the one advertised in Equation eq. (140).

E Computations for the orbifolds of the conifold

In this appendix we study the glide orientifold of orbidolds of the conifold, both chiral and non chiral. In particular we focus on $\mathcal{C}/\mathbb{Z}_2$ and the cone over F_0, the

zeroth Hrizebruch surface. Moreover, we provide an analysis of the duality cascade of the orientifold theory of $\mathcal{C}/\mathbb{Z}_2$, which mimics the one of the conifold.

E.1 Orbifold of the conifold $\mathcal{C}/\mathbb{Z}_2$

Let be a non-chiral orbifold of the conifold, $\mathcal{C}/(\mathbb{Z}_l \times \mathbb{Z}_m)$. The general action is given by

$$\begin{aligned} &\gamma_g V_{1,2} \gamma_g^{-1} = V_{1,2} \\ &\gamma_g A_1 \gamma_g^{-1} = e^{2\pi i/l} A_1 \,, \quad \gamma_g A_2 \gamma_g^{-1} = A_2 \\ &\gamma_g B_1 \gamma_g^{-1} = e^{-2\pi i/l} B_1 \,, \quad \gamma_g B_2 \gamma_g^{-1} = B_2 \,, \end{aligned} \tag{330}$$

and

$$\begin{aligned} &\gamma_g V_{1,2} \gamma_g^{-1} = V_{1,2} \\ &\gamma_g A_1 \gamma_g^{-1} = e^{2\pi i/m} A_1 \,, \quad \gamma_g A_2 \gamma_g^{-1} = A_2 \\ &\gamma_g B_1 \gamma_g^{-1} = B_1 \,, \quad \gamma_g B_2 \gamma_g^{-1} = e^{-2\pi i/m} B_2 \,, \end{aligned} \tag{331}$$

where $V_{1,2}$ are the two adjoint vectors related to the gauge groups. In the case of our first example, $\mathcal{C}/\mathbb{Z}_2$, the action gives the following fields

$$\begin{aligned} V_1 &= \begin{pmatrix} V_1 & 0 \\ 0 & V_3 \end{pmatrix}, \qquad V_2 = \begin{pmatrix} V_2 & 0 \\ 0 & V_4 \end{pmatrix}, \qquad A_1 = \begin{pmatrix} 0 & A_{14} \\ A_{32} & 0 \end{pmatrix}, \\ A_2 &= \begin{pmatrix} A_{12} & 0 \\ 0 & A_{34} \end{pmatrix}, \quad B_1 = \begin{pmatrix} B_{21} & 0 \\ 0 & B_{43} \end{pmatrix}, \quad B_2 = \begin{pmatrix} 0 & B_{23} \\ B_{41} & 0 \end{pmatrix}, \end{aligned} \tag{332}$$

with a superpotential given by

$$W = A_1 B_1 A_2 B_2 - A_1 B_2 A_2 B_1 \,. \tag{333}$$

We consider the following orientifold projection in order to reproduce the glide projection.

$$\begin{aligned} V_{1,2} &= -\gamma_\Omega V_{1,2}^T \gamma_\Omega^{-1} \,, \\ A_{1,2} &= \gamma_\Omega B_{1,2}^T \gamma_\Omega^{-1} \,, \end{aligned} \tag{334}$$

with

$$\gamma_\Omega = \begin{pmatrix} 0 & \mathbb{1}_N \\ \mathbb{1}_N & 0 \end{pmatrix} . \tag{335}$$

The action on mesons, $x = (A_1 B_1)^2$ $y = (A_2 B_2)^2$, $z = A_1 B_2$ and $w = A_2 B_1$, is

$$\begin{aligned} &x \leftrightarrow y \,, \qquad z \to z \,, \qquad w \to w \,, \\ &\Omega_3 = \frac{\mathrm{d}x \wedge \mathrm{d}y \wedge \mathrm{d}z}{2wz^2} \to \Omega_3' = \frac{\mathrm{d}y \wedge \mathrm{d}x \wedge \mathrm{d}z}{2wz^2} = -\Omega_3 \end{aligned} \tag{336}$$

which means that the action preserves supersymmetry on the branes.

The gauge group is $SU(N_1)_1 \times SU(N_2)_2$ and matter content given by

$$\begin{array}{rcl} A_{14} = B_{23}^T \equiv & A & = \ (\,\overline{\square}_{\,1},\ \overline{\square}_{\,2}\,)\,, \\ B_{41} = A_{32}^T \equiv & B & = \ (\,\square_{\,1},\ \square_{\,2}\,)\,, \\ A_{12} = B_{43}^T \equiv & C & = \ (\,\overline{\square}_{\,1},\ \square_{\,2}\,)\,, \\ B_{21} = A_{34}^T \equiv & D & = \ (\,\square_{\,1},\ \overline{\square}_{\,2}\,)\,, \end{array} \tag{337}$$

with superpotential

$$W = ABCD - BAC^T D^T\,. \tag{338}$$

E.2 Zeroth Hirzebruch surface $\mathbf{F}_0$

In this case we take the following actions on the fields

$$\begin{aligned} \gamma_g V_{1,2} \gamma_g^{-1} &= V_{1,2} \\ \gamma_g A_1 \gamma_g^{-1} &= -A_1 \\ \gamma_g A_2 \gamma_g^{-1} &= -A_2 \\ \gamma_g B_1 \gamma_g^{-1} &= B_1 \\ \gamma_g B_2 \gamma_g^{-1} &= B_2\,, \end{aligned} \tag{339}$$

leading to

$$V_1 = \begin{pmatrix} V_1 & 0 \\ 0 & V_3 \end{pmatrix}, \qquad V_2 = \begin{pmatrix} V_2 & 0 \\ 0 & V_4 \end{pmatrix}, \qquad A_1 = \begin{pmatrix} 0 & A_{14}^1 \\ A_{32}^1 & 0 \end{pmatrix},$$
$$A_2 = \begin{pmatrix} 0 & A_{14}^2 \\ A_{32}^2 & 0 \end{pmatrix}, \qquad B_1 = \begin{pmatrix} B_{21}^1 & 0 \\ 0 & B_{43}^1 \end{pmatrix}, \qquad B_2 = \begin{pmatrix} B_{21}^2 & 0 \\ 0 & B_{43}^2 \end{pmatrix}.$$

The orientifold action maps $1 \to 4$ and $2 \to 3$, it can be summarized as

$$\begin{aligned} V_{1,2} &= -\gamma_\Omega V_{1,2}^T \gamma_\Omega^{-1}\,, \\ A_1 &= \gamma_\Omega A_2^T \gamma_\Omega^{-1}\,, \\ B_1 &= \gamma_\Omega B_2^T \gamma_\Omega^{-1}\,, \end{aligned} \tag{340}$$

with

$$\gamma_\Omega = \begin{pmatrix} \mathbb{1}_N & 0 \\ 0 & \mathbb{1}_N \end{pmatrix}. \tag{341}$$

The resulting gauge group is $SU(N)_1 \times SU(N)_2$ and the matter content is given by

$$\begin{array}{rcccl} A^1_{14} = A^{2T}_{14} & \equiv & U_{S,A} & = & \overline{\square\square}_{\,1},\ \overline{\begin{array}{c}\square\\\square\end{array}}_{\,1}\,, \\ A^2_{32} = A^{2T}_{32} & \equiv & Z_{S,A} & = & \square\square_{\,2},\ \begin{array}{c}\square\\\square\end{array}_{\,2}\,, \\ B^1_{21} = B^2_{43} & \equiv & X & = & (\,\square_{\,1},\ \overline{\square}_{\,2})\,, \\ B^2_{21} = B^1_{43} & \equiv & Y & = & (\,\square_{\,1},\ \overline{\square}_{\,2})\,, \end{array} \tag{342}$$

with the following superpotential,

$$W = XU_S Y^T Z_A - X^T Z_S Y U_A\,. \tag{343}$$

In order to compute the action the 3-form, we compute the equations defining the singularity using the geometrical approach described in Section 5.7. The singularity is described by the following equations in $\mathbb{C}^9$

$$\begin{array}{ccc} & z_1 z_3 = z_2 z_4 = z_0^2\,, & \\ z_1 z_2 = z_5^2\,, & & z_2 z_3 = z_7^2\,, \\ z_1 z_4 = z_6^2\,, & & z_3 z_4 = z_8^2\,. \end{array} \tag{344}$$

The action on mesons is

$$z_1 \leftrightarrow z_2\,, \qquad z_3 \leftrightarrow z_4\,, \qquad z_6 \leftrightarrow z_7 \tag{345}$$

while all other coordinates are invariant. The action on the 3-form is

$$\Omega_3 = \mathrm{Res}\frac{\mathrm{d}z_1 \wedge \mathrm{d}z_2 \wedge \mathrm{d}z_3 \wedge \mathrm{d}z_4 \wedge \mathrm{d}z_5 \wedge \mathrm{d}z_6 \wedge \mathrm{d}z_7 \wedge \mathrm{d}z_8 \wedge \mathrm{d}z_0}{\prod_i P_i} \to -\Omega_3\,, \tag{346}$$

since the polynomials are invariant and in the numerator we are exchanging three pairs of coordinates, resulting in an overall minus sign.

E.3 A cascade in the glide projection of $\mathcal{C}/\mathbb{Z}_2$

For a generic choice of ranks, $SU(N+M)_1 \times SU(N)_2$, one finds that the gauge theory has a non-trivial RG-flow and $SU(N+M)_1$ goes more rapidly to strong coupling as we approach the infrared regime of the theory:

$$\beta_1 = 3M\,, \quad \beta_2 = -3M\,. \tag{347}$$

The mesons of the first gauge group are

$$M_1 = BA \quad M_2 = BC\,, \quad M_3 = C^T D^T \quad \text{and} \quad M_4 = DA\,, \tag{348}$$

and one thus finds that this gauge theory is Seiberg dual [31] to $SU(N-M)_1 \times SU(N)_2$ with a matter content given by the mesons M_1, M_2, M_3 and M_4 in addition to the following list of bifundamental fields:

$$a = (\,\square_1,\,\square_2)\,, \quad b = (\,\bar{\square}_1,\,\bar{\square}_2)\,, \quad c = (\,\square_1,\,\bar{\square}_2) \quad \text{and} \quad d = (\,\bar{\square}_1,\,\square_2)\,. \tag{349}$$

The superpotential is given by

$$\begin{aligned} W &= M_2M_4 - M_1M_3 + M_1ab + M_2cb + M_3d^Tc^T + M_4ad \\ &= abd^Tc^T - badc \end{aligned} \tag{350}$$

where the mesons have been integrated out using F-term relations.

The new gauge theory $SU(N-M)_1 \times SU(N)_2$ ends up with the same matter content and superpotential (up to an overall sign) as the initial $SU(N+M)_1 \times SU(N)_2$. This can be seen easily with the following mapping:

$$A \to b\,, \quad B \to a\,, \quad C \to d \quad \text{and} \quad D \to c\,. \tag{351}$$

The M deformation branes thus trigger a cascade of Seiberg dualities à la Klebanov-Strassler [32]. In particular, for N being an integer multiple of M, we expect the cascade flow down to $SU(2M) \times SU(M)$ where the physics should the same as for the deformed conifold. Indeed, we can schematically define baryonic operators $\bar{\mathcal{B}} = \left[AC^T\right]^M$, $\mathcal{B} = \left[BD^T\right]^M$, and a $2M \times 2M$ squared matrix $\mathcal{M}$ in terms of the mesonic operators of eq. (348) that should obey a relation of the form

$$\det\mathcal{M} - \bar{\mathcal{B}}\mathcal{B} = \Lambda_{2M}^{4M}\,, \tag{352}$$

where Λ_{2M} is the strong coupling scale of $SU(2M)$. Going on the baryonic branch $\bar{\mathcal{B}} = \mathcal{B} = i\Lambda_{2M}^{2M}$, one finds that the mesons decouple, leaving a SYM $SU(M)$ dynamics displaying confinement and chiral symmetry breaking.

F Baryonic branch instabilities

In this appendix we investigate the possible instabilities of the Octagon model when exploring the baryonic branch. These directions in the moduli space correspond to the VEV of dibaryons operators. Moving along these directions has the geometric effect of partially resolve the singularity.

In fig. 88 we depict the toric diagram of the Octagon singularity and the corresponding dimer diagram with the fractional brane configuration which gives rise, upon orientifolding, to our DSB model. Neighboring faces with different colors indicate the fact that the rank of gauge groups are different in the considered configuration.

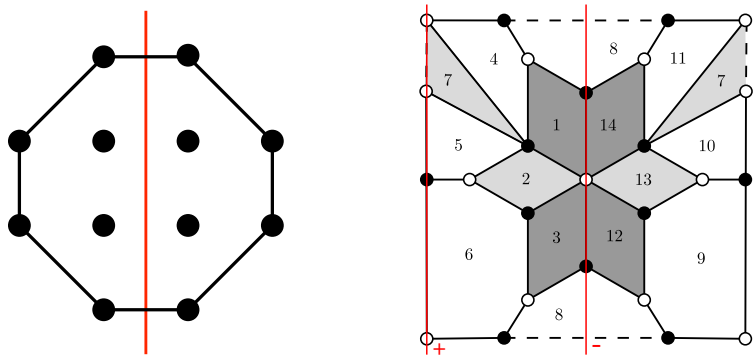

(a) (b)

Figure 88: The Octagon (a) Toric diagram, (b) Dimer diagram with the deformation brane in grey. Red lines represent the orientifold lines.

We list in fig. 89 the first partial resolutions of the Octagon that preserve the orientifold symmetry, as explained in [27]. In order to cause instabilities, the resulting toric diagram has to remain symmetric with respect to the orientifold line and allow for the presence of $\mathcal{N} = 2$ fractional branes. Further partial resolutions consistent with the orientifold projection inexorably lead to orbifolds of the conifold, for which our comments on the case of fig. 89c will remain valid.

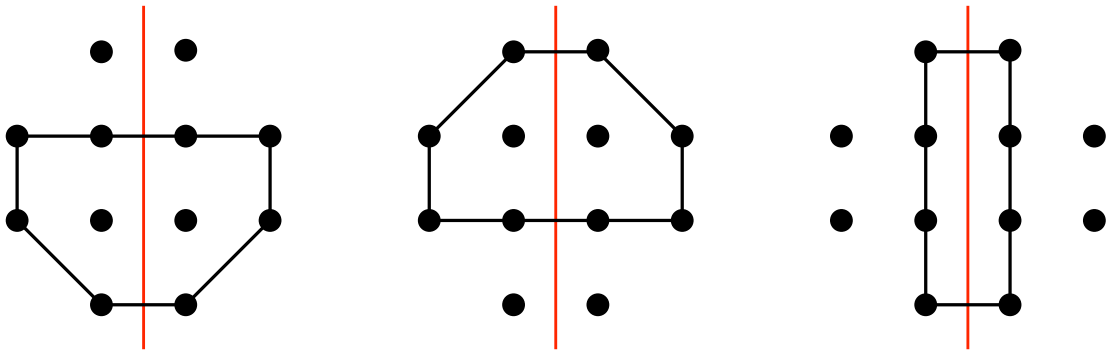

(a) (b) (c)

Figure 89: First partial resolutions of the orientifolded Octagon admitting $\mathcal{N} = 2$ fractional branes.

The corresponding dimer diagrams are obtained following Gulotta's algorithm, [64], and are presented in fig. 90. The algorithm operates the partial resolution by "merging" some ZZP within the dimer diagram of fig. 88b. This action is equivalent to assigning a VEV to the edges on which these ZZP cross each other.

In the cases of fig. 90a and fig. 90b, we see that the partial resolution is in obstruction with the very nature of our deformation brane because it implies the

fusion of faces of different ranks already at the level of the non-orientifolded theory. In the case of fig. 90c, instead, the partial resolution is obstructed because it is obtained giving a VEV to edges separating faces of ranks that differ by the orientifold charge, for example the edge separating faces 1 and 2.

Therefore, we conclude that any partial resolutions of the Octagon singularity which opens-up $\mathcal{N} = 2$ fractional brane directions is indeed obstructed in our model.

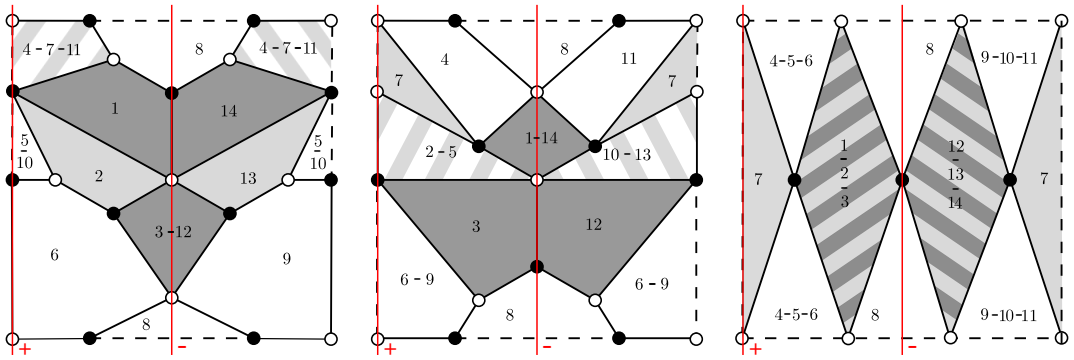

(a) (b) (c)

Figure 90: Dimer diagrams after partial resolutions.

References

[1] R. Argurio, M. Bertolini, S. Meynet, and A. Pasternak, *On supersymmetry breaking vacua from D-branes at orientifold singularities*, *JHEP* **12** (2019) 145, [arXiv:1909.04682].

[2] R. Argurio, M. Bertolini, S. Franco, E. García-Valdecasas, S. Meynet, A. Pasternak, and V. Tatitscheff, *Dimers, Orientifolds and Stability of Supersymmetry Breaking Vacua*, *JHEP* **01** (2021) 061, [arXiv:2007.13762].

[3] R. Argurio, M. Bertolini, S. Franco, E. García-Valdecasas, S. Meynet, A. Pasternak, and V. Tatitscheff, *Dimers, Orientifolds and Anomalies*, *JHEP* **02** (2021) 153, [arXiv:2009.11291].

[4] R. Argurio, M. Bertolini, S. Franco, E. García-Valdecasas, S. Meynet, A. Pasternak, and V. Tatitscheff, *The Octagon and the Non-Supersymmetric String Landscape*, *Phys. Lett. B* **815** (2021) 136153, [arXiv:2005.09671].

[5] E. García-Valdecasas, S. Meynet, A. Pasternak, and V. Tatitscheff, *Dimers in a Bottle*, *JHEP* **04** (2021) 274, [arXiv:2101.02670].

[6] J. Polchinski, *Dirichlet Branes and Ramond-Ramond charges*, *Phys. Rev. Lett.* **75** (1995) 4724–4727, [hep-th/9510017].

[7] J. M. Maldacena, *The Large N limit of superconformal field theories and supergravity*, *Int. J. Theor. Phys.* **38** (1999) 1113–1133, [hep-th/9711200].

[8] S. B. Giddings, S. Kachru, and J. Polchinski, *Hierarchies from fluxes in string compactifications*, *Phys. Rev. D* **66** (2002) 106006, [hep-th/0105097].

[9] C. Vafa, *The String landscape and the swampland*, hep-th/0509212.

[10] T. D. Brennan, F. Carta, and C. Vafa, *The String Landscape, the Swampland, and the Missing Corner*, *PoS* **TASI2017** (2017) 015, [arXiv:1711.00864].

[11] E. Palti, *The Swampland: Introduction and Review*, *Fortsch. Phys.* **67** (2019), no. 6 1900037, [arXiv:1903.06239].

[12] H. Ooguri and C. Vafa, *Non-supersymmetric AdS and the Swampland*, *Adv. Theor. Math. Phys.* **21** (2017) 1787–1801, [arXiv:1610.01533].

[13] B. Freivogel and M. Kleban, *Vacua Morghulis*, arXiv:1610.04564.

[14] G. Buratti, E. Garcia-Valdecasas, and A. M. Uranga, *Supersymmetry Breaking Warped Throats and the Weak Gravity Conjecture*, *JHEP* **04** (2019) 111, [arXiv:1810.07673].

[15] S. Franco, A. Hanany, F. Saad, and A. M. Uranga, *Fractional branes and dynamical supersymmetry breaking*, *JHEP* **01** (2006) 011, [hep-th/0505040].

[16] M. J. Strassler, *The Duality cascade*, in *Theoretical Advanced Study Institute in Elementary Particle Physics (TASI 2003): Recent Trends in String Theory*, pp. 419–510, 5, 2005. hep-th/0505153.

[17] I. Affleck, M. Dine, and N. Seiberg, *Dynamical Supersymmetry Breaking in Supersymmetric QCD*, *Nucl. Phys. B* **241** (1984) 493–534.

[18] M. Yamazaki, *Brane Tilings and Their Applications*, *Fortsch. Phys.* **56** (2008) 555–686, [arXiv:0803.4474].

[19] S. Franco and D. Vegh, *Moduli spaces of gauge theories from dimer models: Proof of the correspondence*, *JHEP* **11** (2006) 054, [hep-th/0601063].

[20] K. Kenyon, *An introduction to the dimer model*, math/0310326.

[21] S. Franco, A. Hanany, K. D. Kennaway, D. Vegh, and B. Wecht, *Brane dimers and quiver gauge theories*, *JHEP* **01** (2006) 096, [hep-th/0504110].

[22] D. P. Thurston, *From dominoes to hexagons*, in *Proceedings of the 2014 Maui and 2015 Qinhuangdao Conferences in Honour of Vaughan FR Jones ,Äô 60th Birthday*, pp. 399–414, Australian National University, Mathematical Sciences Institute, 2017.

[23] A. Hanany and D. Vegh, *Quivers, tilings, branes and rhombi*, *JHEP* **10** (2007) 029, [hep-th/0511063].

[24] A. Butti, *Deformations of Toric Singularities and Fractional Branes*, *JHEP* **10** (2006) 080, [hep-th/0603253].

[25] S. Franco, A. Hanany, D. Krefl, J. Park, A. M. Uranga, and D. Vegh, *Dimers and orientifolds*, *JHEP* **09** (2007) 075, [arXiv:0707.0298].

[26] N. Seiberg, *The Power of holomorphy: Exact results in 4-D SUSY field theories*, in *Particles, Strings, and Cosmology (PASCOS 94)*, pp. 0357–369, 5, 1994. hep-th/9408013.

[27] A. Retolaza and A. Uranga, *Orientifolds of Warped Throats from Toric Calabi-Yau Singularities*, *JHEP* **07** (2016) 135, [arXiv:1605.01732].

[28] M. Yamazaki, *Brane tilings and their applications*, *Fortschritte der Physik* **56** (Jun, 2008) 555,Äì686.

[29] D. Dugger, *Involutions on surfaces*, *Journal of Homotopy and Related Structures* **14** (2019), no. 4 919–992.

[30] W. Thurston, "The geometry and topology of three-manifolds." Notes `http://library.msri.org/books/gt3m/`, 2002.

[31] N. Seiberg, *Electric - magnetic duality in supersymmetric nonAbelian gauge theories*, *Nucl. Phys. B* **435** (1995) 129–146, [hep-th/9411149].

[32] I. R. Klebanov and M. J. Strassler, *Supergravity and a confining gauge theory: Duality cascades and chi SB resolution of naked singularities*, *JHEP* **08** (2000) 052, [hep-th/0007191].

[33] S. Imai and T. Yokono, *Comments on orientifold projection in the conifold and SO x USp duality cascade*, *Phys. Rev. D* **65** (2002) 066007, [hep-th/0110209].

[34] A. Antinucci, S. Mancani, and F. Riccioni, *Infrared duality in unoriented Pseudo del Pezzo*, *Phys. Lett. B* **811** (2020) 135902, [arXiv:2007.14749].

[35] Y. Imamura, K. Kimura, and M. Yamazaki, *Anomalies and O-plane charges in orientifolded brane tilings*, *JHEP* **03** (2008) 058, [arXiv:0801.3528].

[36] A. Dabholkar and J. Park, *Strings on orientifolds*, *Nucl. Phys. B* **477** (1996) 701–714, [hep-th/9604178].

[37] E. Witten, *Toroidal compactification without vector structure*, *JHEP* **02** (1998) 006, [hep-th/9712028].

[38] J. Park and A. M. Uranga, *A Note on superconformal N=2 theories and orientifolds*, *Nucl. Phys. B* **542** (1999) 139–156, [hep-th/9808161].

[39] J. Park, R. Rabadan, and A. Uranga, *N=1 type IIA brane configurations, chirality and T duality*, *Nucl. Phys. B* **570** (2000) 3–37, [hep-th/9907074].

[40] A. M. Uranga, *A New orientifold of C**2 / Z(N) and six-dimensional RG fixed points*, *Nucl. Phys. B* **577** (2000) 73–87, [hep-th/9910155].

[41] I. P. Ennes, C. Lozano, S. G. Naculich, and H. J. Schnitzer, *Elliptic models, type IIB orientifolds and the AdS / CFT correspondence*, *Nucl. Phys. B* **591** (2000) 195–226, [hep-th/0006140].

[42] B. Feng, Y.-H. He, A. Karch, and A. M. Uranga, *Orientifold dual for stuck NS5-branes*, *JHEP* **06** (2001) 065, [hep-th/0103177].

[43] D. Cox, J. Little, and H. Schenck, *Toric Varieties*. Graduate studies in mathematics. American Mathematical Soc., 2011.

[44] R. Argurio and M. Bertolini, *Orientifolds and duality cascades: confinement before the wall*, *JHEP* **02** (2018) 149, [arXiv:1711.08983].

[45] I. García-Etxebarria and D. Regalado, $\mathcal{N} = 3$ *four dimensional field theories*, *JHEP* **03** (2016) 083, [arXiv:1512.06434].

[46] O. Aharony and Y. Tachikawa, *S-folds and 4d N=3 superconformal field theories*, *JHEP* **06** (2016) 044, [arXiv:1602.08638].

[47] D. Berenstein, C. Herzog, P. Ouyang, and S. Pinansky, *Supersymmetry breaking from a Calabi-Yau singularity*, *JHEP* **09** (2005) 084, [hep-th/0505029].

[48] M. Bertolini, F. Bigazzi, and A. Cotrone, *Supersymmetry breaking at the end of a cascade of Seiberg dualities*, *Phys. Rev. D* **72** (2005) 061902, [hep-th/0505055].

[49] R. Blumenhagen, B. Kors, D. Lust, and S. Stieberger, *Four-dimensional String Compactifications with D-Branes, Orientifolds and Fluxes*, *Phys. Rept.* **445** (2007) 1–193, [hep-th/0610327].

[50] R. Argurio, M. Bertolini, G. Ferretti, A. Lerda, and C. Petersson, *Stringy instantons at orbifold singularities*, *JHEP* **06** (2007) 067, [arXiv:0704.0262].

[51] O. Aharony and S. Kachru, *Stringy Instantons and Cascading Quivers*, *JHEP* **09** (2007) 060, [arXiv:0707.3126].

[52] I. Affleck, M. Dine, and N. Seiberg, *Dynamical Supersymmetry Breaking in Chiral Theories*, *Phys. Lett. B* **137** (1984) 187.

[53] I. Affleck, M. Dine, and N. Seiberg, *Dynamical Supersymmetry Breaking in Four-Dimensions and Its Phenomenological Implications*, *Nucl. Phys. B* **256** (1985) 557–599.

[54] V. A. Novikov, M. A. Shifman, A. I. Vainshtein, and V. I. Zakharov, *Exact Gell-Mann-Low Function of Supersymmetric Yang-Mills Theories from Instanton Calculus*, *Nucl. Phys. B* **229** (1983) 381–393.

[55] E. Poppitz and S. P. Trivedi, *Some examples of chiral moduli spaces and dynamical supersymmetry breaking*, *Phys. Lett. B* **365** (1996) 125–131, [hep-th/9507169].

[56] A. Retolaza and A. Uranga, *De Sitter Uplift with Dynamical Susy Breaking*, *JHEP* **04** (2016) 137, [arXiv:1512.06363].

[57] S. Franco, Y.-H. He, C. Herzog, and J. Walcher, *Chaotic duality in string theory*, *Phys. Rev. D* **70** (2004) 046006, [hep-th/0402120].

[58] S. Franco, A. Hanany, and A. M. Uranga, *Multi-flux warped throats and cascading gauge theories*, *JHEP* **09** (2005) 028, [hep-th/0502113].

[59] I. Garcia-Etxebarria, F. Saad, and A. M. Uranga, *Quiver gauge theories at resolved and deformed singularities using dimers*, *JHEP* **06** (2006) 055, [hep-th/0603108].

[60] B. Feng, S. Franco, A. Hanany, and Y.-H. He, *UnHiggsing the del Pezzo*, *JHEP* **08** (2003) 058, [hep-th/0209228].

[61] K. A. Intriligator and B. Wecht, *The Exact superconformal R symmetry maximizes a*, *Nucl. Phys. B* **667** (2003) 183–200, [hep-th/0304128].

[62] S. Franco, Y.-H. He, C. Sun, and Y. Xiao, *A Comprehensive Survey of Brane Tilings*, *Int. J. Mod. Phys. A* **32** (2017), no. 23n24 1750142, [arXiv:1702.03958].

[63] J. Davey, A. Hanany, and R.-K. Seong, *Counting Orbifolds*, *JHEP* **06** (2010) 010, [arXiv:1002.3609].

[64] D. R. Gulotta, *Properly ordered dimers, R-charges, and an efficient inverse algorithm*, *JHEP* **10** (2008) 014, [arXiv:0807.3012].

[65] A. Ishii and K. Ueda, *A note on consistency conditions on dimer models*, 2010.

[66] S. Franco, A. Hanany, D. Martelli, J. Sparks, D. Vegh, and B. Wecht, *Gauge theories from toric geometry and brane tilings*, *JHEP* **01** (2006) 128, [hep-th/0505211].

[67] C. Petersson, *Superpotentials From Stringy Instantons Without Orientifolds*, *JHEP* **05** (2008) 078, [arXiv:0711.1837].

[68] R. Kenyon, *An introduction to the dimer model*, *arXiv preprint math/0310326* (2003).

[69] R. Kenyon, A. Okounkov, and S. Sheffield, *Dimers and amoebae*, `math-ph/0311005`.

[70] A. Hanany and K. D. Kennaway, *Dimer models and toric diagrams*, `hep-th/0503149`.